THE UNIVERSITY OF CHICAGO

INVESTIGATING MOLECULAR MECHANISMS AND DYNAMICS OF ENA/VASP AND OTHER ACTIN BINDING PROTEINS

A DISSERTATION SUBMITTED TO
THE FACULTY OF THE DIVISION OF THE BIOLOGICAL SCIENCES
AND THE PRITZKER SCHOOL OF MEDICINE
IN CANDIDACY FOR THE DEGREE OF
DOCTOR OF PHILOSOPHY

GRADUATE PROGRAM IN BIOCHEMISTRY AND MOLECULAR BIOPHYSICS

BY
ALYSSA JUSTINE HARKER

CHICAGO, ILLINOIS
DECEMBER 2018

Table of Contents

List of Figures

List of Tables

ACKNOWLEDGMENTS

I am very thankful for all the support and assistance I've received during my PhD. None of these projects would have been possible without the work from my collaborators. In addition to my main project, I was able to add to many other people's projects and, while doing so, learned many new topics and different techniques which I greatly appreciate.

I was very fortunate to be able to work in such a great environment as the Kovar Lab. I would like to thank past and present members of the Kovar Lab, specifically Katie Homa, Alisha Morganthaler, Caitlin Anderson, Jenna Christensen, Glen Hocky, Patrick McCall, Dennis Zimmermann, Tom Burke, Kate Proudfoot, and Meghan O'Connell for their scientific insights and making the Kovar Lab a fun, collaborative, and productive place to do science. Furthermore, I would like to thank Jon Winkelman and Cristian Suarez for their training and guidance, especially when I first joined the lab. I would finally like to acknowledge my advisor David Kovar for his guidance and support throughout my entire graduate school career as well as the freedom to explore.

I would like to thank my committee Bob Keenan, Margaret Gardel, and Mike Rust for taking the time to meet with me and give me advice about my project. I appreciate the different persepectives and ideas that they brought during our meetings over the course of my PhD. I would also like to thank the administrators that make the cluster and departments run smoothly, specifically the administrators I worked closely with, Kristine Gaston and Lisa Anderson.

I have also benefited from being part of the larger molecular biosciences community. I appreciate the support my molecular biosciences cohort has given me from when we started this journey during coursework and rotations through the stresses and celebrations that occur throughout graduate school. I would like to thank those who gave me scientific advice and insights, but specifically Ashley Rich and Ana Beiriger who also supported my hobbies and allowed me to maintain balance during graduate school. I would also like to thank my BMB

year Katherine Leon, Chris Katanski, and Phil McGilvray who are an outstanding source of encouragement and laughter. Furthermore, Within the BMB community as a whole, I could rely on sharing of advice, reagents, and knowledge.

My friends and family have given me unending support through my time at University of Chicago. I would specifically like to thank my parents, Mark and Amy Harker, and my sister, Emily Harker, for their limitless encouragement and willingness to assist in any way. I would finally like to thank Corey Rodriguez who supports me in everything I do and is a constant source of motivation and encouragement.

ABSTRACT

Many important cellular functions depend on the architecture of a dynamic actin cytoskeleton forming at the correct location and time during the cell cycle. Cellular division, motility, and endocytosis are a few examples of processes in which actin filaments must be nucleated, polymerized, severed, and depolymerized with spatiotemporal precision in the cell. To create a complete picture of the dynamic actin cytoskeleton, it is vital to collect mechanistic information about the diverse actin networks and their associated proteins. Actin networks gain their distinct properties from the subset of hundreds of actin binding proteins that localize to them. Some of these actin binding proteins, such as formin, have well-studied mechanisms of how the single molecule interacts with actin. However, how these proteins interact with other actin binding proteins and how these interactions affect activity to lead to complex actin networks has only recently become a topic of interest. Nonetheless, it is important that we first discern the molecular mechanisms of actin binding proteins on their own as this gives us a base mechanism to guide further experimentation. Understanding the molecular mechanistic details of actin binding proteins allows us to determine how they can function collectively to create, maintain, and disassemble complex actin networks.

Here I investigate the molecular mechanisms of various actin binding proteins and how they are affected by the presence of other actin binding proteins and actin binding toxins. The main project focuses on Ena/VASP, which are tetrameric actin elongation factors that bind F-actin barbed ends continuously while increasing their elongation rate within dynamic bundled networks such as filopodia. However, we were also interested in how Ena/VASP's molecular mechanism is affected by the presence of different bundling proteins. We used single-molecule TIRFM and developed a kinetic model to dissect Ena/VASP's processive mechanism on bundled filaments. The results demonstrate that Ena tetramers are tailored for enhanced processivity on fascin bundles and avidity of multiple arms associating with multiple filaments is critical for this process.

I also was involved in many collaborations to investigate the dynamics and molecular mechanisms of various actin binding proteins. Many of these projects also surround the bundling proteins that I have studied in relation to Ena/VASP. I found that fascin, which is the main bundling proteins in filopodia and an enhancer of Ena/VASP processivity, also plays a role in reducing Arp2/3 complex-mediated branching. We also showed that fascin sorts with α-actinin due to an intrinsic sorting mechanism dictated by filament spacing. We visualized this sorting by electron microscopy and observed the transition between a fascin domain and an α-actinin domain. Further investigation into α-actinin's bundling properties showed that tropomyosin increases α-actinin dynamics. My other collaborations focused on the pathogenic *Vibrio* bacteria. We found that an excreted toxin formed actin oligomers that inhibited Ena/VASP elongation and caused Ena/VASP to cap filaments. Furthermore, we investigated the molecular mechanism of a *Vibrio* nucleation factor VopL/F and found that they nucleate filaments from the pointed end of F-actin and stay bound at the pointed end before releasing the filament.

Overall, my work has shown the importance of not only characterizing the molecular mechanism of actin binding proteins, but also how these actin binding proteins work in concert with the multiple other actin binding proteins that are found within the cell. The gained knowledge from these studies are a step forward for the field to fully grasp the role each actin binding protein plays in the larger system of the actin cytoskeleton.

CHAPTER 1

INTRODUCTION

As the most abundant protein in most eukaryotic cells, actin participates in more protein-protein interactions than any known protein [40]. All eukaryotes have at least one gene for actin and many form complex actin networks with only a single actin gene, such as budding yeast, fission yeast, and green algae [132]. However, some species have many actin genes that are expressed in different tissues. For example, humans have three genes for α-actin, one gene for β-actin, and two genes for γ-actin and plants can have 10 or more actin genes [132]. Additionally actin is highly conserved among organisms and, even among the three isoforms (α, β, γ-actin) in vertebrates, only varies by a few amino acids near the N-terminus [40]. The actin cytoskeleton plays many biochemical and mechanical roles in the cell and is important for many cellular processes such as polarity establishment, motility, and morphogenesis [13]. To fulfill these roles, the actin cytoskeleton forms distinct and dynamic networks made up of filamentous actin (F-actin) and other actin binding proteins. These networks are formed and degraded at certain times and locations within cells for proper cellular function.

1.1 Actin

Actin is a 42 kDa globular protein and contains four subdomains. The N-terminus is located in subdomain 1, then the polypeptide domain proceeds through subdomains 2, 3, and 4, returning to subdomain 1 with the C-terminus [132]. Subdomains 1 and 3 are structurally similar although they contain little sequence similarity [39, 132]. Subdomains 1 and 2 form the outer domain while subdomains 3 and 4 form the inner, larger domain. Between these domains is a hinge region and two large clefts, a nucleotide binding cleft and a target binding cleft. The nucleotide binding cleft binds ATP and an associated cation (Mg^{2+} in cells). Many proteins bind actin in the target binding cleft between subdomains 1 and 3 [39].

Actin assembles into polar filaments with new subunits being primarily added onto the barbed end (subdomains 1 and 3) versus the pointed end (subdomains 2 and 4). The polarity of the filaments was initially observed when visualizing actin filaments saturated with myosin heads using electron microscopy [75]. The myosin heads formed an arrowhead-shaped object and thus defined the "barbed" and "pointed" end of the filament due to the direction the arrowheads pointed. An actin filament contains two protofilaments that wrap around each other with a right-handed twist along the long-axis [62]. However, the repeated unit of symmetry is a left-handed helix with ~13 actin subunits repeating every 35.9 nm. The G-actin to F-actin transition consists of a 12-13° rotation of the outer domain (subunits 1 and 2) with respect to the inner domain (subunits 3 and 4) with some additional bending movements of subdomains 2 and 4. Therefore, F-actin is flatter than G-actin and the DNase I binding loop (D-loop) in subdomain 2 inserts into the target-binding cleft of the subunit above [40].

Actin monomers bind both ATP or ADP tightly and a nucleotide-free G-actin will rapidly acquire ATP with an affinity in the nanomolar range [38]. A bound nucleotide stabilizes an actin monomer, but is not required for polymerization [132]. Monomers polymerize spontaneously under physiological salt conditions with cations present. Spontaneous assembly has an initial lag period due to the slow nucleation step caused by the instability of actin dimers and trimers [33, 50, 152]. Once a fourth subunit has been added to the actin nucleus, the seed is more stable and elongation occurs at the same rate as longer filaments. Elongation occurs 10 times faster at barbed ends than pointed ends. ATP-actin associates with barbed ends with a rate constant of ~10 μM^{-1} s^{-1} and slowly dissociates at ~1 s^{-1} [130]. Thus the "critical concentration" for monomer addition is 0.1 μM for the barbed end of actin filaments. Once a monomer undergoes the conformational change to bind to a filament, the rate of hydrolysis increases to 0.3 s^{-1}. ATP hydrolysis is thought to occur randomly along the filament [77], though it has been proposed that neighboring subunits could affect the

rate [83]. Once hydrolysis occurs, the phosphate is slow to dissociate [27], leaving ADP-actin which dissociates more easily from both ends of the filament.

The total cellular concentration of actin is between 50-200 μM. In cells, filaments assemble and disassemble on the timescale of tens of seconds. Actin binding proteins cause large differences in actin assembly and disassembly from the *in vitro* rates and allow for almost half of the total actin in cells to be unpolymerized (~25-100 μM) which is far above the critical concentration. Within cells there are millimolar concentrations of Mg-ATP and phosphate, so most cytoplasmic G-actin has bound Mg-ATP. Once the G-actin is added to F-actin, the Mg-ATP is hydrolyzed and then the phosphate is released. Depolymerization of F-actin releases Mg-ADP monomers, where ADP is exchanged for ATP. The ADP to ATP exchange is slow, but can be sped up by an actin monomer binding protein, profilin [132]. Overall actin assembly and disassembly rates are further changed by actin binding proteins that nucleate, elongate, cap, sever, and crosslink filaments.

1.2 Actin networks

The actin filaments in cells are organized into distinct, dynamic networks that allow the cell to carry out processes such as cytokinesis, endocytosis, motility, and adherence. A set of actin binding proteins localize to each distinct network, which allows for each network's unique architecture and function. One simplified model organism, *Schizosaccharomyces pombe* (fission yeast), only has one actin isoform, yet has three distinct primary actin networks: actin patches for endocytosis, actin rings for cytokinesis, and actin cables for polarity establishment. As you progress to more complex organisms the number of networks and actin binding proteins expands. Here I will focus on three actin networks found in higher eukaryotes; lamellipodia, filopodia, and stress fibers.

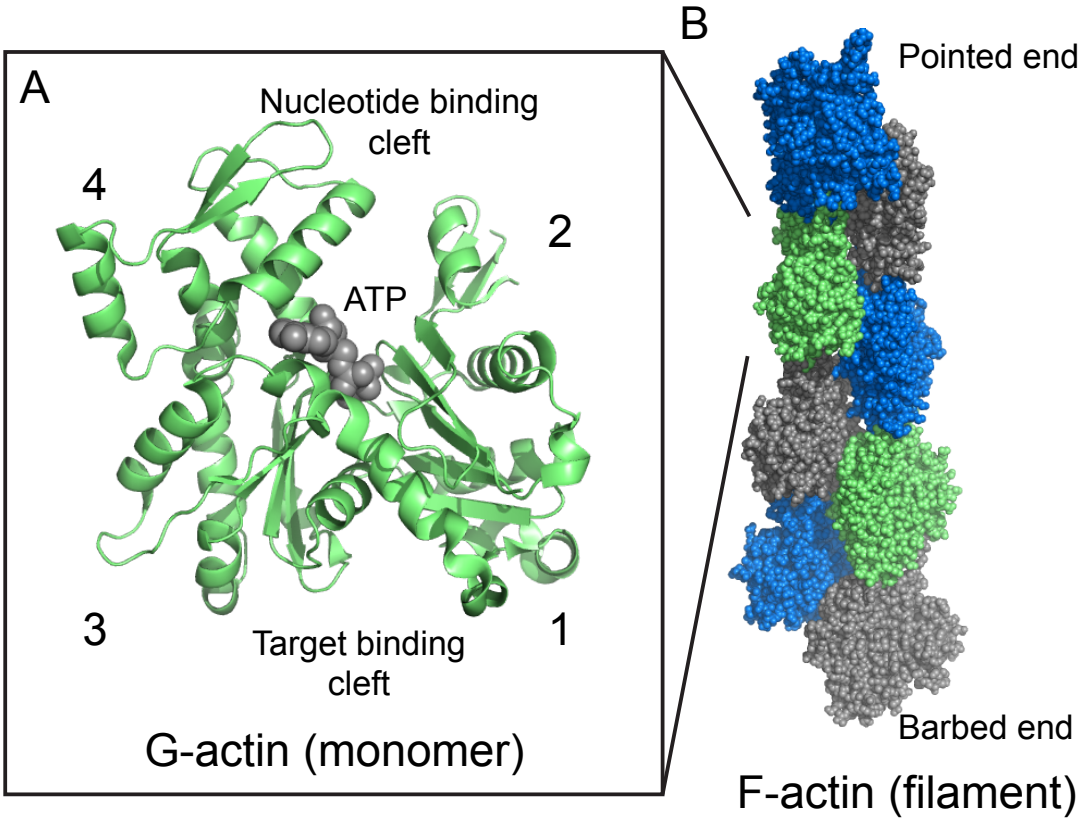

Figure 1.1: **Monomeric G-actin is assembled into filamentous F-actin.** (A) Monomeric globular actin (G-actin) (PDB: 1NWK) contains four subdomains with the N- and C-terminus in subdomain 1. There are two binding clefts within the actin subunit. In the center of the actin subunit, between subdomains 2 and 4, is the nucleotide binding cleft while other actin binding proteins bind in the target binding cleft between subunits 1 and 3. (B) G-actin assembles into filamentous actin (F-actin) (PDB: 6BNO) that is polar with a fast growing barbed end (bottom) and a slow growing pointed end (top).

1.2.1 Lamellipodia

The lamellipodium is made of short, branched actin filaments that form a thin, dense meshwork [164]. Lamellipodia can extend up to tens of microns along the leading edge of motile cells [162]. The branched network is nucleated by the Arp2/3 complex, which must be activated by a nucleation promoting factor (NPF) such as WAVE or WASP proteins [13]. The branches are kept short by capping protein, which blocks barbed end filament growth and filaments are severed for recycling by cofilin. The branched filaments are crosslinked into a dense mesh by the bundling proteins fimbrin, α-actinin, and filamin [164]. The growth of the dense network pushes on the leading edge membrane generating force. Actin polymerization within the lamellipodia network drives the membrane forward when membrane tension is low, but when membrane tension is high, actin polymerization drives retrograde flow. In addition to traction formed by adhesion to a surface, retrograde flow drives cell movement [162].

1.2.2 Filopodia

The dynamic fingerlike projections that emerge from the lamellipodium in motile cells are called filopodia. Filopodia are important for exploration of the mechanical and chemical extracellular space [103]. This is especially important in steering neuronal growth cones, wound healing, and dorsal or ventral closure during development. During these processes cells must be able to follow mechanical and chemical signals in order to move through space towards other cells or locations [15]. Filopodia are made up of 10-30 tightly packed filaments, primarily bundled by the crosslinking protein, fascin [177, 105]. These filaments form uniform parallel bundles, with all their barbed ends organized towards the tip of the filopodia [15].

There are two proposed models for how filopodia form at the leading edge of cells: convergent elongation [186] and de-novo nucleation [44] (Figure 1.2). The convergent elongation model proposes that the filopodial filaments are initially nucleated by Arp2/3 complex in

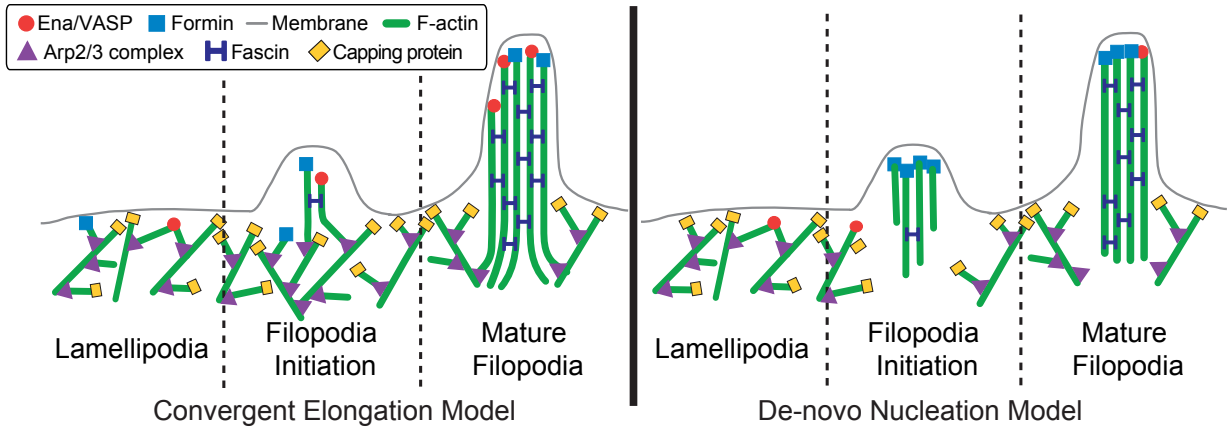

Figure 1.2: **Comparison of models for filopodia formation.** A comparison between two models for filopodia formation. The convergent elongation model (left) proposes that filaments are nucleated by Arp2/3 complex within the lamellipodia and are gathered into parallel fascin-mediated bundles by elongation factors Ena/VASP and formin. The de-novo nucleation model (right) postulates that nucleation of filopodia filaments occur at the membrane by nucleation factors such as formin and are separate from the Arp2/3 complex nucleated filaments in the lamellipodia.

the lamellipodia. These filaments make λ-shaped precursors that can be elongated by elongation factors such as Ena/VASP or formins and bundled by fascin [168, 164]. In contrast, the de-novo nucleation proposes that filopodia formation is distinct from the lamellipodium and nucleation of these filaments is facilitated by formins such as mDia2 [45, 105]. There is no consensus on which model is followed in cells and it could be that different nucleators are driving different types of filopodia in different cell types. Futhermore, some cells can produce different types of filopodia within the same cell. For example, D16 cells from *Drosophila* have short, more dynamic filopodia formed by Ena compared to the long, stable filopodia formed by formin Dia [12]. This is also seen in mammalian cells where VASP or mDia2 expression facilitates varying number of filopodia with different dynamics and morphology [8].

1.2.3 Stress Fibers

Another way that cells can produce force through actin networks is with contractile stress fibers. Stress fibers are formed from actomyosin bundles formed mainly by α-actinin. There are three main types of stress fibers in animal cells: ventral, dorsal, and transverse arcs. Ventral stress fibers are anchored at each end by focal adhesions where dorsal stress fibers are only anchored at one end near the leading edge. Transverse arcs are convex stress fibers that form parallel to the leading edge [23]. Stess fibers and focal adhesions are important for cell adhesion, morphogenesis, and especially mechanotransduction [171]. Stress fibers are the main vehicle for contractile forces in cells. The contractile force is initiated by myosin II that binds alternating with α-actinin along the stress fibers [115].

1.3 Actin binding proteins

Actin binding proteins affect F-actin in a variety of ways including nucleating, elongating, capping, severing, disassembling and crosslinking. Additionally, actin binding proteins such as profilin can bind to actin monomers. Profilin is a small actin binding protein that has high affinity for ATP-actin monomers (Kd = 0.1 μM) [132]. However, profilin binds monomers on the barbed end so it inhibits nucleation and addition at the pointed end, but allows addition at barbed ends. When a profilin-actin complex binds the barbed end, the affinity of profilin for the bound actin subunit decreases, facilitating dissociation [35]. Profilin is also important for catalyzing nucleotide exchange in actin monomers, facilitating the formation of ATP-actin [108, 179]. Between profilin and another actin monomer binding protein, thymosin-β4, there is a low concentration of free actin monomers [132].

Other actin binding proteins can bind to sides of F-actin, such as tropomyosin and myosin. Tropomyosin is a coiled-coil protein that binds along the long-pitch helices of F-actin [41]. Tropomyosin stabilizes filaments and increases its persistence length [165]. Additionally, in muscle cells tropomyosin regulates the binding of myosin. Myosin is a family of ATP-motors

that bind and release actin filaments throughout the ATP hydrolysis cycle. Depending on the type of myosin, this allows processive runs along actin filaments or muscle contraction in sarcomeres. Myosins are important for force generation, transport of cargo along F-actin, anchoring organelles, and mechanotransduction [65].

1.3.1 Nucleation factors

As described earlier, actin nucleation is slow; therefore, actin binding proteins are necessary to catalyze the formation of an F-actin nucleus within the timescale required in cells. There are three major classes of nucleation factors. The first class is Arp2/3 complex, which is made up of seven subunits including actin related protein 2 (Arp2) and actin related protein 3 (Arp3). Arp2/3 complex nucleates filaments by binding to the side of a mother filament and using its Arp2 and Arp3 proteins to template the nucleation of a filament that branches from the mother at a 70° angle. In order to nucleate branches, Arp2/3 needs to be activated via a nucleation promoting factor such as WAVE or WASP. Arp2/3 complex nucleates branched filaments within for networks that supply pushing forces such as the lamellipodia, some stress fibers, sites of endocytosis and internal membrane traffic, and actin patches in *S. pombe* [132, 115, 106].

The second class of nucleation factors are formins, which nucleate unbranched filaments. There are still some open questions surrounding how formins nucleate filaments *in vivo*. Initially, it was thought that formins stabilize actin dimers with their FH2 domain to aid in nucleation, since the FH2 domain is necessary and sufficient for nucleation *in vitro* [190, 123, 136]. However, FH2 domains are inefficient at nucleating profilin-actin, which is thought to be the main substrate available *in vivo*. Recently it has been shown that C-terminal tail regions of certain formins, FH1 domains, and NPFs that bind to some C-terminal tail regions could assist the FH2 domain for profilin-actin nucleation [16]. Formins nucleate filaments for the lamellipodia, filopodia, some stress fibers, and contractile rings [44, 106, 13].

The third class of nucleation factors are WH2 nucleators. This is a much broader class than the other two classes and contains proteins such as Spire, Cobl, and bacterial VopL and VopF (VopL/F) [139, 114, 22, 158]. This is a more recently discovered class of nucleators that use tandem WH2 domains to bind and bring together actin monomers to form a nucleus. The proteins in this class have variable nucleation activities, caused by the differences in the number of WH2 domains and also the length of linkers between them [158]. As an example, VopL/F are virulence factors from bacteria *Vibrio parahaemolyticus* and *Vibrio cholera* that can assemble unproductive F-actin in host cells [100]. VopL/F contains three tandem WH2 domains and dimerizes through a VopL/F C-terminal domain (VCD). However, two different mechanisms were proposed for VopL and VopF, two closely related proteins. One mechanism suggested that VopL nucleates actin filaments from the pointed end [114, 188, 189], while the other mechanism proposed that VopF nucleated filaments then continued to assemble actin at the barbed end, similar to a formin [126].

1.3.2 Elongation factors

Beyond nucleation, there are also assembly factors that aid in actin elongation. Actin will assemble spontaneously at a rate of ~10 μM s^{-1} [130]; however, there are actin binding proteins that associate with the growing barbed end and can change its polymerization rate. Formins are able to increase the elongation rate of F-actin up to 10-fold using profilin-actin [132]. Another elongation factor protein is Enabled/Vasodilator stimulating phosphoprotein (Ena/VASP). These tetrameric proteins use WH2-like domains to associate with the barbed end and can increase F-actin elongation 2- to 3-fold with both free actin monomers and profilin-actin, but are not thought to nucleate new filaments. I will return to these two proteins to look closer into their mechanisms and functions.

Formins and Ena/VASP compete for barbed ends with capping protein. Capping protein is found in almost all eukaryotic cells at micromolar concentrations and consists of a het-

erodimer. Capping protein associates with barbed ends within seconds but remains tightly bound to the barbed end with the half-time of dissociation at 30 minutes [42]. While bound, capping protein blocks both monomer addition as well as monomer dissociation. Therefore, capping protein helps maintain the actin monomer pool by reducing the number of growing barbed ends available for monomer addition and can also stabilize the barbed ends of filaments such as those found in striated muscles [132].

1.3.3 Bundling proteins

There are different families of proteins that are able to crosslink F-actin. These proteins contain more than one actin binding domain so that they can bind to more than one filament at a time. Crosslinking is defined as holding two filaments together at one point. In contrast, bundling is when two filaments are held parallel to each other by multiple crosslinks [132]. I will use bundling protein to describe proteins that are able to bundle filaments *in vitro*, though their main function in cells may be to crosslink rather bundle filaments.

The largest group of bundling proteins fall in the CH domain superfamily, such as fimbrin/plastin, α-actinin, spectrin, and filamin. These proteins use two sets of tandem CH domains to bind to two actin filaments. Fimbrin contains two tandem CH domains to bundle F-actin as a monomer and localizes to the lamellipodia and base of filopodia in cells. Fimbrin bundles have narrow spacing, ~10-12 nm, and can consist of both antiparallel and parallel filaments [60]. α-actinin also uses CH-domains to bundle actin but only contains one tandem CH domain per monomer so to bundle F-actin it forms a dimer using its spectrin repeats. α-actinin bundles have much wider spaced filaments, ~30-36 nm, and can also contain either parallel or antiparallel filaments [159]. Some α-actinins have different spacing due to the number of spectrin repeats that separate the CH domains. For example, we quantified the spacing of filaments within *S. Pombe* Ain1 bundles, which contains just two spectrin repeats, using electron microscopy as 25 $\pm$ 4 nm (data not shown). Ain1 makes

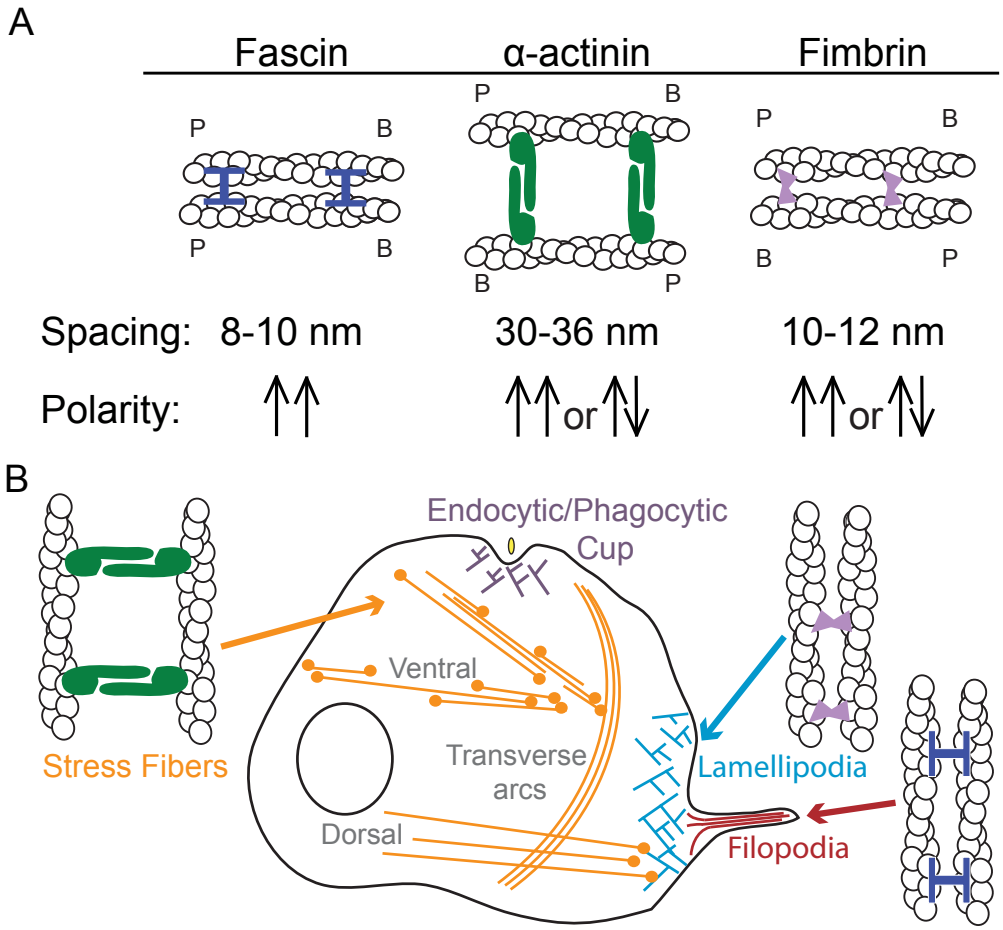

Figure 1.3: **Bundling proteins form diverse bundles.** (A) Fascin forms narrow parallel bundles. α-actinin forms wide parallel and antiparallel bundles. Fimbrin forms narrow parallel and antiparallel bundles. (B) Different bundling proteins localize to distinct actin networks. α-actinin localizes to stress fibers which include ventral, dorsal, and transverse arcs. Fimbrin localizes predominately to the lamellipodia while fascin is found in filopodia.

more narrow spaced bundles compared to human α-actinin IV (30-36 nm), which contains four spectrin repeats [113, 59, 170, 99]. α-actinin and fimbrin bind on the same site of the actin filament [81]. In contrast, fascin bundles F-actin using its four β-trefoil domains [76]. Fascin is a small globular bundling protein that is the main bundling protein in filopodia [177, 105]. Fascin forms bundles that are narrowly spaced, between 8-10 nm, and only consist of parallel filaments [43, 76, 26].

1.4 Ena/VASP and Formins[1]

1.4.1 Comparison of processive actin elongation factors

To gain mechanistic understanding of the actin cytoskeleton and actin binding proteins we must elucidate how each protein works individually, but also how the different proteins affect each other and contribute to proper function of cellular processes. I am interested in the molecular mechanism of actin binding proteins to understand how they properly function, but also how with different diseases and mutations the proteins function abnormally. This detailed mechanistic understanding is the foundation that cell biology can be built upon, leading to deeper knowledge of processes that occur in cells and even organisms.

Here I will focus on the mechanism of two processive protein families, formins and Ena/VASP, which bind to the barbed end of actin filaments and affect actin filament polymerization. Interestingly, though these two families have different structures and use distinct mechanisms, they share similarities in how they increase actin polymerization as well as that they are both localized to the leading edge and involved in filopodia formation. However, their mechanistic differences in terms of processive run lengths, diverse protein binding partners, and formin's reliance on profilin-actin bring up many interesting questions concerning how these proteins are utilized by a cell within different and even the same processes. The

1. Portions of this section were modified from a review in preparation with Jonathan Winkelman.

knowledge of formin's mechanism is a step ahead of Ena/VASP's, exploring the role of force, rotation, and diverse actin regulatory domains on its actin assembly properties. However, this gives us insight by comparing and contrasting the two processive machines and understand how they both individually and concurrently help to assemble the necessary actin networks for proper cellular function.

1.4.2 Cellular processes

Formin

Formin homology proteins (formins) are highly conserved actin binding proteins that function in multiple cellular processes such as cytokinesis, oogenesis, and stress fiber and filopodia formation. Furthermore, formins can interact with both actin and microtubules [6, 70], allowing for communication between these two cytoskeleton systems. Formins were first discovered as mutations at the mouse limb deformity (ld) locus resulting in development defects [184]. Since their discovery the formin family has grown, now counting 15 different formins in mammalian cells. The formins are localized to different areas of the cell including the leading edge, tips of filopodia, cell-cell junctions, and cytokinetic rings [132]. Formins are implicated in nucleation of nascent actin filaments, processive elongation, and competition with capping protein as well as other F-actin barbed end binding proteins. However, there are some proteins within the formin family (i.e. INF2, Daam1) that have been shown to exhibit additional behaviors, such as depolymerization, bundling of filaments, severing, or actin monomer sequestering [56]. Though the mechanism of formin's processive F-actin assembly has been well-studied, the individual characteristics of different formins and how those characteristics influence their distinct roles within the same cell continue to be open questions.

Ena/VASP

Ena/VASP proteins are tetrameric actin polymerases that localize to multiple actin networks including tips of filopodia, lamellipodia, stress fibers, focal adhesions, and adherence junctions. Ena/VASP is important for filopodia formation, cell migration, and is thought to potentially play a role in stress fiber repair [93]. Vasodilator-stimulated phosphoprotein (VASP) was first discovered in human platelets as a substrate of both the cAMP- and cGMP-dependent protein kinases [58]. Simultaneously, *enabled* (*ena*) was found in Drosophila during a genetic screen for surpressors of abelson protein tyrosine kinase mutant phenotypes [51]. Ena and VASP were found to be homologous [1] and homologs have been found in all multicellular metazoan cells and Dictyostelium [151]. Invertebrates (*Drosophila, C. elegans, Dictyostelium* ect.) only have one isoform of Ena/VASP while mammalians have three: Mena (mammalian Enabled), VASP, and EVL (Ena-VASP-like) [52]. Ena/VASP associates with barbed ends of F-actin and increase the elongation rate and *in vitro* has been shown to nucleate and bundle filaments at high concentrations [18, 19, 182, 61, 122, 9]. Like formin, Ena has also been shown to compete with capping protein for barbed ends of F-actin [9].

1.4.3 Domain organization

Formin

The classical formin homology 1 (FH1) and formin homology 2 (FH2) domains are the characteristic domains of the formin family (Figure 1.4A). The N-terminus of formin contains regulatory and localization domains that vary depending on the subfamily of formins. The largest subfamily, Diaphanous-related formins (DRF), is autoregulated by the N-terminal Diaphanous inhibitory domain (DID) binding to a C-terminal Diaphanous autoregulatory domain (DAD). Rho-GTPase binding to the N-terminal GTPase binding domain (GBD) can partially relieve this autoregulation [72]. Subsets outside of DRFs have C-terminal DAD

or Wiskott-Aldrich syndrome homology region 2 (WH2) domains. A formin homology 3 (FH3) domain is present in fungal and metazoan formins for targeting [128]. Other domains are found across the diverse formin family, including those that function in auto-regulation, inhibition, localization, depolymerization, and filament actin (F-actin) binding.

The FH1 and FH2 domains have canonically been associated with the formins' actin assembly properties and dimerization. The FH1 domain contains between one to 15 polyproline repeats that are able to bind to profilin, but with varying affinity. This domain is flexible and allows for increased actin filament elongation in the presence of profilin-actin likely by increasing the local concentration of actin monomers near the polymerizing barbed end as well as orienting the monomers for correct addition [144, 53]. The FH2 domain forms a "donut-shaped" head-to-tail dimer that is thought to stabilize an actin dimer or trimer, thereby promoting nucleation of a nascent actin filament. The dimerized FH2 domains can additionally encircle and remain associated with the barbed end of an actin filament, facilitating the addition of profilin-actin to the barbed end during elongation. For a detailed review of FH1 and FH2 domains, see [124].

Ena/VASP

Ena/VASP contains an N-terminal Ena-VASP homology 1 (EVH1) domain (Figure 1.5A). This domain binds to FP4 (FPPPP) motifs within such proteins as formin, zyxin, lamellipodin, vinculin and is important for Ena/VASP localization within cells [5, 117, 82]. The EVH1 domain is present in all Ena/VASP family members as well as distantly related Wiskott-Aldrich syndrome proteins, WASP and N-WASP, and Homer/Vesl family, though proteins from outside the Ena/VASP family recognize different motifs. Structurally the EVH1 domain is similar to pleckstrin homology (PH) and phosphotyrosine-binding (PTB) domains, though there is little sequence similarity to these domains [135, 142, 5, 46]. The C-terminal Ena/VASP Homology 2 (EVH2) domain contains the actin interacting domains.

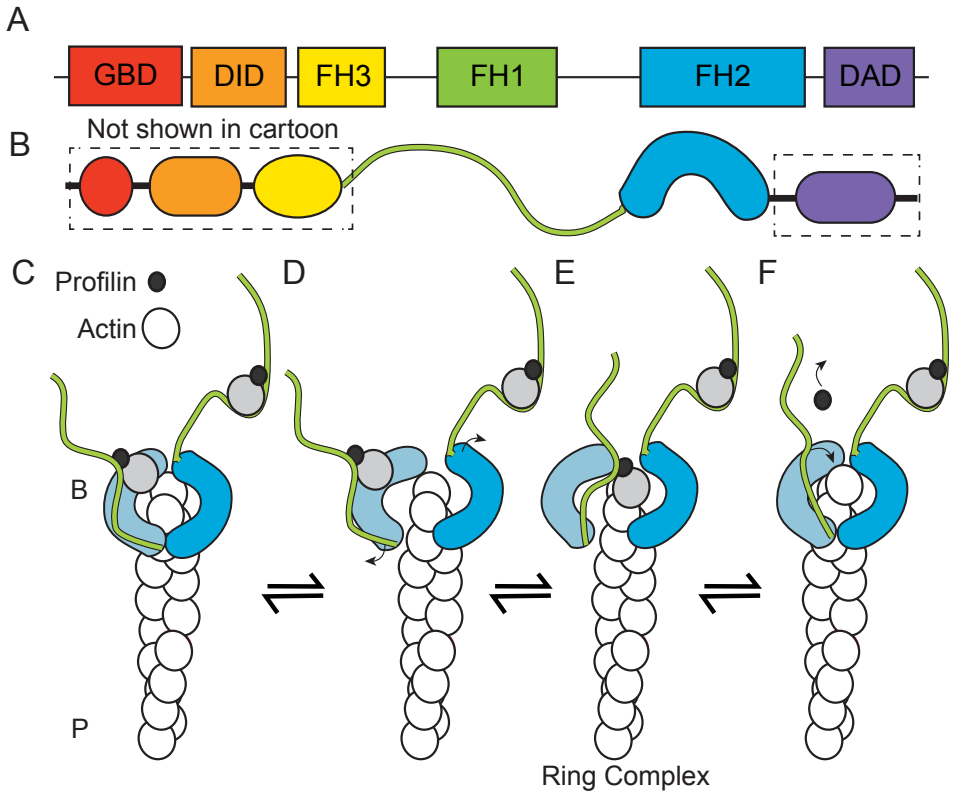

Figure 1.4: **Domain organization and stepping second mechanism of formins.** (A-B) Domain organization and structure cartoon of formin. The N-terminal GTPase binding domain (GBD, red) binds to Rho-GTPase to release autoregulation by the Diaphanous inhibitory domain (DID, orange) binding the Diaphanous autoregulatory domain (DAD, purple). Formin Homology 1 (FH1, green) binds profilin-actin and can transfer it to the barbed end that is bound by a dimerized formin homology 2 (FH2, blue) domain. Some formins also contain a formin homology 3 (FH3, yellow) domain involved in targeting. (C) Profilin-actin binds the FH1 domain and can be added to the barbed end of the filament (D) when the formin FH2 domains are in the open state. (E) A ring complex forms when the profilin actin is transferred from the FH1 domain to the FH2 barbed end. (F) Once the actin monomer is added to the filament, profilin dissociates, and then the FH2 domain translocates one step along the F-actin towards the barbed end.

The G-actin binding domain (GAB) is related to WH2 domains, which also bind actin monomers. The F-actin binding domain (FAB) is able to bind actin filaments while the C-terminal coiled-coil facilitates tetramerization. Between the EVH1 and EVH2 domain is a poly-proline region (PPR). This region can bind to profilin, a small G-actin binding protein, and other SH3 containing molecules such as Abl and Src [97, 52]. It is thought that profilin-actin can bind to both the GAB domain as well as the PPR to facilitate monomer addition to the barbed end [47]. However, Ena/VASP is able to enhance elongation of F-actin without profilin present, in contrast to formins [61, 19, 182, 21].

1.4.4 Mechanism of processive F-actin elongation

Formin

Formin increases the elongation rate of the barbed end in the presence of profilin up to 10-fold. However, the observation that formin decreases the barbed end elongation rate of F-actin in the absence of profilin suggests that the FH2 domain "gates" the addition of new actin monomers [85, 120, 176]. This gating occurs through the FH2 being in a dynamic equilibrium between a tightly bound “closed” state and loosely bound “open” state. When the FH2 domain is in the closed state there is an over-rotation of the actin filament from the native F-actin state of 167° to 180°. New actin monomers cannot be added while the FH2 domain is in the closed state due to this over-rotation because it does not contain favorable contacts for an incoming subunit at the barbed end [120].

There are two main models proposed for the formin processive elongation mechanism, stair-stepping and stepping second. Stair stepping, the first proposed model, begins with the FH2 in the closed state bound tightly to three actin subunits with four actin binding contacts. To transition to the open state the FH2 domain must dissociate two actin binding contacts and "step" towards the barbed end. While in the open state, an actin monomer can bind to the F-actin barbed end and the FH2 domain at one of the recently dissociated

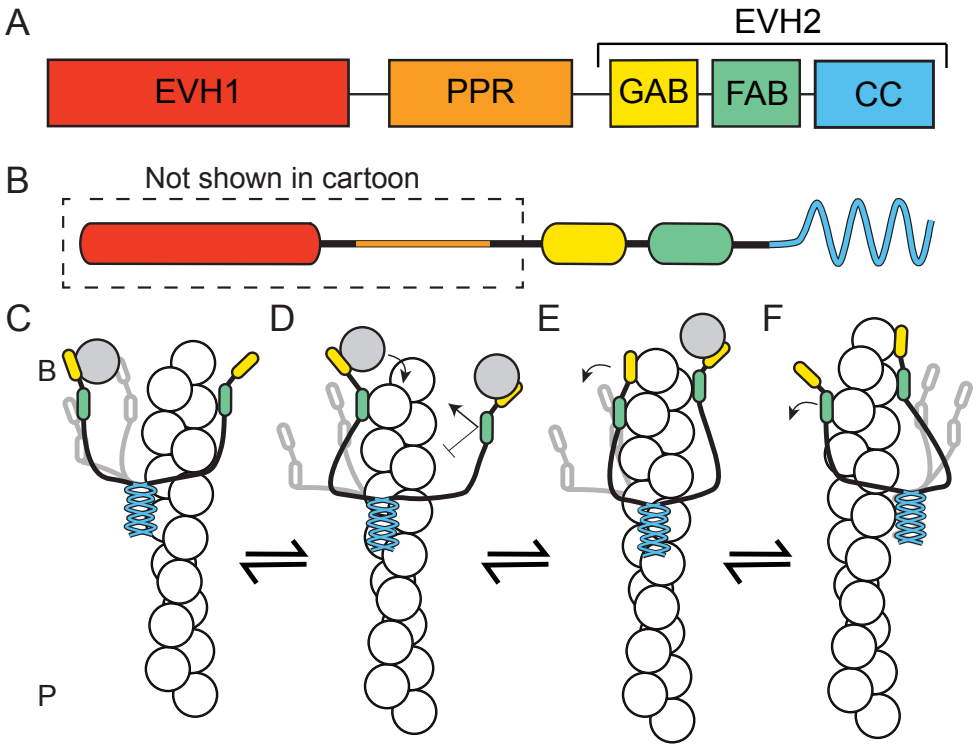

Figure 1.5: **Domain organization and mechanism of Ena/VASP.** (A-B) Ena/VASP domain organization and cartoon structure of Ena/VASP: Ena/VASP homology domain 1 (EVH1, red), polyproline region (PPR, orange), Ena/VASP homology domain 2 (EVH2) includes G-actin binding domain (GAB, yellow), F-actin binding domain (FAB, green), coiled coil region (CC, blue). (C-F) Potential mechanism of Ena/VASP. (C) First G-actin binds the GAB domain and (D) can be transfered to the barbed end. Though only one monomer may be added at a time. (E) Once a monomer is added the GAB domain dissociates. (F) An "arm" of Ena can bind to the side of the filament to prevent diffusion away from the barbed end while another monomer is added.

binding sites. With the addition of a new actin monomer, the FH2 domain returns back to the closed state. Therefore, the stair stepping mechanism predicts that the FH2 domain translocates first, followed by monomer addition [120]. Importantly, the translocation state is the most loosely bound state where formin is most likely to dissociate. Conversely in the stepping second model, the FH2 domain translocates after addition of the actin monomer. The FH2 domain again starts in the closed state with four actin-binding contacts. Within an equilibrium, the FH2 domain releases two contacts with the barbed end to transition to the open state. During the open state monomer addition can occur, but the formin cannot step forward. After an actin monomer binds to the barbed end, the formin is transiently bound to two interior subunits. The FH2 domain can then move onto the new barbed end by passing through a dissociative translocating state and return to the closed state binding the newly added actin monomer [123, 124] (Figure 1.4B). The stair-stepping model proposes that formin enters its most unstably bound (open) state independent of monomer addition, while the stepping second model predicts that formin only enters the dissociative state after monomer addition. Therefore the stepping second model predicts that formin's dissociation rate should be proportional to the number of actin monomers added whereas the stair-stepping model predicts that dissociation should be a function of time [124]. It was observed that formin dissociates as a function of the number of actin monomers added, lending support to the stepping second model [123].

Whether the FH2 domain is in a closed or open state can dictate whether additional monomers can be added to the barbed end of a filament. Modulating the open-closed state equilibrium would allow fine-tuning of formin-mediated elongation rates. Using microfluidics, recent studies have shown that formin-mediated elongation rate is sensitive to tension on the formin and filament [34, 78]. Jégou et al. showed that the formin mDia1's elongation rate is increased up to two-fold when under tension. Similarly, Courtemanche et al. have shown that the elongation rate of the formin Bni1 also increases when a pulling force is applied,

though only in the presence of profilin. Both groups suggest that a pulling force shifts the gating equilibrium of the FH2 domain towards the open state, which then causes an increase in elongation. Interestingly, when the FH1 domains are pulled straight the elongation rate still increases. This suggests that the size of the area which FH1 domains can explore to find monomers is not a major factor because reducing FH1 mobility does not cause reduced elongation rates. The sensitivity to tension opens up the possibility that within cells formins can sense mechanotransduction of forces, which could tune formin elongation rates. A recent study by Zimmermann et al. showed formin mechanosensitivity, localized in the FH1 domain in the fission yeast cytokinesis formin, Cdc12. When myosin pulls on filaments being elongated by Cdc12, it causes Cdc12 to pause the filament's elongation. Even more surprising, mDia2 does not have this mechanosensitive property with elongating filaments under myosin tension, suggesting this could be important for Cdc12's role in cytokinesis [191].

The models of formin processivity also predict that rotation must occur for formins to track the helical twist of the actin filament as it elongates filaments. However, early work suggested that this rotational tracking doesn't occur, because formins stuck on a glass coverslip buckle rather than supercoil the actin that is adhered to the glass coverslip at its pointed end. To relieve the torque, it was proposed that the formin would "slip" on the end of the F-actin [86, 156]. Recently, advances in microscopy have allowed us to gain a clearer understanding of formin rotation during elongation. Mizuno et al. found that helical rotation is an intrinsic property of formins using fluorescence polarization. They observed a periodic oscillation of a sparsely tetramethylrhodamine (TMR) labeled filament elongated by a formin (mDia1) which was biotinylated to a surface. The periodic movement of the actin label corresponded to the long-pitch helical length of F-actin, therefore the actin filament was rotating. In this experimental setup, the filament was forced to rotate rather than the formin because the formin was linked to the surface. However, *in vivo* it is more likely that formins

rotate rather than filaments during elongation, especially within crosslinked F-actin networks [107]. This work raises many new questions including whether formin binding partners would rotate with the formins and if this would affect their actin assembly properties. It also opens new possibilities for mechanisms of regulation involving formin rotation.

Ena/VASP

Ena/VASP can increase the elongation of F-actin using both actin monomers and profilin-actin [79, 61, 182]. It is thought that profilin-actin loads on the PPR and GAB domains as actin monomers bind to the GAB domain while profilin can still bind to the PPR. Profilin-actin has a 6- to 11-fold higher affinity for the PPR than profilin alone which reduces non-efficient loading of profilin over profilin-actin [47]. Furthermore, it was shown that profilin-actin has a 5-fold higher affinity for the GAB domain than actin monomers alone, suggesting that Ena/VASP would elongate actin filaments using profilin-actin over free actin monomers [29]. However, even though profilin-actin is preferred, Ena/VASP effectively elongates F-actin *in vitro* in the absence of profilin, in contrast to formins [61, 182]. After being bound to an "arm" of Ena via the PPR and GAB domains, the actin monomer or profilin-actin can then be added to the barbed end of the actin filament [29, 47, 19]. Once the actin monomer adds to the filament and undergoes a conformational change, the affinity of the GAB domain for the newly added monomer is reduced and is therefore released [29]. Hansen et al. showed using human VASP that the number of subunits added to the filament is proportional to the concentration of actin, while the dwell time is constant [61]. This is in contrast to formins that can only take a certain number of steps or equivalently add a certain number of monomers on average before dissociating. This presents an interesting extrapolation *in vivo* where actin concentrations are higher and suggests that VASP could be more effective in the presence of these higher concentrations.

Ena/VASP was originally thought to be processive only when clustered on beads [18],

but was later observed to processively elongate actin filaments as single molecules in solution [61, 182, 19]. It is not well understood how Ena/VASP is functioning in cells during filopodia initiation and maintenance. Ena/VASP localizes in a cluster at the tips of filopodia, so the current model is that Ena/VASP is clustering at the plasma membrane in cells [168, 96]. One open question about Ena/VASP's mechanism is whether it tracks the helical pitch of F-actin as it elongates, similar to the formin mDia1. Since Ena/VASP is thought to work in clusters and on bundled filaments in filopodia, our hypothesis is that instead of rotating along F-actin's helical pitch, Ena/VASP rather tip-tracks the barbed end of the filament. Furthermore, since Ena/VASP is a tetramer, understanding if all arms function in equal roles during filament elongation is also another open mechanistic question about Ena/VASP.

1.4.5 Behaviors

Formin

The main functions of formins include F-actin nucleation, processive elongation, and actin filament crosslinking [132]. However, there are multiple different formins in cells that are tuned for diverse processes. Different formins balance these main functions as well as some additional properties that allow them to carry out their unique processes. For example, there are three formin isoforms in fission yeast (Cdc12, Fus1, and For3) that are responsible for distinct actin networks. Each of these formins have varied nucleation rates, processivity, elongation enhancement, and ability to bundle [150]. Cdc12 and Fus1 can efficiently nucleate filaments and are 70-fold better nucleators than For3. Cdc12 and For3 are both highly processive and elongate filaments at a moderate rate, while Fus1 is 10-fold less processive and only elongates filaments at half the rate of Cdc12 in the presence of profilin. Where Cdc12 adds 27 times more monomers than Fus1 on an average processive run, Fus1 is the only fission yeast formin that can bundle filaments. These varying behaviors of the different formin isoforms found within the same organism raises the question of how these formins

are tuned to their unique role within the cell. Furthermore, how do proteins differentially interact with these formins, and how can that contribute to or change these properties?

The actin assembly activity of formins can also be tuned to the environment in the cell. Higashida et al. have shown that mDia1 rapidly increases processive F-actin assembly with the release of cell tension using sequential fluorescence decay after photoactivation (s-FDAPplus) to visualize the nucleation and elongation activity of mDia1 [71]. A recent study from Zimmermann et al. showed that fission yeast Cdc12 is mechanoregulated by myosin. Cdc12-mediated elongation of F-actin is inhibited while the filament is under myosin produced tension [191]. The mechanosensitivity plays an important role for fission yeast cytokinesis and was predicted by mathematical modeling of the process [176]. How actin and binding proteins are able to sense cell stress and forces is not very well understood. It will be important to look into what protein(s) are initially sensing the forces on the cell and how this is translated to modifying actin networks.

Previous formin research has often focused on the two characteristic FH1 and FH2 domains to understand their actin assembly properties. However, formins contain other domains that vary across the formin family, including those that function in auto-regulation, inhibition, depolymerization, and actin filament binding. More recent studies have shown that the C-terminal tails of different formins play an important role in their actin assembly and nucleation properties. Cappuccino (Capu) [180], FMNL3 [67], and mDia1 [54] can bind G-actin monomers with their C-terminal tails to help the FH2 domains nucleate F-actin filaments. Furthermore, Vizcarra et al. suggest that Capu's C-terminal tail also enhances elongation by forming nonspecific electrostatic interactions with F-actin that can assist in stabilizing the open-state FH2 dimer binding to the actin filament. Additionally, INF2 has domains present in the C-terminal tail that can bind and sequester actin monomers [30]. However, even though many formins depend on their C-terminal tail for their specific function, they do not all function equally. Replacing the C-terminal tail of Capu with the

C-terminal tail of DRF formins changed its nucleation and processivity properties [180]. The growing evidences of the role of the C-terminal tail in tuning of nucleation and processivity opens up the possibility of differential regulation and function of formin isoforms present in the same cell. Whether these C-terminal interactions have important contributions to formin function and regulation overriding that of the FH1FH2 is unclear.

Beyond binding to actin, Capu's C-terminal tail along with specific residues of the FH2 have been shown to promote high affinity microtubule binding, though this occurs separately from Capu's actin assembly properties [145]. Actin and microtubule dynamics are linked within the cell and the details of this relationship remain a current question in the field. Recently it has been shown that formins mDia1, mDia2, and mDia3 are involved in ErbB2-dependent microtubule capture through their FH2 domains [37]. Additionally, TIRFM was used to visualize the interaction between microtubule plus end localizing CLIP-170 and formin mDia1, which stimulates actin growth from microtubule plus ends [70]. This opens up many new questions about how various formins could be regulating actin-microtubule crosstalk.

Ena/VASP

Ena/VASP's main function is an actin elongation factor. Studies of different Ena/VASP homologs have observed differences in the rate of actin elongation and time that Ena/VASP is bound to the barbed end [18, 19, 61, 182]. These properties are thought to be a tuning of the affinity of the GAB domain for actin, though differences in the FAB affinity could also play a role. Interestingly, mammalian paralogues can form heterotetramers through conservation of the coiled-coil domain [143]. However, it was observed that the paralogues did not equally associate *in vivo*. This opens up interesting questions about how different paralogues are regulated and how mixed heterotetramers affect processes in cells.

While Ena/VASP is associated with barbed ends, it can compete with capping protein.

However, once capping protein binds to the barbed end Ena/VASP cannot uncap the filament [2, 9, 182, 7]. This function is thought to be important in cells as Ena/VASP is localized to the leading edge of motile cells, which is also where capping protein localizes. Especially within the convergent elongation model for filopodia formation, the competition for capping protein allows some of the short filaments within the lamellipodium to be protected and elongated, facilitating filopodia initiation [168]. In addition to barbed end binding, Ena/VASP has been shown to bundle filaments, especially at higher concentrations *in vitro* [3, 7]. However, it is not known how important this function is in cells since Ena/VASP is seen to localize to filopodia tips and not the shaft as fascin does [168, 96]. Another function of Ena/VASP observed *in vitro* is nucleation. Ena/VASP has been shown to nucleate filaments in bulk assays, yet *in vivo* experiments have not shown that this is a physiological function [9]. Both of these functions have been shown to be salt dependent, so one possibility is that at physiological conditions these activities are very weak.

1.4.6 Regulation

Formin

It is well established that DRF formins are autoregulated by interaction of the DID-DAD domains, which can be relieved by Rho-GTPase binding. Recently, a structure has been solved of full-length mDia1 that confirms that the DID-CC domain sterically occludes where actin binds on FH2 during nucleation [102]. Furthermore, it was shown that the formin does not quickly return to its autoinhibited state during processive elongation, which opens further questions about how, or if, formins are stopped once a processive run has been initiated. Other insights into autoregulation have been highlighted by the structure of Rho-GTPase Cdc42 with formins FMNL1 and FMNL2. The structure along with biochemical data suggests that specific interactions between formin FMNL2 and the Rho-GTPase insert helix are at play when determining specificity of Rho-GTPases to release formin autoinhibition [94].

Beyond autoregulation, it has been shown that PIP2 can inhibit mDia1 by binding to its C-terminal tail. Phospholipids can recruit mDia1 to the membrane [175], which then causes an accumulation of PIP2 so phospholipids are able to regulate formin localization to the membrane and inactivation [140].

Recent studies focusing on formin binding partners has opened up even further opportunities for regulation. The formin mDia1 can interact with adenomatous polyposis coli (APC) through its tail, forming a complex that acts as a potent nucleator [17, 119]. Likewise, nucleation-promoting factor Bud6 is known to enhance the nucleation of formin Bni1 [111]. Capu and closely related FMN2 have been shown to interact with the nucleating protein Spire with their C-terminal domains [110, 109, 125, 181]. Recent studies have visualized a "decision complex" of capping protein and formins mDia1 and FMNL2. Previous genetic and biochemical work suggested that formins and capping protein were entirely antagonistic [87], yet single-molecule TIRF microscopy has shown that both of these proteins can bind simultaneously to a barbed end for a set amount of time before one gains sole control [14, 155]. Further questions remain about how different formins are regulated to act at the precise time and location within a cell. Exploring the interaction between a formin and different protein binding partners and macromolecules can open up new possibilities for regulation.

Ena/VASP

Ena/VASP proteins were originally identified as substrates for different kinases [58, 51]. Additional studies have shown that vertebrate Ena/VASPs are substrates for cAMP- and cGMP-induced protein kinases with serine/threonine phosphorylation sites in both the PPR and EVH1 domain, with the latter being the preferred site [52, 95, 63, 24]. Phosphorylation at these sites have shown decreased Ena/VASP activity both *in vitro* and *in vivo* [101, 74, 11, 24]. Beyond regulation by phosphorylation, different isoforms of profilin can affect the activity of Ena/VASP [61, 112]. Different mammalian Ena/VASP proteins are able to utilize

specific isoforms of profilin to increase their activity. This specificity, along with the ability of mammalian paralogues to form mixed tetramers, could result in a tunable system based on the Ena/VASP monomers and profilin isoform spatial-temporal localization in cells.

1.4.7 Ena/VASP and formin interaction

Although their biochemical mechanisms and rate constants are quite different, Ena/VASP and formins both stimulate the assembly of long, straight filaments within cells in two ways: both families 1) protect actin filaments from capping protein by processive association with the barbed end and 2) increase elongation rate of filaments during this processive association. In line with these activities, both protein families induce the assembly of filopodia [12, 73] and localize to zones of actin assembly at distal tips of these structures. However, Ena/VASPs and formins appear to drive distinct types of filopodia [8, 12, 118, 73]. In general, formin-induced filopodia are much longer, and the actin is not highly connected with other actin networks. Conversely, Ena/VASP-induced filopodia are shorter and deeply rooted in lamellar networks. During dorsal closure in fly embryos, motile epithelial cells displayed filopodia more characteristic of Ena, while underlying non-motile amnioserosal cells displayed filopodia more characteristic of formin Dia [118]. However, both proteins played roles in both tissue types. It is possible that in each tissue type, activities of each elongation factor are modulated accordingly to drive different functions. For example, it has been suggested that Ena/VASP may work primarily in reorganizing preexisting networks in the leading edge of motile cells through a convergent elongation-type mechanism [168]. Formin, which can also nucleate actin filaments, may not require a preexisting lamellipodial network and assemble its own filaments for filopodia de novo [44], and therefore may function more in non-motile cells.

However, Ena/VASPs and formins directly bind to each other and colocalize at the distal tips of some filopodia. These observations led different groups to question why these proteins with generally similar assembly properties would colocalize in filopodia and how their direct

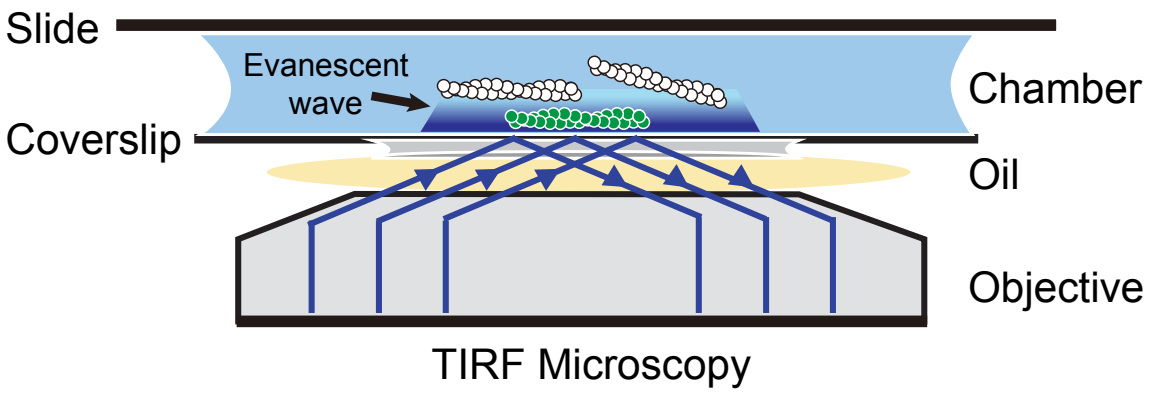

Figure 1.6: **Diagram of Total Internal Reflection Fluorescence Microscopy (TIRFM)** Total Internal Reflection Fluroesence Microscopy (TIRFM) consists of a fluorescent sample being placed in a flow chamber between a coverslip and glass slide. The flow chamber is placed on an oil objective and visualized using a laser at a critical angle that allows for total reflection within the coverslip, forming an evanescent wave that only excites fluorophores within a few hundred nanometers of the coverslip.

binding might regulate each other's activity. Ena/VASP's EVH1 domain mediates this interaction either through formin's FH1 [12] and/or FH2 domain [8, 148]. Ena's EVH1 domain binds to the fly formin Diaphanous with a Kd of 13 μM, similar to the low affinity EVH1-FPPP4 interaction that the EVH1 uses to bind a large number of other proteins [135]. This interaction may negatively regulate formin by interfering with the core assembly machinery.

Recent data shows that in addition to Ena/VASP and formin driving distinct filopodial morphology and dynamics, Ena/VASP is necessary for proper function in some cells. Bilancia et al., found that Ena could negatively regulate the formin Diaphanous both in vivo and in vitro [12]. Work from the Gertler lab extended these ideas by showing the physiological consequences of driving filopodia formation with either formin or Ena/VASP [7]. This study found that although formins can generate filopodia, Ena/VASP is necessary for initiating focal contacts and integrin-dependent signaling. It is not currently clear if these dynamics play out in all cell types, and will be an important area of future research. In addition, the effect of formin on Ena/VASP activity, if any, is also an open question in the field.

1.5 Single-molecule total internal reflection microscopy (TIRFM)

The main experimental set-up that we have used to study actin binding proteins and their activity and dynamics is total internal reflection microscopy (TIRFM). This microscopy uses a special objective that allows for a low angle of incidence of the incoming laser [48]. The laser is then internally reflected within the glass coverslip, causing an exponentially decaying evanescent wave that can illuminate fluorophores within 150 μm. By only illuminating this small area, we get much better signal to noise by reduction of background fluorescence beyond the 150 μm. TIRFM is especially beneficial for observing single molecules due to the reduced background. Single-molecule TIRFM allows us to measure single events at low concentrations of our protein of interest. Specifically for studying the actin cytoskeleton [192], we are able to watch filaments assemble in real time and monitor how actin binding proteins interact with F-actin and their dynamics. Compared to bulk actin assays such as fluorescent pyrene assays, we are able to distinguish polymerization, nucleation, and measure actual elongation rates of the filaments. We are also able to localize where proteins are interacting along the actin filament as well as with other actin binding proteins. One of the biggest advantages of visualizing actin binding proteins with TIRFM is the ability to measure rates of both binding to and dissociation from the F-actin. This kinetic information can inform the molecular mechanisms of actin binding proteins.

CHAPTER 2

ENA/VASP PROCESSIVE ELONGATION IS MODULATED BY AVIDITY ON ACTIN FILAMENTS BUNDLED BY THE FILOPODIA CROSSLINKER FASCIN

2.1 Abstract[1]

Ena/VASP tetramers are processive actin elongation factors that localize to diverse F-actin networks composed of filaments bundled by different crosslinking proteins, such as filopodia (fascin), lamellipodia (fimbrin), and stress fibers (α-actinin). Previously, we found that *Drosophila* Ena takes ~3-fold longer processive runs on trailing barbed ends of fascin-bundled actin filaments. Here, we used single-molecule TIRFM and developed a kinetic model to further dissect Ena/VASP's processive mechanism on bundled filaments. We discovered that Ena's enhanced processivity on trailing barbed ends is specific to fascin bundles, with no enhancement on fimbrin or α-actinin bundles. Notably, Ena/VASP's processive run length increases with the number of both fascin-bundled filaments and Ena "arms", revealing avidity facilitates enhanced processivity. Moreover, Ena tetramers form more filopodia than mutant dimer and trimers in *Drosophila* culture cells. Finally, enhanced processivity on trailing barbed ends of fascin-bundled filaments is an evolutionarily conserved property of Ena/VASP homologs human VASP and *C. elegans* UNC-34. These results demonstrate that Ena tetramers are tailored for enhanced processivity on fascin bundles and avidity of multiple arms associating with multiple filaments is critical for this process. Furthermore, we discovered a novel regulatory process whereby bundle size and bundling protein specificity control activities of a processive assembly factor.

1. Citation for chapter: Alyssa J. Harker, Harshwardhan H. Katkar, Tamara C. Bidone, Fikret Aydin, Gregory A. Voth, Derek A. Applewhite, David R. Kovar. Ena/VASP processive elongation is modulated by avidity on actin filaments bundled by the filopodia crosslinker fascin. *In revision at Molecular Biology of the Cell.*

2.2 Introduction

Many important cellular functions depend on formation of actin cytoskeleton networks at the correct time and location with specific architectures and dynamics [134, 25]. For example, filopodia are filamentous actin (F-actin)-rich finger-like protrusions that elongate from the lamellipodium, a dense, branched F-actin network kept short by capping protein [133] at the cell periphery. Filopodia are important for cell motility and environment sensing. Filopodial actin filaments are assembled by actin elongation factors such as formins and Enabled/vasodilator-stimulated phosphoprotein (Ena/VASP) [103]. During filopodia initiation, Ena/VASP localizes to the edge of the lamellipodium, where it competes with capping protein for barbed ends [10, 168, 7, 2, 9, 182] and then facilitates generation of long, straight filaments by remaining processively associated with barbed ends and increasing their elongation rate 2- to 7-fold [18, 19, 122, 61, 182, 21]. The 10-30 filaments in filopodia are bundled primarily by fascin, a globular crosslinking protein containing β-trefoil domains [177, 76, 105]. Fascin bundles are composed of parallel filaments with narrow spacing, between 8-10 nm [26, 43, 76, 187]. Ena/VASP continues to localize to the tips of mature filopodia, where fascin-bundled filaments ultimately are the same length [45, 55], presumably assuring uniform thickness of filopodia required for protrusive force [168, 182].

Ena/VASP is a multidomain homotetramer with homologs in all metazoan cells [151]. A few Ena/VASP homologs have been biochemically characterized, including human VASP [3, 29, 18, 122, 61], *Drosophila* Enabled [182], and *Dictyostelium* VASP [18]. Ena/VASP proteins contain two conserved Ena/VASP homology domains, EVH1 and EVH2 (Figure 2.1A). The N-terminus EVH1 domain is important for cellular localization and binds to proteins with FPPPP (FP4) repeats, such as lamellipodin, zyxin, and formin [4, 12]. The C-terminus EVH2 domain consists of three smaller subdomains: G-actin binding domain (GAB) [3, 47], F-actin binding domain (FAB) [40], and a C-terminal coiled-coil tetramerization domain [3, 92]. Between the EVH1 and EVH2 domains there is a poly-proline rich region that binds

profilin as well as SH3 domains [47, 61].

In addition to the leading edge and tips of filopodia, Ena/VASP proteins also localize to focal adhesions and stress fibers [141, 20], which are composed of filaments crosslinked by CH domain superfamily crosslinkers, fimbrin/plastin and α-actinin. Fimbrin also localizes to the lamellipodia and base of filopodia, and it bundles both parallel and antiparallel filaments with narrow spacing (10-12 nm), similar to fascin [60]. In comparison, α-actinin bundles filaments of mixed polarity with much wider spacing (30-36 nm) [159].

We previously discovered that for F-actin bundles made by human fascin, *Drosophila* Enabled (Ena) remains processively associated with trailing barbed ends (shorter filaments) ~3-fold longer than leading barbed ends (longest filament) (Figure 2.1B) [182]. However, the underlying molecular mechanisms that facilitate Ena's enhanced processivity on bundled filaments remain unclear. We therefore used a combination of in vitro reconstitution with single-molecule multi-color total internal reflection fluorescence microscopy (TIRFM), kinetic modeling, and analysis of *Drosophila* culture cells to characterize the dynamics and function of processive elongation of single and bundled filaments by multiple Ena/VASP homologs including Ena, human VASP, and *C. elegans* UNC-34. Together, our experiments and simulations inform our mechanistic understanding of Ena/VASP on single and bundled filaments, demonstrate that avidity of multiple filaments within fascin bundles and multiple Ena arms leads to increased processivity of tetrameric Ena on trailing barbed ends, and reveal a novel regulatory process whereby the particular F-actin bundling protein matters for Ena/VASP processivity.

2.3 Results

2.3.1 Ena is more processive on trailing barbed ends of both human and fly fascin (Singed) bundles

To understand what features are important for *Drosophila* Ena's enhanced processivity on trailing barbed ends within human fascin bundles (Figure 2.1B) [182], we first tested if a different fascin homolog also facilitates enhanced residence times. We used two-color TIRFM to directly visualize the assembly of 1.5 μM Mg-ATP-actin monomers (15% Oregon green-labeled) with 15 pM fluorescently labeled SNAP(549)-EnaΔL (referred to as Ena) (Figure 2.1A) and human fascin or fly fascin, Singed. TIRFM allows direct visualization of individual Ena molecule dynamics on single and bundled actin filament barbed ends. Ena's processive run lengths were measured for leading and single filament barbed ends (collectively referred to as leading) as well as trailing barbed ends (Figure 2.1C-D). Kaplan-Meier survival curves were calculated from individual Ena processive runs (Figure 2.1E-F), revealing that Ena remains associated with trailing barbed ends (τ_{fascin} = 23.7 s, τ_{Singed} = 28.1 s) 3-fold longer than leading barbed ends (τ_{fascin} = 8.4 s, τ_{Singed} = 10.1 s) for both human fascin and fly Singed (Figure 2.1I, Table 2.1), consistent with our previous findings [182]. Therefore, enhancement of Ena's processive elongation on trailing barbed ends is not specific to a particular fascin homolog.

2.3.2 Ena's residence time is not enhanced on trailing barbed ends of fimbrin and α-actinin bundles

To determine if diverse bundle architectures are similarly sufficient to enhance Ena's processivity on trailing barbed ends, we tested the effect of bundling proteins with distinct properties (fimbrin and α-actinin, see introduction). First, we measured elongation rates of Ena-bound leading and trailing barbed ends of filaments bundled by human fascin, fly fascin

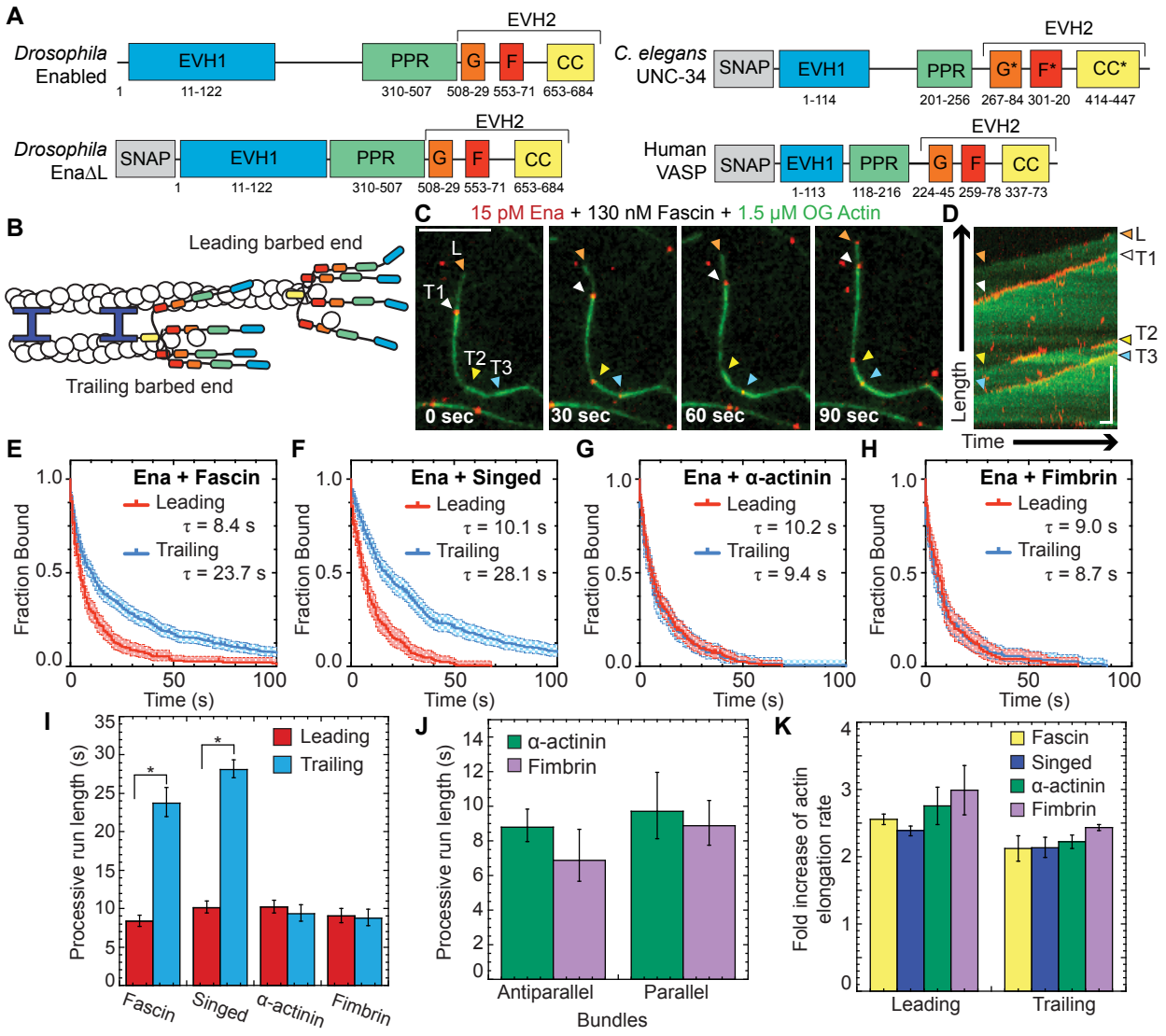

Figure 2.1: **Ena has enhanced processivity on F-actin bundles formed specifically by fascin.** (A) Ena/VASP domain organization and constructs used for Ena, UNC-34, and VASP: Self-labeling tag (SNAP), Ena/VASP homology domain 1 (EVH1), polyproline region (PPR), Ena/VASP homology domain 2 (EVH2) includes G-actin binding domain (G), F-actin binding domain (F), coiled coil region (CC). *Putative domain. Two-color TIRFM visualization of 1.5 μM Mg-ATP-actin (15% Oregon green-actin) with 15 pM SNAP(549)-EnaΔL and unlabeled 130 nM human fascin, 250 nM fly fascin Singed, 125 nM α-actinin, or 100 nM fimbrin. (B) Cartoon Ena/VASPs bound to leading and trailing barbed ends in a fascin bundle. (C and D) Representative experiment of OG-actin with SNAP(549)-EnaΔL and fascin. Arrows indicate leading (orange), 1st trailing (white), 2nd trailing (yellow) and 3rd trailing (blue) barbed ends. (C) Merged timelapse micrographs. Scale bar, 5 μm. (D) Merged kymograph of filament length (scale bar, 5 μm) over time (time bar, 10 s).

Figure 2.1: (continued) (E-H) Kaplan-Meier curves representing average processive run lengths (τ) for Ena with (E) fascin, (F) Singed, (G) α-actinin, or (H) fimbrin on leading (red) and trailing (blue) barbed ends. Error bars, 95% CI. n $\geq$ 127. (I) Average processive run lengths for leading (red) and trailing (blue) barbed ends shown in E-H for 2-filament bundles with fascin, Singed, α-actinin, or fimbrin. P values (*<0.0001). Error bars, 95% CI. (J) Average processive run lengths for antiparallel and parallel 2-filament α-actinin (green) or fimbrin (purple) bundles. Error bars, 95% CI. n $\geq$ 64. (K) Fold increase of barbed end elongation rates of Ena on fascin (yellow), Singed (blue), α-actinin (green), or fimbrin (purple) bundled filaments. Error bars, SEM. n $\geq$ 5 barbed ends from at least 2 movies.

Singed, α-actinin, or fimbrin. Two-color TIRFM visualization of control and Ena-bound barbed ends revealed a similar fold increase in Ena-mediated actin elongation for leading (~2.2- to 3-fold) and trailing (~2- to 2.5-fold) barbed ends with all four bundling proteins (Figures 2.1K, 2.2, Tables 2.2, 2.3). Therefore, Ena's barbed end elongation enhancement is bundling protein independent.

Conversely, Ena's enhanced processivity on trailing barbed ends is specific to fascin bundles. The average processive run length on leading barbed ends with all four bundling proteins is similar, ~10 sec (Figure 2.1I). However, there is no enhancement of Ena's average residence time on trailing barbed ends of α-actinin (τ = 9.4 s) or fimbrin (τ = 8.7 s) bundles (Figure 2.1G-I, Table 2.1). Therefore, F-actin bundling proteins are not universally sufficient to enhance Ena's processivity on trailing barbed ends. Although fascin exclusively forms parallel bundles, α-actinin and fimbrin form bundles composed of filaments with mixed polarities. We therefore compared Ena's residence time on trailing barbed ends in parallel and antiparallel two-filament bundles. For both fimbrin and α-actinin bundles, the average residence time for trailing parallel and antiparallel barbed ends is equivalent; thus, neither bundler enhances Ena's processivity (Figures 2.1J, Table 2.4). Fimbrin can bind to single filaments [160], so to control for potential hindrance of Ena/VASP association with F-actin by fimbrin binding to single filaments we tested a low concentration of fimbrin that could still bundle (Figure 2.3). We found that even with low concentrations of fimbrin that there was no enhancement of Ena processivity. Therefore, neither "fascin-like" filament spacing

Ena/VASP	Bundling Protein	Leading[a] (s)	Trailing[a] (s)	L/T p-value[b]
Ena Tetramer	Fascin	8.4 [7.7,9.1] (254)	23.7 [22.0,25.8] (511)	< 0.0001
Ena Tetramer	Singed	10.1 [9.4,11.0] (184)	28.1 [27.0,29.4] (328)	< 0.0001
Ena Tetramer	α-actinin	10.2 [9.5,11.1] (284)	9.4 [8.4,10.5] (176)	0.64
Ena Tetramer	Fimbrin	9.0 [8.2,10.0] (127)	8.7 [7.7,10.0] (183)	0.91
VASP Tetramer	Fascin	1.2 [0.9,1.6] (213)	3.3 [3.1,3.5] (348)	< 0.0001
VASP Tetramer	Singed	1.0 [0.7,1.5] (187)	3.5 [3.2,3.8] (463)	< 0.0001
UNC-34 Tetramer	Fascin	1.7 [1.4,2.2] (82)	3.7 [3.4,4.0] (266)	< 0.0001
Ena Trimer	Fascin	6.2 [5.6,6.9] (322)	9.8 [9.2,10.4] (299)	< 0.0001
Ena Dimer	Fascin	1.3 [1.0,1.7] (376)	1.8 [1.5,2.4] (418)	0.01

Table 2.1: **Comparison of Ena/VASP proteins' residence time on leading and trailing barbed ends.**
[a] Values of average processive lifetime (s) [95%CI] (n) where n is the number of Ena/VASP binding events measured in at least three movies for Leading or Trailing barbed ends.
[b] Log Rank p-value comparing Leading and Trailing average processive lifetime.

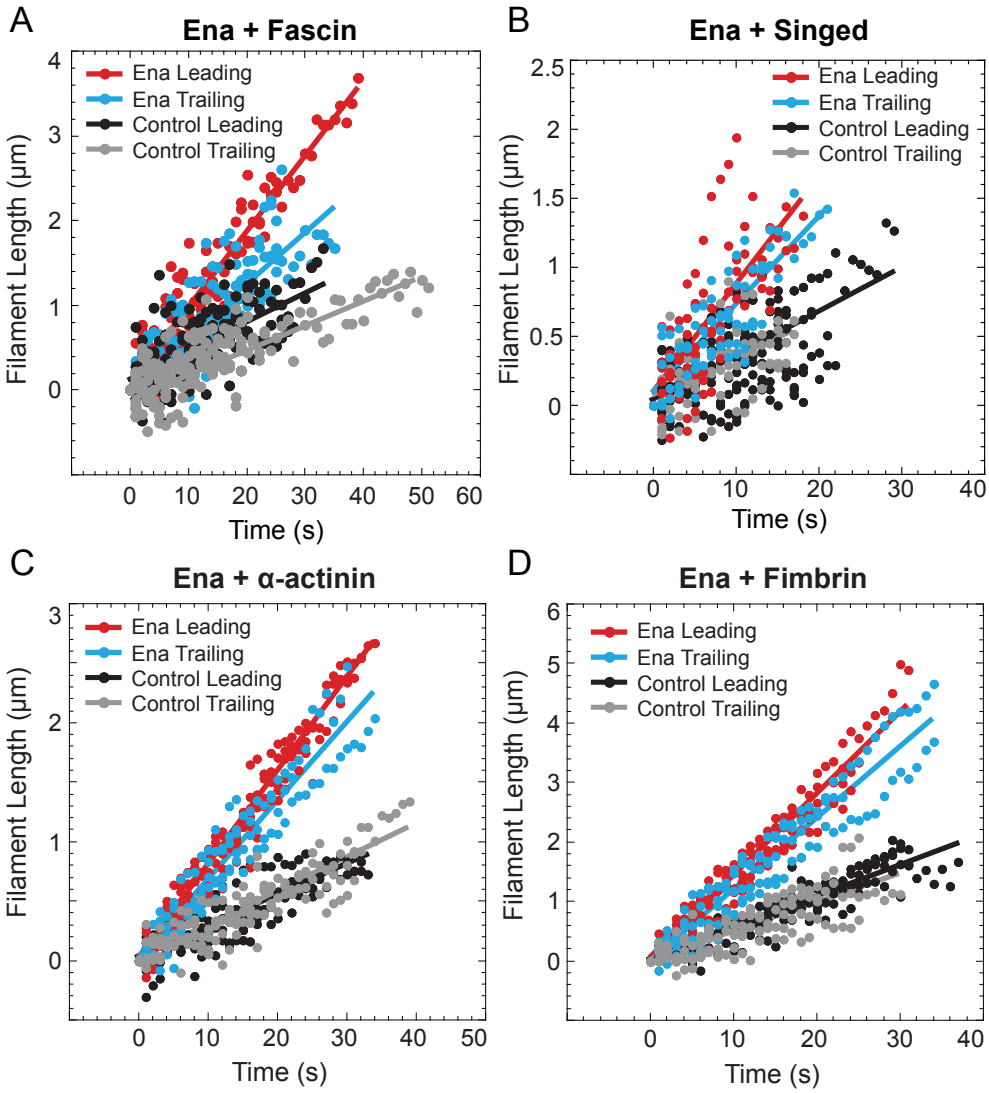

Figure 2.2: **Bulk elongation show average elongation rates of Ena-bound and control filaments.** Example scatter plots fit with a linear equation for the length of control filaments or Ena-bound filaments over time in the presence of 15 pM SNAP(549)-EnaΔL with either (A) 130 nM human fascin, (B) 250 nM fly fascin Singed, (C) 125 nM α-actinin, or (D) 100 nM fimbrin. A linear fit gives the bulk elongation rate for a single movie. Average elongation rates are given in Table 2.2.

(8-10 nm) nor polarity (parallel) of actin filaments within bundles is sufficient to facilitate increased processivity on trailing barbed ends. Given that Ena's ~3-fold enhancement of processivity on trailing barbed ends is specific to fascin, different bundling proteins could regulate Ena's specific activity for different F-actin networks.

Ena/ VASP	Bundling Protein	Bound Leading[a] (sub/s)	Bound Trailing[a] (sub/s)	Control Leading[b] (sub/s)	Control Trailing[b] (sub/s)	Fold Change Leading[c]	Fold Change Trailing[c]	n[d]
Ena Tetramer	Fascin	25.6 ±0.8	16.8 ±1.1	10.0 ±1.0	7.9 ±0.2	2.56 ±0.08	2.1 ±0.2	2
Ena Tetramer	Singed	22.4 ±0.6	20.0 ±0.1	10.0 ±0.9	10.0 ±0.2	2.24 ±0.06	2.00 ±0.02	2
Ena Tetramer	α-actinin	27.6 ±2.7	25.43 ±0.03	10.0 ±0.2	11.5 ±0.5	2.8 ±0.3	2.2 ±0.1	2
Ena Tetramer	Fimbrin	29.9 ±3.7	21.9 ±1.0	10.0 ±0.1	9.0 ±0.3	3.0 ±0.4	2.43 ±0.04	2
VASP Tetramer	Fascin	23.6 ±3.9	18.8 ±4.6	10.0 ±1.4	8.0 ±0.5	2.4 ±0.4	2.4 ±0.7	2
UNC-34 Tetramer	Fascin	27.2 ±2.3	20.2 ±3.4	10.0 ±1.8	8.0 ±1.5	2.7 ±0.2	2.7 ±0.9	2
Ena Trimer	Fascin	17.4 ±1.3	14.1 ±0.8	10.0 ±0.2	8.70 ±0.05	1.7 ±0.1	1.6 ±0.1	2
Ena Dimer	Fascin	14.5 ±0.2	14.1 ±2.2	10.0 ±0.2	9.8 ±0.9	1.45 ±0.02	1.5 ±0.4	2

Table 2.2: **Comparison of actin elongation rates with and without (control) Ena/VASP bound.**
[a] Normalized actin elongation rate (sub/s) of Ena/VASP bound Leading or Trailing barbed ends to Control Leading.
[b] Normalized actin elongation rate (sub/s) of Ena/VASP free Leading or Trailing barbed ends to Control Leading.
[c] Fold change in actin elongation rate of Ena/VASP bound over Ena/VASP free Leading or Trailing barbed ends.
[d] n is the number of movies analyzed. Each movie had at least five filaments with at least 50 length measurements for each movie.

Leading/Trailing[a]	Fascin	Singed	α-actinin	Fimbrin
Fascin	1 / 1	0.3 / 1	0.6 / 0.7	0.4 / 0.3
Singed	0.3 / 1	1 / 1	0.4 / 0.7	0.3 / 0.3
α-actinin	0.6 / 0.7	0.4 / 0.7	1 / 1	0.7 / 0.3
Fimbrin	0.4 / 0.3	0.3 / 0.3	0.7 / 0.3	1 / 1

Table 2.3: **p-values for comparisons of fold change in actin elongation rate with Ena on different bundling proteins for both leading and trailing filaments.**
[a] p-values from student's two-tailed t-test with unequal variance between fold change of actin elongation rates when Ena is bound to the Leading or Trailing barbed end.

Ena/VASP	Bundling Protein	Parallel[a] (s)	Antiparallel[a] (s)	A/P p-value[b]
Ena Tetramer	Fascin	16.8 [14.3,19.7] (201)	N/A	N/A
Ena Tetramer	Singed	21.7 [20.4,23.3] (155)	N/A	N/A
Ena Tetramer	α-actinin	9.7 [8.1,12.0] (77)	8.8 [8.0,9.8] (90)	0.52
Ena Tetramer	Fimbrin	8.9 [7.7,10.4] (64)	6.9 [5.7,8.7] (106)	0.53

Table 2.4: **Comparison of Ena/VASP proteins' residence time on parallel and antiparallel bundled F-actin.**
[a] Values of average processive lifetime (s) [95%CI] (n) where n is the number of Ena/VASP binding events measured in at least three movies for parallel or antiparallel barbed ends on 2-filament bundles. Fascin results are equal to the values in 2 filaments because fascin only makes parallel bundles.
[b] Log Rank p-value comparing average processive lifetime trailing barbed ends in parallel and antiparallel bundles.

2.3.3 Ena's processive run length increases with bundle size

Filopodia are composed of ~10-30 actin filaments bundled by fascin [168, 45], suggesting an avidity mechanism where enhanced processivity depends on Ena simultaneously associating with a barbed end and sides of neighboring filaments. To test whether the number of filaments in a fascin bundle positively correlates with processive run length, we determined the dependence of Ena's enhanced processivity on fascin bundle size (Figure 2.4A). Average run lengths on trailing barbed ends (Figure 2.1E-F) was thereby parsed into 2-filament bundles or 3- or more filament bundles for both human and fly fascin (Figure 2.4B-D, Table 2.1). Ena's average residence time on trailing barbed ends of a 2-filament bundle (τ_{fascin} = 16.8 s, τ_{Singed} = 21.7 s) is ~2-fold longer than on single filament barbed ends (τ_{fascin} = 8.9 s,

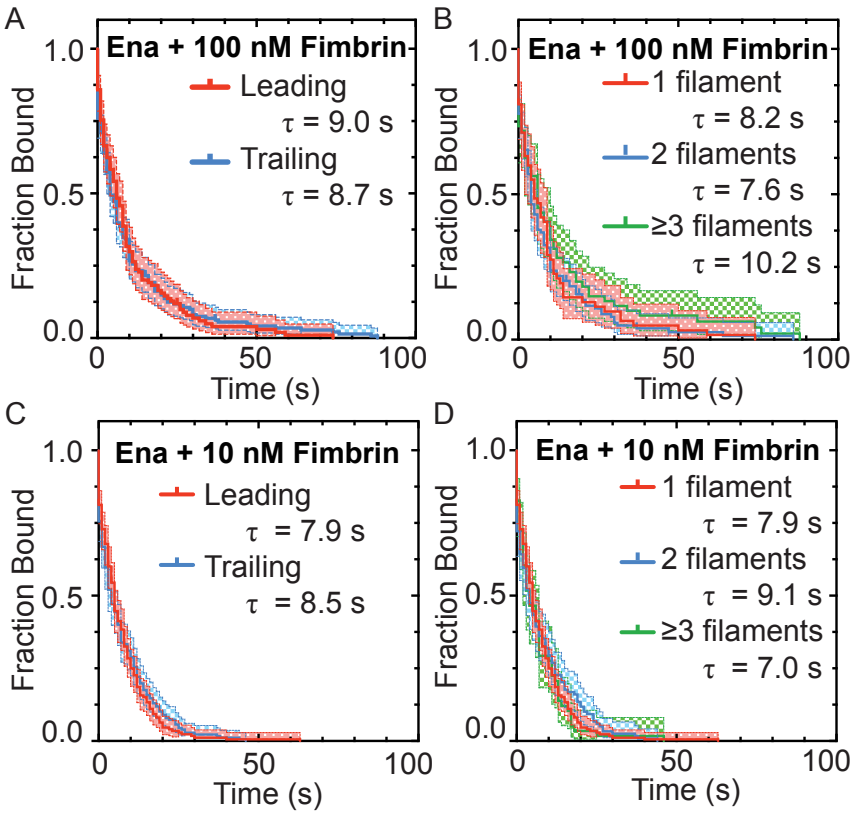

Figure 2.3: **Low concentrations of fimbrin also do not enhance Ena processivity.** Kaplan-Meier curves representing average processive run lengths (τ) for Ena with (A-B) 100 nM fimbrin or (C-D) 10 nM fimbrin on (A,C) leading (red) and trailing (blue) barbed ends or further separated into (B,D) single filaments (red), or bundles with 2 (blue) and ≥3 (green) filaments. Error bars, 95% CI. n ≥ 58. Kaplan-Meier curve in (A) also shown in Figure 2.1H.

τ_{Singed} = 10.0 s). Furthermore, there is an additional ~1.5-fold increase in processivity when Ena is bound to trailing barbed ends of 3- or more filament bundles (τ_{fascin} = 26.0 s, τ_{Singed} = 32.2 s) (Figure 2.4D). Therefore, consistent with an avidity effect, Ena's processivity increases with the number of fascin-bundled filaments. In contrast, when comparing Ena's residence time on single filaments compared to the trailing barbed end of a 2-filament bundle, there is no difference with respect to fascin concentration (Figure 2.5, Table 2.6). This suggests that changing the fascin concentration in solution does not affect the property of fascin that causes a specific enhancement of Ena's processivity.

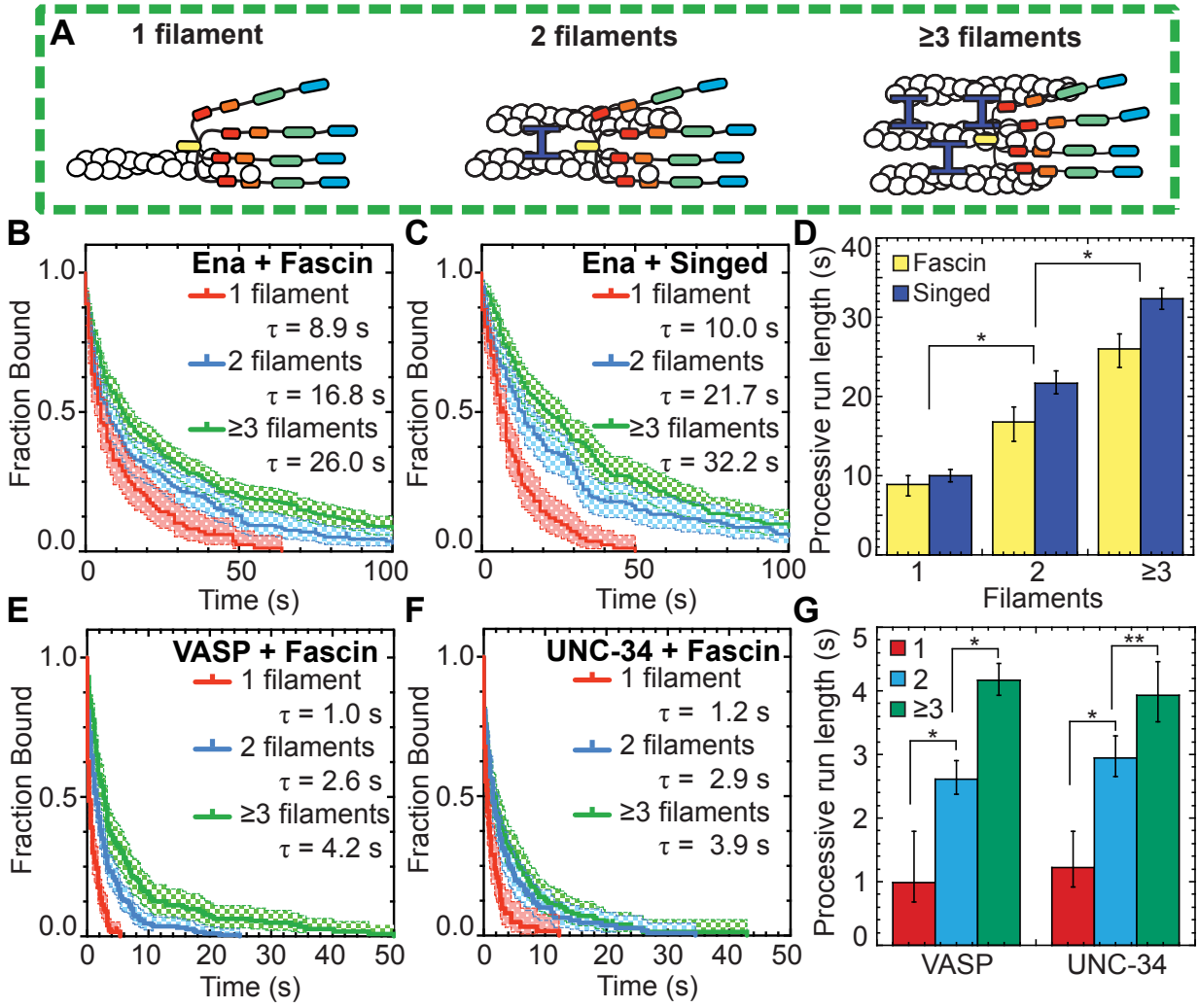

Figure 2.4: **Ena/VASP's processive run length increases with the number of filaments in a fascin bundle.** (A) Cartoons of Ena/VASP on a single filament and 2- and 3-filament fascin bundles. (B-G) Two-color TIRFM visualization of 1.5 μM Mg-ATP-actin (15% Oregon green-actin) with fly SNAP(549)-EnaΔL (red), human SNAP(549)-VASP or worm SNAP(549)-UNC-34 and unlabeled 130 nM human fascin or 250 nM Singed as indicated. (B and C) Kaplan-Meier curves representing average processive run lengths (τ) for 15 pM Ena with (B) fascin or (C) Singed on single filaments (red), or bundles with 2 (blue) and $\geq$3 (green) filaments. Error bars, 95% CI. n $\geq$ 98. (D) Average processive run lengths for increasing number of filaments in fascin (yellow) or Singed (blue) bundles shown in B and C. Error bars, 95% CI. P values (*<0.0001). (E and F) Kaplan-Meier curves representing run lengths (τ) for (E) 25 pM VASP or (F) 18 pM UNC-34 with fascin on single filaments (red), or bundles with 2 (blue) and $\geq$3 (green) filaments. Error bars, 95% CI. n $\geq$ 60. (G) VASP and UNC-34 average processive run lengths for increasing number of filaments in fascin bundles shown in E and F. Error bars, 95% CI. P values (*<0.0001, **0.002).

Ena/VASP	Bundling Protein	1 fil.[a] (s)	2 fil.[a] (s)	≥3 fil.[c] (s)	1/2/≥3 p-value[b]	1/2 p-value[b]	2/3 p-value[b]
Ena Tetramer	Fascin	8.9 [7.5,10.6] (107)	16.8 [14.3,19.7] (201)	26.0 [23.7,28.6] (308)	< 0.0001	< 0.0001	< 0.0001
Ena Tetramer	Singed	10.0 [9.2,10.8] (98)	21.7 [20.4,23.3] (155)	32.3 [31.0,33.6] (176)	< 0.0001	< 0.0001	< 0.0001
Ena Tetramer	α-actinin	9.1 [8.3,10.2] (165)	8.9 [7.7,10.6] (116)	8.7 [7.8,9.9] (60)	0.6	0.8	0.9
Ena Tetramer	Fimbrin	8.2 [7.1,9.8] (63)	7.6 [6.6,9.1] (121)	10.2 [8.6,12.6] (64)	0.3	0.2	0.1
VASP Tetramer	Fascin	1.0 [0.7,1.8] (123)	2.6 [2.4,2.9] (207)	4.2 [3.9,4.4] (143)	< 0.0001	< 0.0001	< 0.0001
VASP Tetramer	Singed	0.9 [0.6, 1.6] (118)	2.8 [2.6,3.2] (224)	4.1 [3.7,4.7] (220)	< 0.0001	< 0.0001	< 0.0001
UNC-34 Tetramer	Fascin	1.2 [0.9,1.8] (65)	2.9 [2.7,3.3] (123)	3.9 [3.5,4.5] (144)	< 0.0001	< 0.0001	0.002
Ena Trimer	Fascin	5.3 [4.7,6.1] (151)	8.9 [8.3,9.6] (206)	11.2 [10.2,12.6] (93)	< 0.0001	< 0.0001	0.0008
Ena Dimer	Fascin	1.2 [0.9,1.9] (197)	1.5 [1.2,2.0] (261)	2.5 [1.9,3.8] (122)	0.03	0.3	0.03

Table 2.5: **Comparison of Ena/VASP proteins' residence time on various bundled F-actin.**
[a] Values of average processive lifetime (s) [95%CI] (n) where n is the number of Ena/VASP binding events measured in at least three movies for 1 filament (fil.), 2 filaments, or greater than or equal to 3 filaments barbed ends.
[b] Log Rank p-value comparing 1 filament, 2 filaments, or greater than or equal to 3 filaments average processive lifetime.

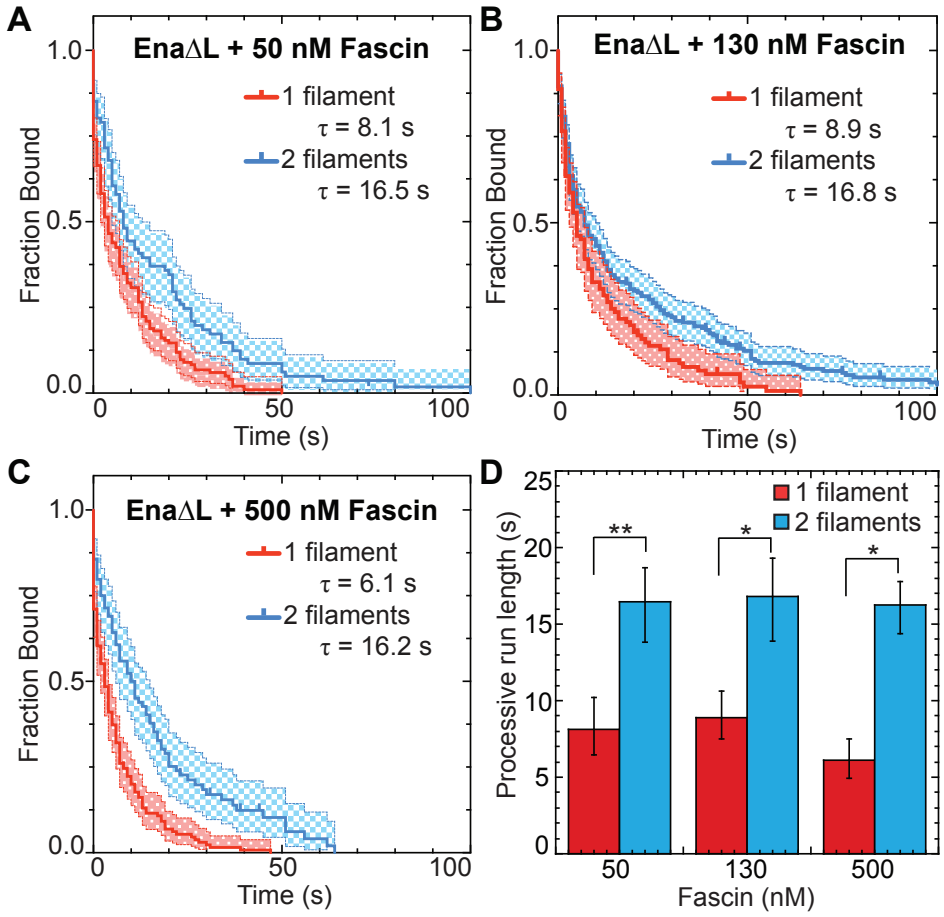

Figure 2.5: **Ena's enhanced processivity is consistent over a range of fascin.** (A-C) Kaplan-Meier curves representing average processive run lengths (τ) for 15 pM Ena with (A) 50 nM (B) 130 nM or (C) 500 nM fascin on single filaments (red), or 2-filament bundles (blue). Error bars, 95% CI. n $\geq$ 77. (D) Average processive run lengths on single filaments (red) and 2-filament bundles (blue) with increasing concentration of fascin. Error bars, 95% CI. P values (*<0.0001, **0.0002). 130 nM fascin data in (B) and (D) was also reported in 2.4B and D respectively.

Bundling protein	1 fil.[a] (s)	2 fil.[a] (s)	1/2 p-value[b]	Fold change[c]
50 nM Fascin	8.1 [6.5,10.2] (142)	16.5 [14.2,19.1] (80)	0.0002	2.3
130 nM Fascin[d]	8.9 [7.5,10.6] (107)	16.8 [14.3,19.1] (201)	< 0.0001	1.9
500 nM Fascin	6.1 [5.0,7.5] (136)	16.2 [14.7,18.0] (77)	< 0.0001	3.0

Table 2.6: **Average processive lifetime and p-values for Ena tetramers with different fascin concentrations.**
[a] Values of average $\text{Ena}_{\text{Tetramer}}$ processive lifetime on Leading or 2-filament barbed ends (s) [95%CI] (n) where n is the number of Ena/VASP binding events measured in at least two movies for barbed ends of leading filaments or 2-filament bundles.
[b] Log Rank p-value comparing average processive lifetime of barbed ends of leading filaments and 2-filament bundles.
[c] Fold change in average processive lifetime between leading and 2-filament bundle barbed ends.
[d] Data also shown in Table 2.5.

2.3.4 Human VASP and worm UNC-34 also have enhanced processive properties on fascin bundles

To determine whether enhanced processivity on fascin-bundled trailing filament barbed ends is conserved among Ena/VASP family members, we extended our analysis to human VASP and worm UNC-34 (Figure 2.1A). Human VASP is a well-characterized Ena/VASP protein [3, 29, 18, 122, 61], whereas UNC-34 had not yet been biochemically characterized in vitro despite multiple in vivo studies [154, 49, 66].

For our initial characterization of the three homologs, we measured the affinity for barbed ends and effect on actin elongation for Ena, VASP, and UNC-34. Initially, the effect of Ena/VASP homologs on actin elongation rates and their apparent affinity (Kd, app) for barbed ends was determined by single-color TIRFM visualization of spontaneous assembly of 1.5 μM Mg-ATP-actin (15% Oregon Green) over a range of concentrations for each unlabeled Ena/VASP homolog (Figure 2.6A-F). All three Ena/VASP homologs increase actin elongation by a similar amount, ~1.6- to ~2.7-fold, at or near saturating conditions but have somewhat varying affinities for actin filament barbed ends ranging from 3.2 nM (Ena) to

6.7 nM (UNC-34) to 12.2 nM (VASP) (Figure 2.6F). Likewise, bulk seeded pyrene actin assembly assays also show that all three Ena/VASP homologs increase actin elongation rates by similar amounts, and fits of assembly rate over a range of Ena/VASP concentrations revealed apparent affinities for barbed ends ranging from 0.7 nM (Ena) to 10.2 nM (UNC-34) to 10.8 nM (VASP) (Figure 2.6G-H). We then used two-color TIRFM visualizations of red-labeled Ena, VASP, and UNC-34 on fascin bundles to measure actin elongation rates of Ena/VASP-bound leading and trailing barbed ends (Figure 2.6I). All three Ena/VASP homologs similarly increase actin elongation ~2- to 3-fold on both leading and trailing barbed ends (Figure 2.6J, Tables 2.3, 2.7). Enhancement of actin elongation rates by Ena and VASP are similar to previously reported values [61, 182, 21] and the actin elongation properties of UNC-34 are in good agreement with the other homologs. Therefore, though Ena, VASP, and UNC-34 vary in their barbed end affinity, they all similarly increase the actin elongation rate of both leading and trailing barbed ends of fascin-bundled filaments.

Leading/Trailing[a]	$Ena_{Tetramer}$	VASP	UNC-34	Ena_{Trimer}	Ena_{Dimer}
$Ena_{Tetramer}$	1 / 1	0.7 / 0.8	0.6 / 0.6	<u>0.05</u> / 0.2	<u>0.03</u> / 0.3
VASP	0.7 / 0.8	1 / 1	0.5 / 0.8	0.3 / 0.5	0.3 / 0.4
UNC-34	0.6 / 0.6	0.5 / 0.8	1 / 1	0.09 / 0.4	0.1 / 0.4
Ena_{Trimer}	<u>0.05</u> / 0.2	0.3 / 0.5	0.09 / 0.4	1 / 1	0.3 / 0.8
Ena_{Dimer}	<u>0.03</u> / 0.3	0.3 / 0.4	0.1 / 0.4	0.3 / 0.8	1 / 1

Table 2.7: **p-values for comparisons of fold change in actin elongation rate with different Ena/VASPs on both leading and trailing filaments of fascin bundles.**
[a] p-values from student's two-tailed t-test with unequal variance between fold change of actin elongation rates when Ena/VASP is bound to the leading or trailing barbed end. Underlining shows p-values ≤ 0.05.

To test if different Ena/VASP homologs have similarly enhanced processive properties on fascin bundles, two-color TIRFM visualization of 1.5 μM Mg-ATP-actin (15% Oregon Green) was used to quantify the processive run lengths of fluorescently labeled VASP and UNC-34 on fascin bundles (Figure 2.4E-G). The average residence time of both VASP (1.0 s) and UNC-34 (1.2 s) on single filament barbed ends is ~9-fold shorter than Ena (8.9 s),

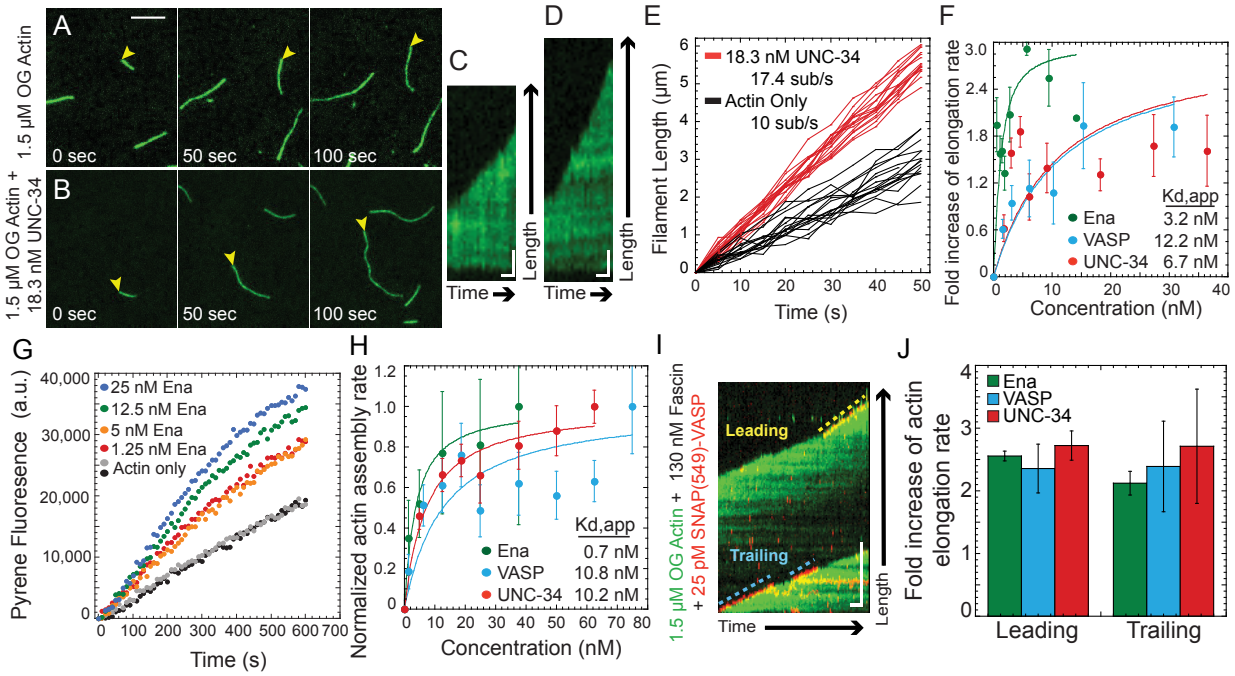

Figure 2.6: **Ena/VASP homologs have generally conserved processive actin elongation properties.** (A-F) Single-color TIRFM of the spontaneous assembly of 1.5 μM Mg-ATP-actin (15% Oregon Green) with worm UNC-34, fly Ena, and human VASP. (A and B) Timelapse micrographs (scale bar, 5 μm), and (C and D) corresponding kymographs (scale bar, 1 μm; time bar, 5 s) for (A and C) actin alone or with (B and D) 18 nM UNC-34. Yellow arrowheads indicate barbed ends. (E) Length of individual filaments over time for actin only (black) and UNC-34 (red). (F) Fold increase in elongation rate over increasing concentration of Ena (green), VASP (blue), and UNC-34 (red). Curve fits revealed the indicated apparent dissociation constants (Kd, app) of Ena/VASP for the barbed end. $n \geq 5$ filaments for at least 2 movies. (G and H) Seeded assembly: addition of 0.5 μM Mg-ATP-actin monomers (20% pyrene-labeled) to the barbed end of 0.5 μM preassembled actin filaments. (G) Time course of seeded assembly alone (black and gray) or with a range of Ena concentrations. (H) Dependence of the initial barbed end assembly rate on Ena/VASP concentration. Curve fits revealed the indicated apparent dissociation constants (Kd, app) of Ena/VASP for the barbed end. Error, SEM. $n \geq 3$. (I and J) Two-color TIRFM visualization of 1.5 μM Mg-ATP-actin (15% Oregon Green) with 25 pM SNAP(549)-VASP, 18 pM SNAP(549)-UNC-34 or 15 pM SNAP(549)-Ena, and unlabeled 130 nM human fascin. (I) Kymograph of leading and trailing barbed ends of a fascin bundle with SNAP(549)-VASP (red) and OG actin (green). Dashed blue (trailing) and yellow (leading) lines indicate bound VASP. Scale bar, 5 μm. Time bar, 10 s. (J) Average elongation rate of leading and trailing filament barbed ends on fascin bundles with actin alone, Ena, VASP, or UNC-34. Error bars, SEM. $n \geq 5$ filaments for at least 2 movies. Elongation rate for Ena in (J) also shown in Figure 2.1K.

as expected from lower apparent affinities for barbed ends and previously reported values [61]. Yet, like Ena, both VASP and UNC-34 have ~2.5-fold longer processive run lengths on trailing barbed ends of 2-filament bundles (τ_{VASP} = 2.6 s, τ_{UNC-34} = 2.9 s), with an additional ~1.5-fold increase on trailing barbed ends of 3- or more filament bundles (τ_{VASP} = 4.2 s, τ_{UNC-34} = 3.9 s) (Figure 2.4E–G, Table 2.1). Therefore, enhanced processivity on fascin-bundled trailing barbed ends is conserved from worms to flies to humans, suggesting that enhanced processivity is important for Ena/VASP's activity in cells.

2.3.5 Enhanced elongation and processive run length increases with the number of Ena arms

Wildtype Ena is a tetrameric protein [92, 182], with four arms that could facilitate simultaneous association with a barbed end, neighboring actin filaments, and/or actin monomers for processive elongation. Since we observed that Ena's average processive run length increases with number of fascin-bundled filaments (Figure 2.4), we investigated the importance of Ena's oligomeric state by measuring actin elongation and processive properties of dimeric and trimeric Ena. Dimer and trimer constructs were formed by replacing Ena's coiled-coil tetramerization domain with a GCN4 dimerization domain [64] or a Foldon trimerization domain (Figure 2.7A) [57, 121]; and the oligomeric state was verified by gel filtration and multi-angle light scattering (Figure 2.8A-C). Two-color TIRFM was used to visualize 1.5 μM Mg-ATP-actin (15% Alexa-488 labeled) with SNAP(549)-EnaΔLΔCC-GCN4 (referred to as $\text{Ena}_{\text{Dimer}}$) or SNAP(549)-EnaΔLΔCC-Foldon (referred to as $\text{Ena}_{\text{Trimer}}$) on fascin bundles. First, we measured actin elongation rates of Ena-bound leading and trailing barbed ends (Figure 2.7B, Tables 2.2, 2.7). While all constructs increase actin's elongation rate on both leading and trailing filaments, the fold increase is positively correlated with the number of Ena arms. $\text{Ena}_{\text{Tetramer}}$ has the largest enhancement of actin elongation (2.56-fold leading, 2.1-fold trailing), followed by $\text{Ena}_{\text{Trimer}}$ (1.74-fold leading, 1.62-fold trailing), and then

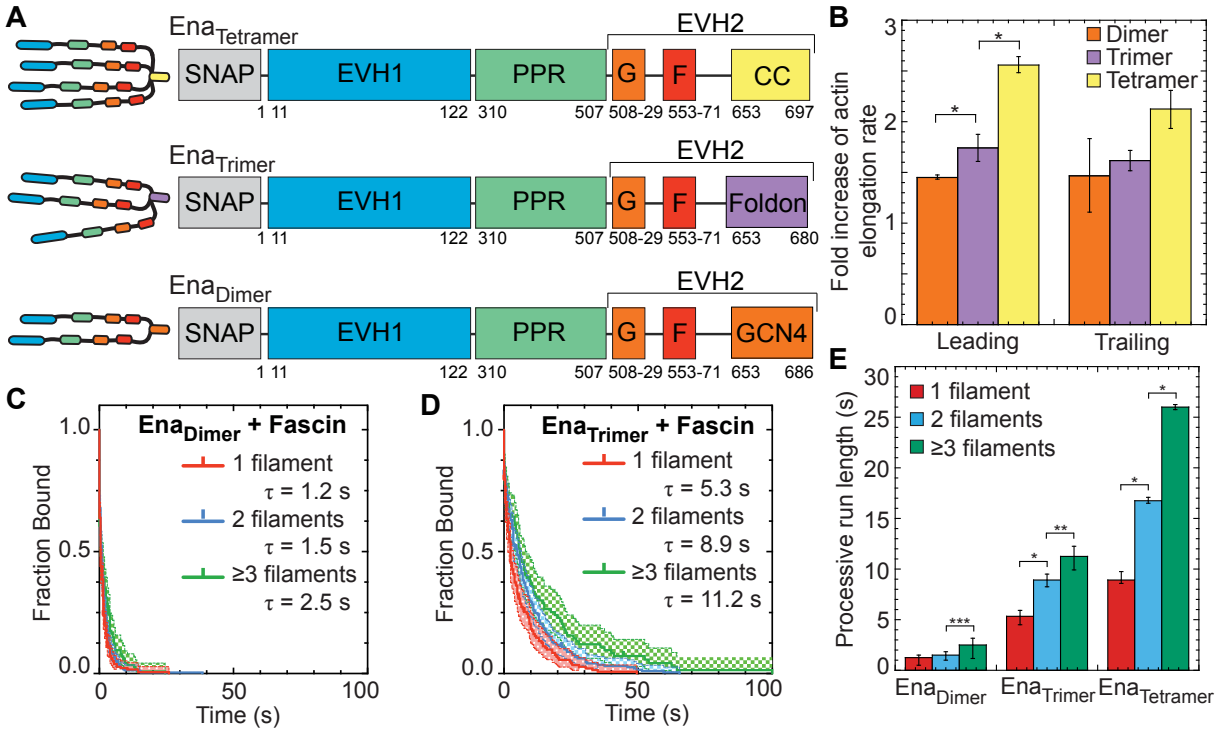

Figure 2.7: **Ena's processive run length increases with the number of Ena 'arms'.** (A) Cartoon and domain organizations of $Ena_{Tetramer}$, Ena_{Trimer}, and Ena_{Dimer}. (B-E) Two-color TIRFM visualization of 1.5 μM Mg-ATP-actin (15% Alexa 488-actin) with indicated SNAP(549)-Ena construct and 130 nM fascin. (B) Fold increase of barbed end elongation rates of Ena_{Dimer} (orange), Ena_{Trimer} (purple), and $Ena_{Tetramer}$ (yellow). Error bars, SEM. n $\geq$ 5 barbed ends from at least 2 movies. P values (*$\leq$0.05) (C and D) Kaplan-Meier curves representing average processive run lengths (τ) for (C) 50 pM MBP-SNAP(549)-EnaΔLΔCC-GCN4 or (D) 70 pM MBP-SNAP(549)-EnaΔLΔCC-Foldon with fascin on single filaments (red) or bundles with 2 (blue) and $\geq$3 (green) filaments. Error bars, 95% CI. n $\geq$ 93. (E) Average processive run length for increasing number of Ena "arms" on single filaments (red), or fascin bundles with 2 (blue) and $\geq$3 (green) filaments shown in C and D. Error bars, 95% CI. P values (*<0.0001, **0.0008, ***0.03). $Ena_{Tetramer}$ data in (B) and (E) was also reported in 2.1K and 2.4D respectively.

Ena_{Dimer} (1.45-fold leading, 1.46-fold trailing).

Similar to actin elongation rates, average processive run length is also positively correlated with the number of Ena arms (Figure 2.7C-E). Remarkably, although reduced ~10-fold compared to $Ena_{Tetramer}$, Ena_{Dimer} does remain processively associated with single filament (τ = 1.2 s), 2-filament trailing (τ = 1.5 s), and 3- or more filament trailing (τ = 2.5 s) barbed ends (Figure 2.7C,E, Table 2.1). Ena_{Trimer} has intermediate processivity on single filament (τ = 5.3 s), 2-filament trailing (τ = 8.9 s), and 3- or more filament trailing (τ = 11.2 s) barbed ends (Figure 2.7D,E, Table 2.1). For each construct, the fluorescence intensity is not correlated with run length (Figure 2.8D-G), indicating that processive activity is not affected by Ena construct multimerization. Ena_{Trimer}'s processive run lengths are similar to the residence time of $Ena_{Tetramer}$ on single filaments but are not comparably enhanced on trailing barbed ends (Figure 2.7E). Therefore, Ena_{Dimer} is sufficient for processive elongation, Ena_{Trimer} is necessary for longer processive runs on single filaments, but $Ena_{Tetramer}$ is necessary for the longest processive runs on trailing barbed ends of fascin bundles (Figure 2.7E). Interestingly, the avidity effect of multiple filaments in a fascin bundle is apparent even with fewer arms than the wildtype tetramer. The positive correlation between processive elongation and Ena arms is consistent with a recent study on chimeric human VASP with *Dictyostelium* GAB domains on single actin filaments [21].

2.3.6 Tetrameric Ena is more efficient at forming filopodia in Drosophila culture cells

$Ena_{Tetramer}$ is significantly better at processive actin filament assembly than either Ena_{Dimer} or Ena_{Trimer}, where $Ena_{Tetramer}$ increases the actin elongation rate ~2- to 2.5-fold and remains processively associated with trailing barbed ends of fascin bundles for ~25 sec (Figure 2.7B,E). To determine whether WT $Ena_{Tetramer}$ is therefore necessary for proper function in cells, we evaluated the ability of Ena oligomerization constructs to facilitate filopodia

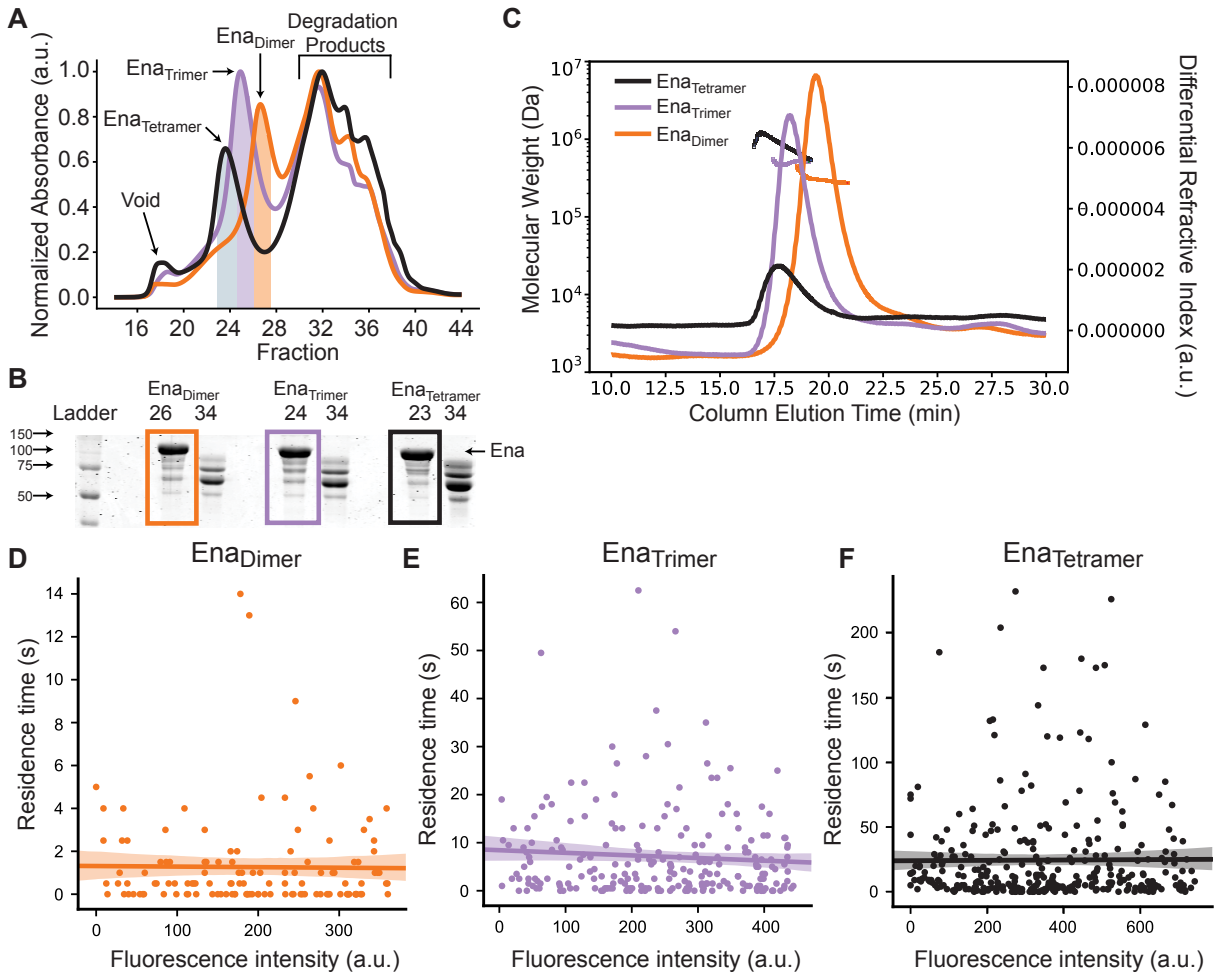

G

Construct	Intensity and Residence Time Pearson's Correlation
Ena_{Dimer}	0.16 (p-value 6.3 e-18)
Ena_{Trimer}	0.037 (p-value 2.2 e-4)
$Ena_{Tetramer}$	-0.034 (p-value 2.6 e-8)

Figure 2.8: **Ena constructs have the predicted oligomerization state.** (A) UV traces for Ena_{Dimer} (orange), Ena_{Trimer} (purple), and $Ena_{Tetramer}$ (black) from size exclusion gel filtration using a Sepharose 6 Increase column. Peaks are labeled and fractions collected are shaded. (B) The 12.5% SDS-PAGE of fractions from A. Fractions showing each construct are boxed. (C) Size exclusion chromatography followed by multi-angle light scattering (SEC-MALS) was used to determine the relative size of Ena_{Dimer} (orange), Ena_{Trimer} (purple), and $Ena_{Tetramer}$ (black). Dependence of (D) Ena_{Dimer}, (E) Ena_{Trimer}, or (F) $Ena_{Tetramer}$ processive run length on its respective fluorescence intensity for an individual movie. Linear correlation fit shown with 95% CI shaded.

Figure 2.8: (continued) (G) Values for the Pearson's correlation of the Ena construct fluorescence intensity and its residence time for all movies analyzed. There is no correlation between an Ena construct's intensity and its bound lifetime. **SEC-MALS performed by Elena Solomaha, University of Chicago Biophysics Core.**

in ML-DmD16-c3 *Drosophila* culture cells, derived from third instar larval wing discs (Figure 2.9). We knocked down endogenous Ena with dsRNAi against the 3'UTR and then expressed mCherry-Ena (referred to as mCherry-Ena$_{\text{Tetramer}}$), mCherry-EnaΔCC-GCN4 (referred to as mCherry-Ena$_{\text{Dimer}}$) or mCherry-EnaΔCC-Foldon (referred to as mCherry-Ena$_{\text{Trimer}}$) constructs from a constitutive pIZ plasmid (Figure 2.9A-C). The activity of the different Ena constructs was determined by quantifying filopodia density, the number of filopodia per perimeter of the cell (Figure 2.9D). Compared to control cells (0.19 $\pm$ 0.06 filopodia/micron), RNAi treated cells without exogenous Ena have a 2.7-fold decrease in filopodia density (0.07 $\pm$ 0.03 filopodia/micron). Strikingly, mCherry-Ena$_{\text{Tetramer}}$ forms significantly more filopodia (0.24 $\pm$ 0.05 filopodia/micron) compared to mCherry-Ena$_{\text{Trimer}}$ (0.15 $\pm$ 0.05 filopodia/micron) and mCherry-Ena$_{\text{Dimer}}$ (0.15 $\pm$ 0.04 filopodia/micron). There was no correlation between filopodia density and GFP-actin fluorescence or mCherry fluorescence (Figure 2.10). Therefore, Ena tetramers facilitate the production of significantly more filopodia than dimer and trimer constructs following knockdown of endogenous Ena.

2.3.7 Kinetic model of Ena shows a direct correlation between processivity and both bundle size and Ena oligomerization

We observed that Ena's processivity depends on the number of filaments in a fascin bundle (Figure 2.4D) and number of Ena arms (Figure 2.7E). Therefore, it is likely that the underlying molecular mechanism for Ena's increased processivity on trailing barbed ends depends on Ena's ability to simultaneously bind to an elongating barbed end and sides of filaments via its multiple arms (Figure 2.1B). To investigate this avidity effect, we developed a kinetic model of Ena with varying number of arms, N, binding bundles composed of varying number

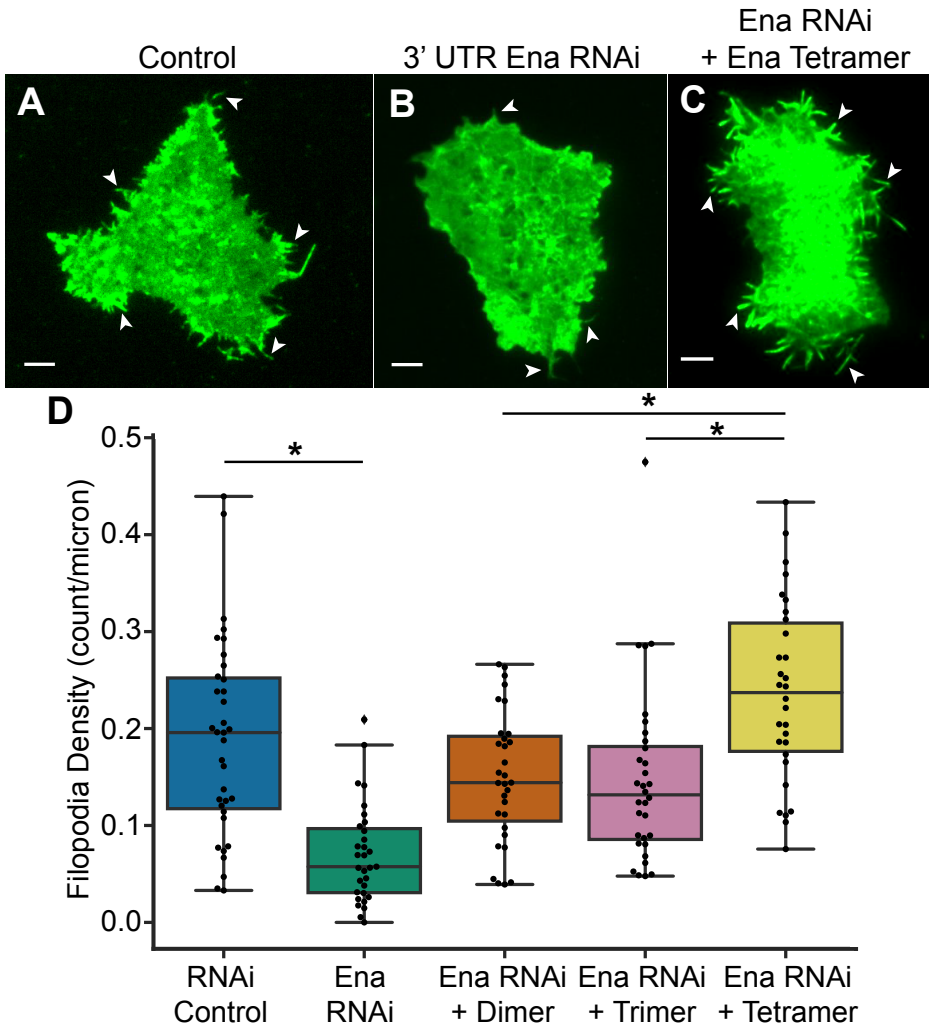

Figure 2.9: **Tetrameric Ena is necessary for proper filopodia density.** (A-C) Representative fluorescent micrographs of D16 cells with GFP-actin for (A) control treatment, (B) Ena 3' UTR RNAi, and (C) RNAi with transfection of mCherry-$\text{Ena}_{\text{Tetramer}}$. White arrows indicate representative filopodia. (D) Boxplot of filopodia density, number of filopodia per micron of cell perimeter, for control cells, Ena 3'UTR RNAi, and RNAi transfected with mCherry-EnaΔCC-GCN4 ($\text{Ena}_{\text{Dimer}}$), mCherry-EnaΔCC-Foldon ($\text{Ena}_{\text{Trimer}}$), and mCherry-$\text{Ena}_{\text{Tetramer}}$. n = 3 with at least 10 cells for each experiment. P values (*<0.0005). **D16 cell culture and images captured by Derek Applewhite.**

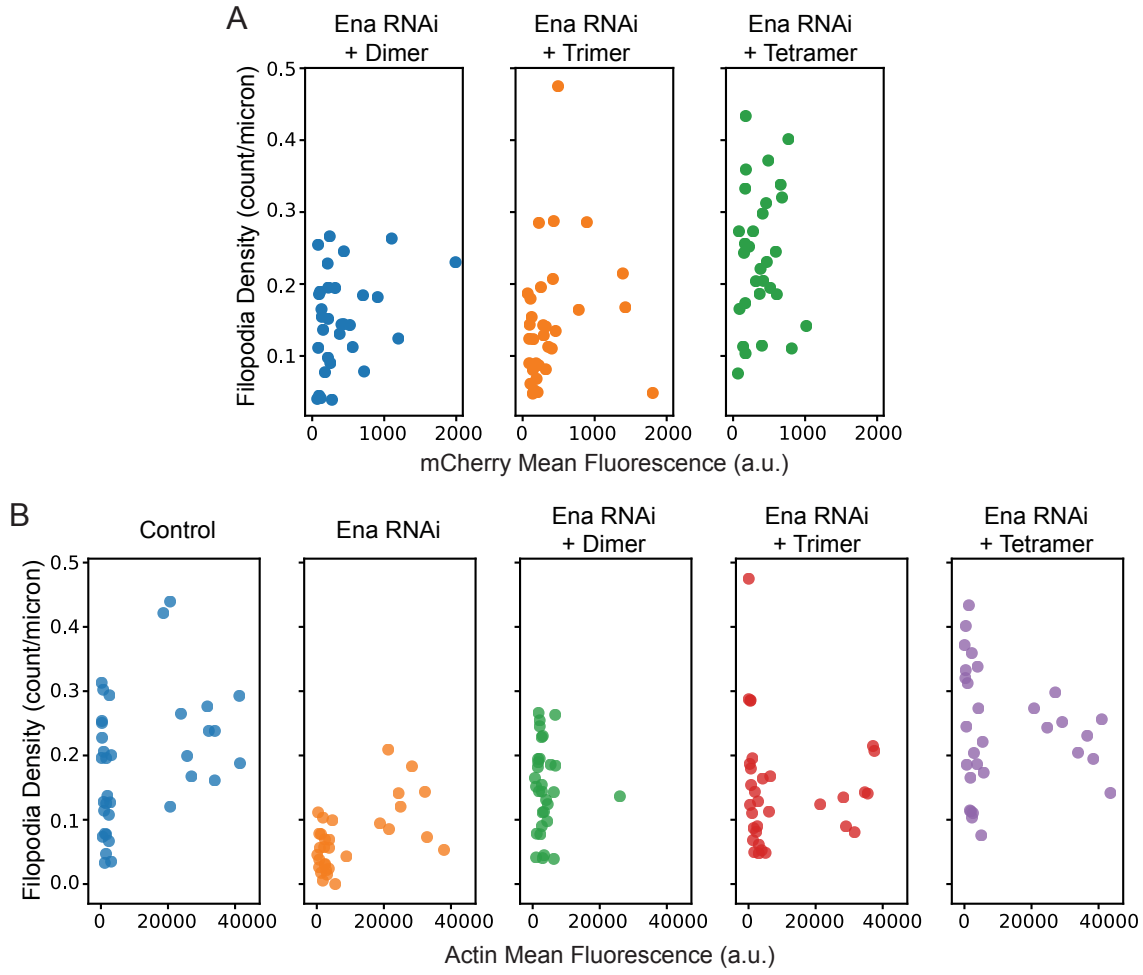

Figure 2.10: **D16 culture cell expression is independent of construct.** (A) Dependence of filopodia density on mCherry fluorescence of RNAi treated cells transfected with mCherry-Ena$_{\text{Dimer}}$, mCherry-Ena$_{\text{Trimer}}$, or mCherry-Ena$_{\text{Tetramer}}$. (B) Dependence of filopodia density on the GFP-actin fluorescence intensity for control or RNAi treated control and mCherry-Ena$_{\text{Dimer}}$, mCherry-Ena$_{\text{Trimer}}$, or mCherry-Ena$_{\text{Tetramer}}$ transfected cells.

of actin filaments, n (Figure 2.11A, 2.12A).

Our model considers binding and unbinding kinetics of all N Ena arms on various binding sites of individual actin filaments in a bundle, which together dictate the kinetics of the Ena "molecule" as a whole (Figure 2.11A). An Ena arm initially binds to the trailing barbed end with an on rate of $k^t_{on,1}$ and unbinds with an off rate of $k^t_{off,1}$ (Figure 2.11A1). The remaining Ena arms are available to bind and unbind to the side of the trailing filament with a rate k^t_{on} and k^t_{off} or to the side of other filaments in the bundle with a rate k^l_{on} and k^l_{off} (Figure 2.11A2-3). A Monte Carlo algorithm was used to integrate rates of binding and unbinding of Ena arms over time as described in the SI. The model parameter $k^t_{on,1}$ was 0.007 s^{-1}, estimated using the TIRFM measured off rate of 0.109 s^{-1} for Ena, and an equilibrium constant of Ena for the barbed end of 0.8 nM [182]. We therefore considered the local concentration of Ena near the barbed end as 50 pM. The other model parameters were optimized using TIRFM off rates for $N \in (2, 3, 4)$ and $n \in (1, 2, \geq 3)$ (Figure 2.7E), as described in the Supplementary Information.

We used the model to characterize Ena's processive run length at the trailing barbed end. Increasing both the number of filaments in a bundle and the number of Ena arms increases Ena's processive run length, which strongly supports the avidity hypothesis. The modeling results are also in excellent agreement with the trends observed from our TIRFM data (Figure 2.11B). Using the model, we tested conditions over a range of both k^l_{on} and k^l_{off} to mimic α-actinin and fimbrin bundles (Figure 2.1I), where Ena processivity is not enhanced on trailing barbed ends (Figure 2.12B-F). The model shows a broad regime that results in the same average processive run length on both leading and trailing barbed ends (Figure 2.11C, dashed region). This indicates that differences between bundlers could be due to an effect on Ena's association and dissociation rates caused by differences in how CH domain bundlers and fascin bind F-actin.

Finally, we used the model to estimate rates of Ena-mediated filament elongation. While

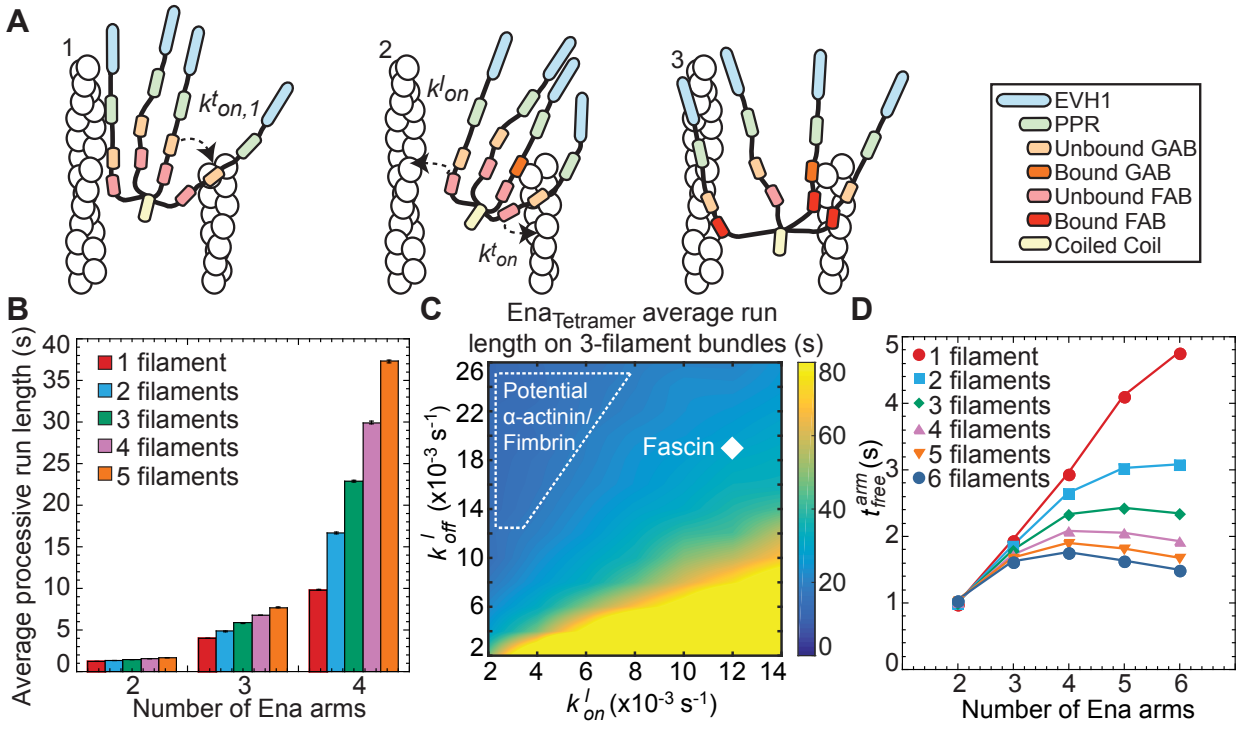

Figure 2.11: **Kinetic model of Ena/VASP on actin bundles shows processivity positively correlates with both number of Ena arms and bundle size.** (A) Modeling schematics showing (from left to right). [1] An Ena arm's GAB domain binds the trailing barbed end with binding rate $k^t_{on,1}$. [2] Once the GAB domain is bound, the FAB domains from the other arms bind to sides of either the trailing filament (k^t_{on}) or leading filaments (k^l_{on}). [3] Arms can be bound to the trailing filament, while others bind leading filaments. (B) Bar graph of the average processive run length as a function of number of Ena arms and bundle size. Error bars, SEM. (C) Heat map showing average Ena run length in the case of 3-filament bundles and four Ena arms, with systematic variations of k^l_{on} and k^l_{off}. Diamond denotes optimized rates for fascin bundles and region within dotted line shows potential rates for α-actinin and fimbrin. (D) Average time between binding events (τ^{arm}_{free}) for varying arm number and bundle size. **Kinetic Model by Harshwardhan Katkar, Tamara Bidone, and Fikret Aydin.**

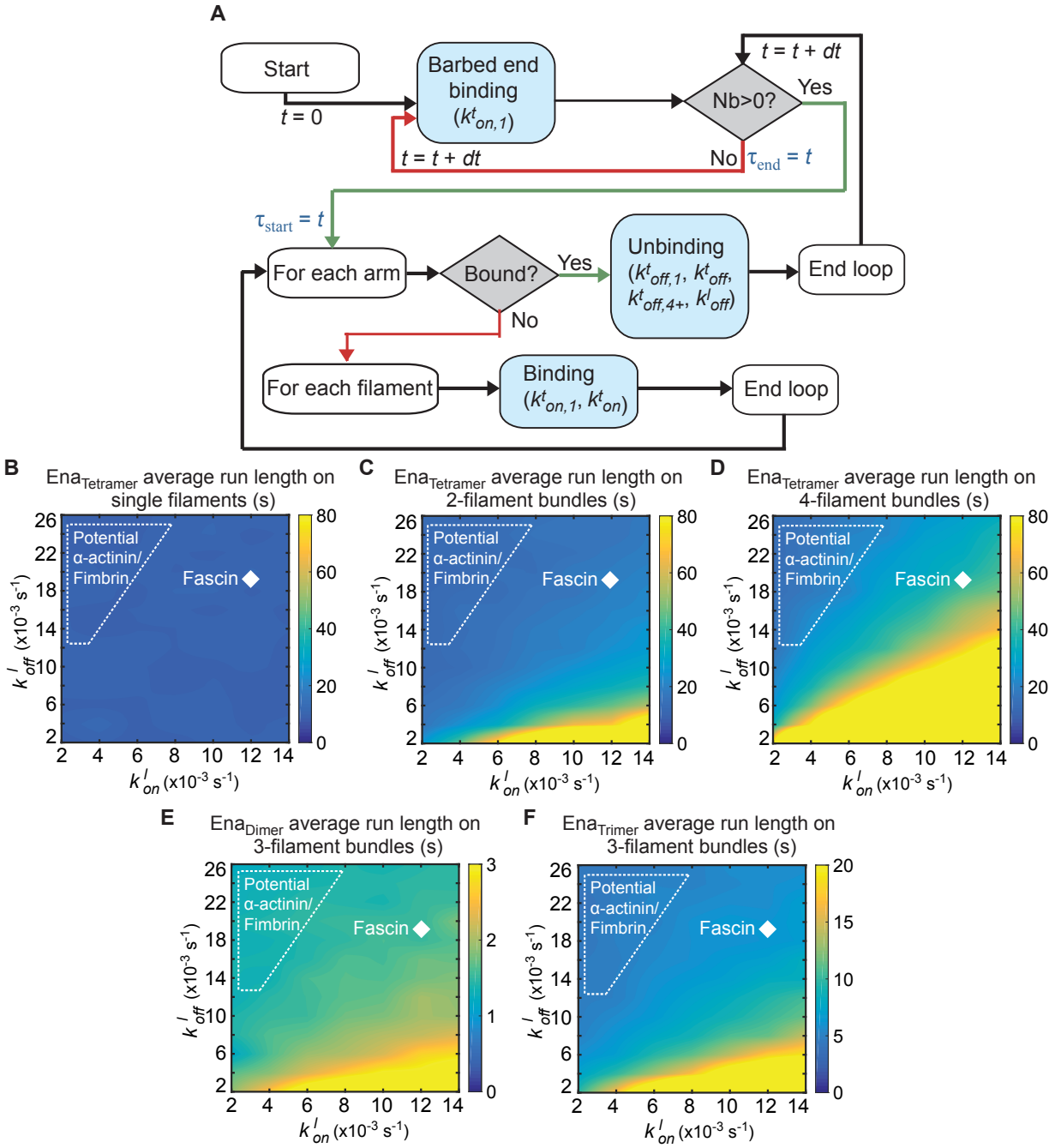

Figure 2.12: **Kinetic model can explore different parameter spaces.** (A) Diagram showing the key steps in the algorithm. Nb represents the number of arms bound at time t. τ_{start} and τ_{end} mark the start and end of Ena "molecule" binding events. The processive run length τ is estimated as the average of the difference $\tau_{end} - \tau_{start}$ across several events.

Figure 2.12: (continued) (B – F) Heat maps showing average Ena processive run length with systematic variations of k_{on}^{l} and k_{off}^{l}. Heat maps of average processive run length for (B) single filaments (C) 2-filament bundles or (D) 4-filament bundles with four Ena arms. These are comparable to Figure 2.11C with 3-filament bundles. Heat maps of average processive run length for 3-filament bundles with (E) two or (F) three Ena arms. **Kinetic Model by Harshwardhan Katkar, Tamara Bidone, and Fikret Aydin.**

at least one Ena arm associates with the barbed end, its other arms undergo binding and dissociation events. When free, an arm can bind G-actin from solution and transfer it to the barbed end. The elongation rate of the Ena bound filament should be proportional to the average time that individual arms are free. From the model, the average time that individual arms remain unbound while the Ena molecule is in the bound state, τ_{free}^{arm}, increases with N, and decreases with n (Figure 2.11D). This result is consistent with the TIRFM data for the fold increase of actin elongation rate due to Ena on the leading ($n = 1$ in the model) and trailing barbed ends ($n > 1$ in the model) (Figure 2.1K, 3B).

2.3.8 Ena binds longer to sides of fascin bundles compared to fimbrin and α-actinin bundles.

Our kinetic model suggested an area of kinetic rates for Ena binding to the side of a leading filament that could account for the specificity of Ena's enhanced processivity to fascin bundles. To test if there is a difference for Ena binding or dissociating from sides of fascin bundles compared to other bundling proteins we used two approaches, steady-state sedimentation assays and TIRF microscopy.

We first tested if there is a difference in Ena's F-actin binding in the presence and absence of fascin using a bulk sedimentation assay. We used two different truncation constructs to test Ena's F-actin binding affinity, GABFAB and EVH2 (Figure 2.13A). GABFAB contains the GAB and FAB domains and is a monomeric protein while EVH2 contains the GAB, FAB, and CC domains and, therefore, is a tetramer. We saw no significant difference in

either the GABFAB (Figure 2.13B-C) or EVH2 F-actin binding (Figure 2.13D-E). These results suggests that there is no difference in FAB binding to the sides of bundled filaments that can be measured in a bulk steady-state assay.

Next, we further analyzed our TIRFM data to measure Ena's affinity for sides of bundles at the resolution that we measure its processivity on barbed ends. We measured the residence time of Ena on sides of single filaments and 2-filament bundles in the presence of fascin, fimbrin, and α-actinin (Figure 2.14A-C, Table 2.8). Surprisingly, Ena binds longer to the sides of 2-filament bundles only when the bundles are formed by fascin (Figure 2.14D). This suggests that the specificity we see for Ena's enhanced processivity on the barbed end is due to a difference in affinity of Ena's F-actin binding domain for fascin bundles.

Bundling protein	Side 1 fil.(s)[a]	Side 2 fil.(s)[a]	1/2 p-value[b]	Bundling protein[c]	Comparison p-value [d]
Fascin	0.4 [0,1.0] (125)	1.9 [1.4,2.5] (161)	< 0.0001	α-actinin	0.008
Fimbrin	0.3 [0,0.6] (68)	0.3 [0.1,0.5] (58)	0.5	Fascin	0.0002
α-actinin	0.3 [0.2,0.5] (129)	0.7 [0.4,1.2] (174)	0.2	Fimbrin	0.2

Table 2.8: **Side binding residence times and p-values for $\mathbf{Ena_{Tetramer}}$ with different bundling proteins.**

[a] Values of average $Ena_{Tetramer}$ lifetime on filament sides (s) [95%CI] (n) where n is the number of Ena/VASP binding events measured in at least two movies for single filaments or 2-filament bundles.

[b] Log Rank p-value comparing average lifetime of filament sides for single filaments and 2-filament bundles.

[c] Bundling protein to compare average lifetime on sides of 2-filament bundles

[d] Log Rank p-value comparing average lifetime on sides of 2-filament bundles for two specified bundling proteins.

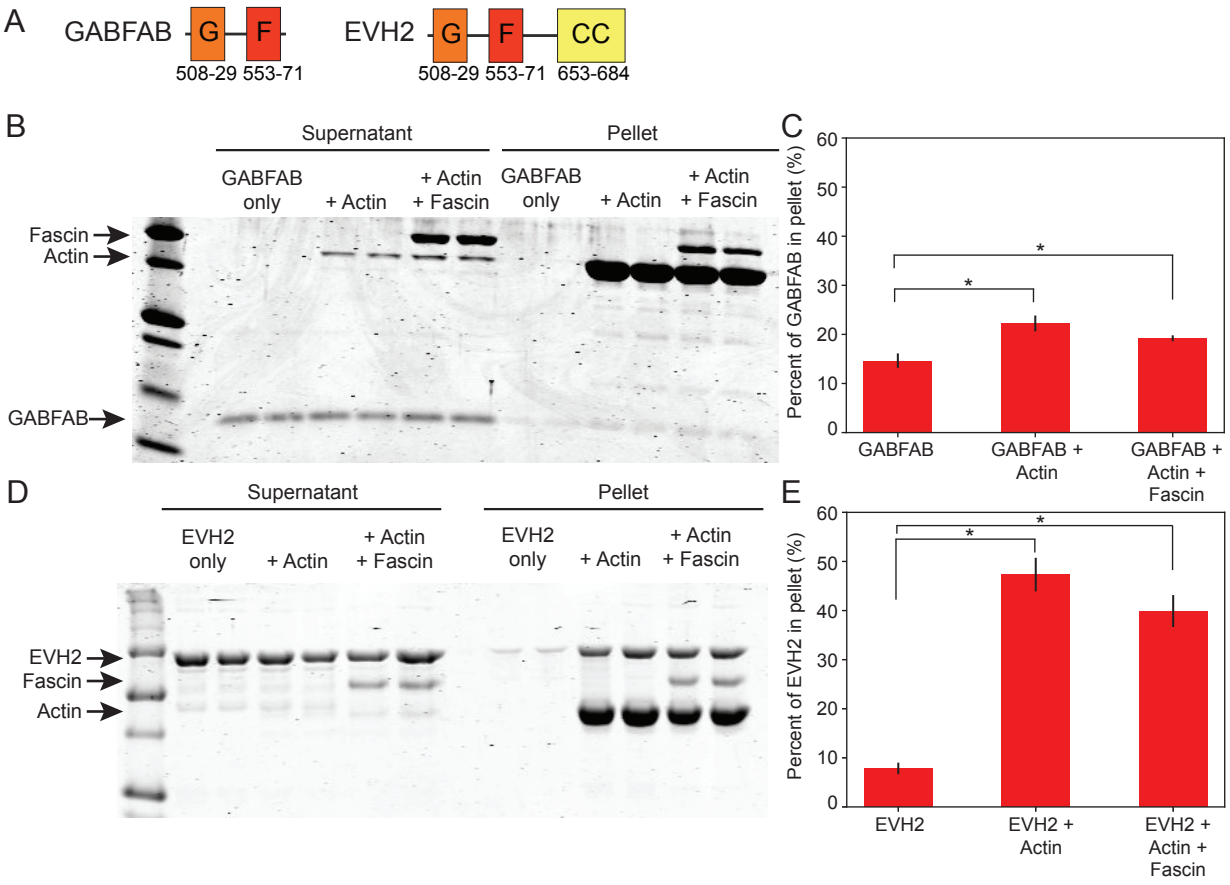

Figure 2.13: **GABFAB and EVH2 bind similarly to single filaments and fascin bundles in bulk sedimentation.** (A) Domain organization for constructs used in sedimentation. G-actin binding domain (G), F-actin binding domain (F), coiled coil region (CC). (B) 15% SDS-PAGE gel showing supernatant (left) and pellet (right) for the specified combination of 5 μM GABFAB, 5 μM actin, and 1 μM fascin. The reactions were done in duplicate. (C) Percent of GABFAB found in pellet for GABFAB alone, GABFAB with actin, and GABFAB with actin and fascin. Error bars, SEM. n = 8. P values (* < 0.05). (D) 12.5% SDS-PAGE gel showing supernatant (left) and pellet (right) for specified combinations of 2.5 μM EVH2, 5 μM actin, and 1 μM fascin. The reactions were done in duplicate. (E) Percent of EVH2 found in pellet for EVH2 alone, EVH2 with actin, and EVH2 with actin and fascin. Error bars, SEM. n = 8. P values (* < 0.05).

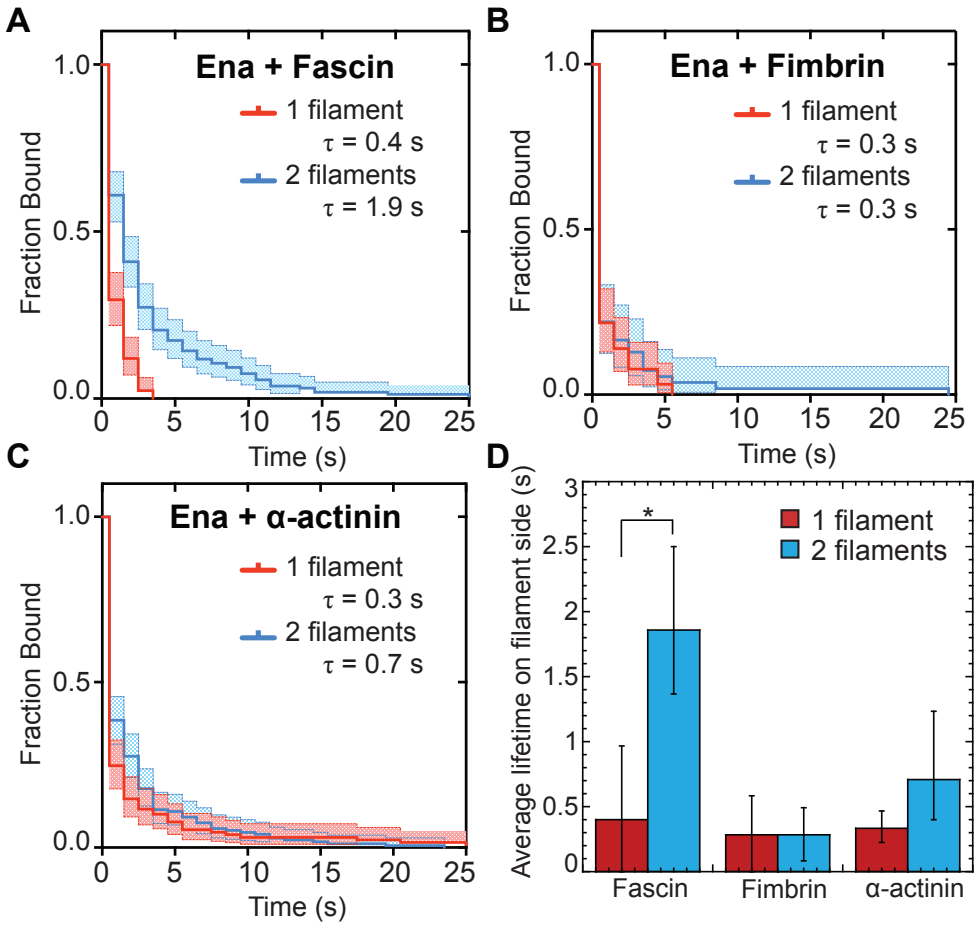

Figure 2.14: **Ena binds longer on sides of fascin bundles.** (A-C) Kaplan-Meier curves representing average lifetimes (τ) for 15 pM SNAP(549)-EnaΔL with (A) 130 nM fascin, (B) 100 nM fimbrin, or (C) 125 nM α-actinin on single filaments (red) and 2-filament bundles (blue). Error bars, 95% CI. $n \geq 58$. (D) Average lifetime for Ena binding to sides of single filaments (red) and 2-filament bundles (blue) shown in A-C with fascin, fimbrin, or α-actinin. Error bars, 95% CI. P values (*<0.0001).

2.4 Discussion

2.4.1 Ena's processivity is enhanced specifically on fascin bundles

Ena/VASP proteins are important processive actin elongation factors that are localized to diverse F-actin networks composed of filaments bundled by different crosslinking proteins, including fascin, fimbrin, and α-actinin. Previously, we found that Ena takes ~3-fold longer processive runs on trailing barbed ends of fascin-bundled F-actin [182]. Here we investigated the mechanism and conservation of Ena/VASP's processivity at the barbed end of single filaments and filaments bundled by different crosslinking proteins, as well as the physiological relevance of Ena/VASP tetramerization.

We found that although fly Ena's processivity is enhanced ~3-fold on trailing barbed ends in fascin bundles, there is no processivity enhancement on trailing barbed ends of α-actinin or fimbrin bundles (Figure 2.1I). Fimbrin and α-actinin use two CH domains to bundle F-actin, whereas fascin uses β-trefoil domains. Though the exact mechanism for Ena's specificity for fascin bundles remains unclear, we suggest several hypotheses. First, fascin could hold the trailing filament in a specific register with respect to the leading filament, allowing for easier Ena/VASP binding. Second, fascin's strong cooperativity [185, 183] could promote bundling closer to the growing trailing barbed ends, thereby promoting longer processive runs by keeping trailing barbed ends closer to sides of leading filaments. Third, it is also possible that Ena weakly associates with fascin, although no interaction has yet been detected. If Ena does associate with fascin, it would need to be carefully tuned because a strong interaction could pull Ena from the barbed end. Furthermore, we show that with increasing concentration of fascin that Ena's enhanced processivity is consistent which suggests the absence of a direct interaction (Figure 2.5D).

The fourth hypothesis is based off of a result from our kinetic model, which revealed a broad region of Ena binding kinetics to sides of bundled filaments (k^l_{on} and k^l_{off}) that

could explain Ena's lack of enhanced processivity on fimbrin and α-actinin bundles (Figure 2.11B). We show that in steady-state assays that there is no difference in Ena's affinity for F-actin (Figure 2.13). However, in TIRFM experiments we observe longer residence times on 2-filament fascin bundles compared to fimbrin and α-actinin bundles (Figure 2.14D). This difference in dissociation rates could be due to a particular structure of the fascin bundle as suggested previously. Alternatively, it is possible that Ena's on and off rates are affected by competition between Ena and the CH domain bundling proteins for similar binding sites on sides of actin filaments.

Further studies of how fascin forms F-actin networks differently than α-actinin and fimbrin will be required to fully elucidate the underlying molecular mechanism. However, this important observation reveals for the first time that bundling proteins and the F-actin networks they form can differentially regulate the activity of processive actin assembly factors, thereby providing a mechanism to allow Ena/VASP proteins to facilitate the assembly of diverse bundled networks with different dynamics in cells. Understanding how different bundling proteins associate with and help form specific F-actin networks in cells will therefore be of critical importance.

2.4.2 The mechanism of tetrameric Ena acting on fascin bundles for filopodia formation

Given that Ena localizes to filopodia with fascin, lamellipodia with fimbrin, and stress fibers with α-actinin, sensitivity to diverse bundles could play an important role in regulating Ena activity in cells. Filopodia are unique amongst these networks with long, straight filaments that emerge from a network capped by capping proteins. Lamellipodia have short, branched filaments and stress fibers are contractile, bipolar networks. Thus, filopodia are the ideal network for enhanced Ena/VASP processivity facilitating elongation of longer filaments that requires stronger competition against capping protein to form a protrusive network. The in-

creased residence time on trailing barbed ends could play a critical role in a feedback mechanism between Ena and fascin in emerging filopodia [182]. Ena/VASP-associated barbed ends elongate faster, assembling longer actin filaments that contain more fascin binding sites, which subsequently enhance Ena/VASP's processivity. Trailing barbed ends that have longer Ena processive runs can catch up to the leading barbed end, allowing all filaments to reach the same length and resulting in mature filopodia with uniform thickness and aligned barbed ends.

2.4.3 Avidity promotes enhanced Ena processivity on fascin bundles.

We hypothesize that avidity between multiple actin filaments in a fascin bundle and multiple Ena arms promotes the formation of long filopodia filaments. We investigated the avidity effect by testing how the number of filaments in a fascin bundle and number of Ena arms affects Ena's processive run length. Our results strongly indicate that avidity plays a major role, as there is a ~2-fold increase in Ena's residence time on trailing barbed ends in 2-filament bundles and an additional ~1.5-fold increase on bundles with 3- or more filaments compared to single filament barbed ends (Figure 2.4B-D). Similarly, the residence time of both VASP and UNC-34 is longer on trailing barbed ends and is correlated with number of actin filaments in a fascin bundle (Figure 2.4E-G). Furthermore, the residence time of $\text{Ena}_{\text{Trimer}}$ and $\text{Ena}_{\text{Tetramer}}$ is ~4.5- and ~10-fold longer than $\text{Ena}_{\text{Dimer}}$ on fascin bundles with 3- or more filaments (Figure 2.7C-E). A recent study measuring processive elongation using chimeric human VASP with *Dictyostelium* GAB domains on single filaments [21] supports our conclusions that enhanced elongation and processive run length are positively correlated with the number of Ena arms. Observing this positive correlation under more physiological conditions, a construct using Ena's unmodified EVH2 domains and on fascin bundles, indicates that these properties are relevant for Ena's activity in cells and specifically for filopodia.

We further tested the avidity hypothesis by developing a kinetic model that incorporates Ena with differing number of arms binding to single or multiple filaments (Figure 2.11). Previous models have focused exclusively on modeling the kinetics of Ena/VASP-mediated barbed end elongation of single actin filaments [61, 19, 21]. As predicted by these models, VASP-mediated single filament elongation rates were shown to increase linearly with the number of VASP arms in solution [19]. However, this model overlooks the binding kinetics of arms that are not associated with the barbed end. Hence, we developed a kinetic model that explicitly incorporates the binding and unbinding rates of each Ena arm on multiple filaments (Figure 2.11A). After an Ena arm binds to the barbed end ($k^t_{on,1}$), the remaining arm(s) are free to bind to the side of the leading filament(s) (k^l_{on}) or the trailing filament (k^t_{on}). We quantified the processive run length for various numbers of bundled filaments and Ena arms.

The model demonstrates that the avidity effect of Ena emerges from an effective increase in local concentration of F-actin that allows for more FAB binding sites and from multiple Ena arms with available FAB domains. The avidity effect results in longer residence times near the trailing barbed end. Importantly, if an arm dissociates from the trailing barbed end, Ena will continue to processively elongate the barbed end and not diffuse away given that other arms' FAB domains are associated with nearby actin filaments. Furthermore, our model that includes multiple arms binding to multiple actin filaments still has a linear correlation of elongation rates with number of Ena arms on single filaments (Figure 2.11D), as predicted by a previous model [19]. The τ^{arm}_{free} is linear with respect to increasing additional Ena arms on single filaments, but with increasing number of filaments there are diminishing returns by adding more Ena arms. τ^{arm}_{free} peaks at a tetramer on larger bundles, which gives an additional argument of why a tetramer of Ena/VASP is evolutionarily preferred. We also observe that an Ena tetramer is more efficient at forming filopodia in *Drosophila* culture cells compared to dimer and trimer constructs (Figure 2.9). Since the tetramer has

increased residence time on trailing barbed ends and increases actin's elongation rate above the dimer and trimer, this suggests that the tetramer is necessary for proper actin elongation rates and competition with capping protein to allow for the formation of the correct number of filopodia.

2.5 Materials and Methods

2.5.1 Total internal reflection fluorescence microscopy (TIRFM)

TIRFM images were collected at 250 ms-1 s intervals with a cellTIRF 4Line system (Olympus, Center Valley, PA) fitted to an Olympus IX-71 microscope with through-the-objective TIRF illumination and an iXon EMCCD camera (Andor Technology, Belfast, UK). Mg-ATP-actin (15% Oregon Green or Alexa 488-labeled) was mixed with polymerization TIRF buffer [10 mM imidazole (pH 7.0), 50 mM KCl, 1 mM $MgCl_2$, 1 mM EGTA, 50 mM DTT, 0.2 mM ATP, 50 μM $CaCl_2$, 15 mM glucose, 20 μg/mL catalase, 100 μg/mL glucose oxidase, and 0.5% (400 centipoise) methylcellulose] to induce F-actin assembly and any additional actin binding proteins. This mixture was transferred to a flow cell for imaging at room temperature. For two color TIRFM, we cyclically imaged labeled actin (1 frame, 488 nm excitation for 50ms) and SNAP(549)-Ena/VASP (1 frame, 561 nm excitation for 50ms) [182].

2.5.2 D16 cell culture

ML-DmD16-c3 (DGRC, Bloomington, IN) cells were cultured in Schneider's Media with 10% Fetal Bovine Serum (Gibco, Waltham, MA), Anti-Anti (Gibco, Waltham, MA), and 10 μg/mL recombinant human insulin (Gibco, Waltham, MA), transfected with FugeneHD (Promega, Madison, WI), and imaged on extracellular matrix (ECM) coated glass-bottom dishes after 48–72 hr. ECM was harvested from ML-DmD17-c3 (DGRC, Bloomington, IN) [36]. All imaging was performed on a total internal reflection fluorescence (TIRF) system

mounted on an inverted microscope (Ti-E, Nikon, Tokyo, Japan) using a 100X/1.49NA oil immersion TIRF objective driven by Nikon Elements software. Images were captured using an Orca-Flash 4.0 (Hamamatsu, Hamamatsu, Japan) and were processed for brightness and contrast using ImageJ [149] analysis. We quantified >30 cells using CellGeo [172]. Filopodia were quantified with the criteria of >0.78 μm long and <0.91 μm wide.

2.5.3 Plasmid Construction

Enabled (Ena) constructs were prepared by removing the 6x-His tag from the C-terminus of previously described Ena constructs [MBP-SNAP-EnaΔL or MBP-EnaΔL] [182] and insertion into a MBP containing plasmid (pet21A) by standard restriction digest and infusion (Clontech, Mountain View, CA) following PCR amplification (iProof; Bio-Rad, Hercules, California). $\text{Ena}_{\text{Dimer}}$ and $\text{Ena}_{\text{Trimer}}$ constructs were prepared by removing the coiled-coil domain and adding a Foldon domain [57, 121] [MBP-SNAP-EnaΔLΔCC-Foldon] or GCN4 domain [64] [MBP-SNAP-EnaΔLΔCC-GCN4] from MBP-SNAP-EnaΔL. UNC-34 was cloned from worm cDNA and inserted into a pet21A vector with MBP-SNAP (New England Biolabs, Ipswich, MA) at XmaI/PacI sites, while also including a flexible linker (GGSGGS) in the forward primer sequence of SNAP constructs. Singed and VASP constructs were cloned from fly and human cDNA libraries, respectively. VASP was inserted into a MBP-SNAP and SNAP containing vector while Singed was inserted into a pGEX KT Ext plasmid containing GST with a Thrombin cleavage site at XbaI/XhoI sites. Plasmids for transfection of mCherry-EnaΔCC-GCN4 and mCherry-EnaΔCC-Foldon were cloned into a pIZ-mCherry-Ena [12] construct using infusion (Clontech, Mountain View, CA). The RNAi was designed using Primer3Plus [174] targeting the 3' UTR of *enabled* using forward primer 5' TAATACGACTCACTATAGGGAGACCACGTGATGGCATGTGCATAGGC 3' and reverse primer 5' TAATACGACTCACTATAGGGAGACCACTGCTGAAGACTTGCTGGTTC 3'. The 3'UTR was extracted from w1118 strain fly genome and

the DNA region of interest was isolated by PCR amplification and placed in a bluescript SK vector. dsDNA was produced using PCR amplification and dsRNA was produced from the resulting dsDNA using MEGAscript T7 Transcription kit (Invitrogen, Waltham, MA).

2.5.4 Protein Expression and Purification

Recombinant Ena/VASP proteins were purified by expressing in *Escherichia coli* strain BL21-Codon Plus (DE3)-RP (Agilent Technologies, Santa Clara, CA) with 0.25 mM isopropyl β-D-1-thiogalactopyranoside for 16 h at 16 °C. Cells were lysed with an Emulsi-Flex-C3 (Avestin, Ottawa, Canada) in extraction buffer [20 mM TRIS-HCl (pH 8.0), 200 mM NaCl, 10% glycerol, 0.1 mM DTT] with 0.5 μM PMSF and cOmplete, EDTA-free Protease Inhibitor Cocktail (Roche, Basel, Switzerland) and were clarified. The extract was incubated for 1 h at 4 °C with amylose resin (New England Biolabs, Ipswich, MA) and the beads were washed with extraction buffer followed by batch elution with elution buffer [20 mM TRIS-HCl (pH 8.0), 200 mM NaCl, 10% glycerol, 0.1 mM DTT, 40 mM maltose]. Ena/VASP was incubated overnight without and with 1 μM TEV protease to cleave MBP and filtered on an Superdex 200 10/300 GL or Superose 6 Increase 10/300 GL column (GE Healthcare, Little Chalfont, UK) where they eluted as stable oligomers. Ena/VASP constructs were dialyzed against SNAP buffer [20 mM Hepes (pH 7.4), 200 mM KCl, 0.01% NaN3, and 10% Glycerol, and 0.1 mM DTT]. SEC-MALS was performed using DAWN HELEOS II and Optilab T-rEX (Wyatt Technology, Goleta, CA) with a Superdex 200 Increase 10/300 GL column and Akta FPLC (GE Healthcare, Little Chalfont, UK). SEC-MALS data was analyzed using Astra 6.0 (Wyatt Technology, Goleta, CA). SNAP-tagged proteins were labeled with BG-549 (New England Biolabs, Ipswich, MA) following the manufacturers' protocols. Concentrations of SNAP-tagged proteins were determined by densitometry of Coomassie stained bands on SDS/PAGE gels compared with standards or by absorbance at 280 nm. Ena/VASP was flash-frozen in liquid nitrogen and stored at -80°C. N-terminal SNAP and MBP tags

did not affect Ena/VASP's activity. Actin was purified from rabbit skeletal muscle acetone powder (Pel-Freez, Rogers, AR) or self-prepared chicken skeletal muscle acetone powder by a cycle of polymerization and depolymerization and gel filtration [166]. Gel-filtered actin was labeled with Oregon Green [91] or Alexa 488. Human fascin, human α-actinin IV, and *S. pombe* fimbrin were expressed in bacteria and purified as described [178, 161, 98]. Singed was purified in the same manner as previously reported for human fascin [178] except cleavage by thrombin was done off of the column after overnight incubation.

2.5.5 Glass Preparation

Microscope slides and coverslips (#1.5; Fisher Scientific, Waltham, MA) were washed for 30 min with acetone and for 10 min with 95% ethanol, were sonicated for 2 h with Helmanex III detergent (Hellma Analytics, Müllheim, Germany), incubated for 2 h with piranha solution (66.6% H_2SO_4, 33.3% H_2O_2), washed with deionized water, and dried. Glass then was incubated for 18 h with 1 mg/mL mPeg-Silane (5,000 MW) in 95% ethanol, pH 2.0. Parallel strips of double-sided tape were placed on the coverslip to create multiple flow chambers [192].

2.5.6 Calculation of Residence Time and Elongation Rates

To calculate Ena/VASP's residence time on barbed ends, SNAP(549)-Ena/VASP fluorescent spots associated with the barbed end were manually tracked using MTrackJ [104] in ImageJ. Spots that did not move were not scored, because they were assumed to be adsorbed to the glass. Events that contained joined barbed ends with no clear leading or trailing barbed bend were not included in the average lifetime calculation. Residence times for single SNAP(549)-EnaΔL tetramers were determined by fitting a Kaplan-Meier [80] survival curve with a single exponential equation, $f(x) = x_0 * exp^{(-x/\tau)}$ to calculate the average lifetime. Kaplan-Meier survival curves were used to account for processive runs that started before imaging began or

ends after imaging terminated. Log rank statistical significance tests were done using Prism 7 (GraphPad Software, San Diego, CA). Barbed end elongation rates were calculated by measuring filament lengths over time with ImageJ software. Multiple filament lengths were plotted over time and the distribution was fit with a linear equation using KaleidaGraph 4.5 (Synergy Software, Reading, PA). To calculate the number of filaments in a bundle the TIRFM movie was used to follow the history of the filaments. This could most accurately differentiate between two-filament bundles and three or more filament bundles. Due to photobleaching of the filaments over time the actin fluorescence was not used to determine the number of filaments within the bundle.

2.5.7 Fluorescence Spectroscopy

Bulk actin assembly was measured from the fluorescence of pyrene-actin with a Safire2 or Infinite M200 Pro (Tecan Systems, Inc., Männedorf, Switzerland) fluorescent plate reader [116, 192]. Briefly, unlabeled Mg-ATP-actin was preassembled into seeds for 1 hour by adding 50 mM KCl, 1 mM $MgCl_2$, 1 mM EGTA, 10 mM imidazole, pH 7.0. The assay measures the elongation rate of actin by addition of 20% pyrene-labeled Mg-ATP-actin monomers and actin binding proteins to be assayed. Final protein concentrations are indicated in the figure legends.

2.5.8 Sedimentation Assay

A stock solution of 20 μM Mg-ATP actin monomers in 10 mM imidazole (pH 7.0), 30 mM KCl, 1 mM $MgCl_2$, 1 mM EGTA, 0.5 mM DTT, 0.2 mM ATP, and 90 μM $CaCl_2$ were assembled with the addition of any specified bundling proteins and/or Ena construct for 1 h to generate filaments. Any additional specified Ena construct was added and F-actin was then diluted to $5mu$M final concentration for 20 min at 25°C and spun at 100,000 x g (high-speed) at 24°C. Supernatant and pellets were separated by either 15% (GABFAB) or

12.5% (EVH2) SDS–PAGE and stained with Coomassie blue for 30 min, destained for 16 h, and analyzed by densitometry on an Odyssey Infrared Imager (Li-Cor Biosciences, Lincoln, NE).

2.6 Acknowledgements

We thank Elena Solomaha of the University of Chicago BioPhysics Core Facility for performing SEC-MALS and Jonathan Winkelman for cloning VASP and UNC-34. We thank Caitlin Anderson, Katie Homa, Cristian Suarez and other members of the D.R.K. laboratory for helpful discussions. We thank the Drosophila Genomics Resource Center, supported by NIH grant 2P40OD010949, for Drosophila cells. This material is based upon work supported by the National Science Foundation Graduate Research Fellowship under Grant No. DGE-1144082 and DGE-1746045 (to A.J.H.), National Institute for Health's Molecular and Cellular Biology Training Grant T32 GM007183 (to A.J.H.), National Institute for Health's Grant RO1 GM079265 (to D.R.K.), Department of Defense Army Research Office's MURI grant W911NF1410403 (to G.A.V. and D.R.K.), and by the University of Chicago Materials Research Science and Engineering Center, funded by National Science Foundation award DMR-1420709 (to G.A.V. and D.R.K.). Acknowledgement is made to the computational resources provided by the Research Computing Center at The University of Chicago.

2.7 Supplementary Information

2.7.1 Development of kinetic model

In order to test, mechanistically, the hypothesis that avidity of Ena binding multiple actin filaments with multiple arms determines an increase in time spent at the trailing barbed end for fascin-crosslinked bundles, we developed a kinetic model. The model is based on a kinetic Monte Carlo algorithm that at each time step evaluates binding and unbinding probabilities

of each Ena arm for each filament and, accordingly, changes the arm "state". The kinetic Monte Carlo scheme is chosen because it can, in principle, give the exact evolution of the system, in terms of bound and unbound states of each Ena arm over time, thus providing a strong approximation of the sequence of events given individual Ena arm's binding and unbinding rates, with respect to individual filaments. The kinetic model used in this work consisted of the following elementary reactions:

I. Initial binding of an arm of Ena to the barbed end of the trailing filament with a rate of $k^t_{on,1}$

II. At every subsequent step, binding and unbinding of:

   a. an arm of Ena to the barbed end of the trailing filament, with rates $k^t_{on,1}$ and $k^t_{off,1}$

   b. up to two other arms of Ena to the side of the trailing filament, with rates k^t_{on} and k^t_{off}

   c. additional arms of Ena beyond three to the side of the trailing filament, with rates $k^t_{on,4+}$ and $k^t_{off,4+}$

   d. other arms of Ena to the sides of other filaments in the bundle, with rates k^l_{on} and k^l_{off}

In summary, once any arm is bound to the barbed end of the trailing filament, the Ena "molecule" is considered to be in the bound state. The Ena molecule unbinds only when none of its arms are bound to any of the filaments in the bundle. Thus, after initiation of the bound state for an Ena molecule, the arm bound to the barbed end can unbind and bind multiple times before the molecule unbinds. The model was made efficient by only simulating events involving binding and unbinding of the Ena molecule to the barbed end of a trailing filament. Further, we did not intend to calculate the binding rate of the Ena

molecule using the model, and instead optimized the model parameters based on TIRFM data (see below) for calculating the unbinding rates of Ena molecules, and predicting the kinetics of individual Ena arms while the molecule was bound. This gave rise to the following possible scenarios while the Ena molecule is in the bound state.

I. Only one arm is bound to either

   a. the barbed end

   b. the side of the trailing filament

   c. the side of another filament in the bundle

II. Two or more arms are bound

   a. one to the barbed end, others to the side of the same filament

   b. one to the barbed end, others to the side of another filament

   c. one to the barbed end, others to the sides of the same and other filament(s)

   d. some to the side of the same filament and the remaining to the side of another filament

   e. all to the side of the same filament

   f. all to the side of another filament

Model parameters.

Since Ena is a homotetramer, all arms in this work are structurally identical to each other. Hence, not all of the eight kinetic rate constants $k^t_{on,1}$, $k^t_{off,1}$, k^t_{on}, k^t_{off}, $k^t_{on,4+}$, $k^t_{off,4+}$, k^l_{on} and k^l_{off} in the model (Figure 2.11A) are independent. We set $k^t_{on,1} = 0.007$, estimated using the TIRFM measured off rate of 0.109 s^{-1} for Ena, and an equilibrium constant of Ena for the barbed end of 0.8 nM [182]. The model assumes that binding rates of the rest of

the arms to sides of filaments are identical ($k^t_{on} = k^t_{on,4+} = k^l_{on}$), consistent with the idea that avidity results from binding and unbinding of multiple Ena arms to multiple filaments, rather than from different kinetics of individual arms. The corresponding unbinding rates were, however, assumed to be different owing to the following reasons. An arm bound to the barbed end interacts with the barbed end of the filament through its GAB domain and potentially its FAB domain, while an arm bound to the side of a filament interacts only through its FAB domain. Thus, $k^t_{off,1}$ is considered an independent parameter. The number of FAB domain binding sites available on the trailing filament can be assumed to be less than those on leading filaments since it is the shortest filament in the bundle. Thus, k^t_{off} and k^l_{off} are *a priori* considered to be distinct parameters. Our TIRFM data (Figure 2.7B) suggests that the fold increase in processive run length between a trimer and a tetramer binding to a single filament is smaller than the fold increase between a dimer and a trimer. Thus, the fourth arm binding to the same filament is assumed to have different unbinding kinetics represented using the rates $k^t_{off,4+}$. This translates to having an upper limit on the number of arms that can simultaneously bind to a given filament.

Optimization procedure for parameter estimation

With the above assumptions, the number of undetermined parameters to be estimated reduces to five: $k^t_{on,1}$, k^t_{on}, k^t_{off}, $k^t_{off,4+}$ and k^l_{off}. These parameters were estimated using all 9 data points for the processive run length data in Figure 2.7B using the Levenberg-Marquardt algorithm implemented in the MATLAB® function "fsolve". Let $\tau(n, N)$ represent the processive run length of Ena with N arms on the trailing barbed end of a bundle consisting of n actin filaments. The rate ratio vector y is defined as

$$y = [\frac{\tau(1,4)}{\tau(1,2)}, \frac{\tau(1,3)}{\tau(1,2)}, \frac{\tau(2,4)}{\tau(1,4)}, \frac{\tau(2,3)}{\tau(1,3)}, \frac{\tau(2,2)}{\tau(1,2)}, \frac{\tau(4,4)}{\tau(1,4)}, \frac{\tau(4,3)}{\tau(1,3)}, \frac{\tau(4,2)}{\tau(1,2)}] \tag{2.1}$$

the error was then defined as

$$error = [(y_{model} - y_{TIRFM})/y_{TIRFM}]^2 \tag{2.2}$$

and minimized iteratively using the five undetermined parameters. For each iteration, the kinetic model was solved for each pair of $N \in (2, 3, 4)$ and $n \in (1, 2, 4)$ and the corresponding average processive run length (defined below) was calculated. The TIRFM data for $n \geq 3$ in Figure 2.7E, corresponding to three or more filaments in the bundle, was considered to be equivalent to $n = 4$ in the model, consistent with our observation that most bundles in the TIRF data fell between 3 and 5 filaments for an average "large" bundle.

For computational efficiency, we adopted a two-step strategy to obtain the optimum set of parameters. In the first step, we performed error minimization using 50 distinct initial guesses for the parameters and chose six optimized parameter sets with the lowest errors. In the second step, we performed error minimization using 100 sets of initial guesses, each perturbed within $\pm 10\%$ of the average of these six sets from the first step. The parameter set with the least error was chosen as the final set (Table 2.9). A comparison of the rate ratio vectors from the model with corresponding data from TIRFM is shown in Table 2.10. The optimized parameter set was found to predict rate ratios in good agreement with the corresponding ratios from TIRFM data (Figure 2.7E).

Algorithm

Using the values of reaction rates provided in Table 2.9, the system evolved using a Monte Carlo algorithm with a constant time-step implemented in MATLAB®. The states of the arm binding the barbed end and the other arms binding sides of filaments was stored along corresponding columns in a *state* array, with an entry of 0 representing an unbound state and 1 representing a bound state. Each row in the array corresponded to a simulation step. The

identity of the filament in the bundle that each Ena arm bound to was stored in a separate *filamentid* array, with filament identities ranging from 1 to n.

The simulation was initialized with all arms of Ena in the unbound state. At each timestep $t + dt$, a reaction move (either binding or unbinding) and the corresponding rate constants were selected depending on the previous state of the system at timestep t (Figure 2.12A). For example, if the barbed end was bound at timestep t, the unbinding reaction with the rate constant of $k^t_{off,1}$ was selected at timestep $t+dt$. N random numbers were generated, one corresponding to each arm, and compared with the rate constant of the selected reaction move. The move was accepted if the random number was less than the corresponding rate constant times dt, and the entries *state* and *filamentid* arrays were updated accordingly.

Model verification and predictions

The quantities in the model with units of timesteps were converted to real time in seconds by multiplying with a single factor of 5.4374×10^{-3} that accounted for the "timescale" and was chosen to exactly match the processive run length for a dimer on a single filament between the model (defined below) and the TIRFM data (leftmost red bar in Figure 2.7E). For computational efficiency, we used $dt = 0.1$ s. Assuming that any difference in fascin, α-actinin and fimbrin bundles due to spacing between filaments or different interactions should be reflected in the binding and unbinding kinetics, we systematically varied binding/unbinding rates k^l_{on} and k^l_{off} from 0.002 to 0.026 s^{-1}, keeping other model parameters fixed (Figure 2.12B-F). For a single filament, the processive run length of an Ena tetramer is independent from k^l_{on} and k^l_{off} as expected (Figure 2.12B). With more than one filament, the processive run length increases with k^l_{on}, for increasing values of k^l_{off} below ~0.010 s^{-1} (Figure 2.12C) or below ~0.026 s^{-1}(Figure 2.12D). We also systematically changed k^l_{on} and k^l_{off} using dimers and trimers on 3-filament bundles. Similar to the Ena tetramer, the Ena trimer and dimer showed processive run lengths that increased with k^l_{on} for values of k^l_{off} below ~0.014 s^{-1}

(Figure 2.12E-F). In the tested range of values for k^l_{on} and k^l_{off}, the maximum run length with dimers is 3 s (Figure 2.12E) and trimers is 20 s (Figure 2.12F). Our results show that the processive run length is determined by an interplay between the numbers of arms and filaments, and crosslinker effects on binding rates to sides of leading filaments.

Definitions

Processive run length (τ). The Ena molecule binding was considered the beginning of a processive run event (τ_{start}, Figure 2.12A) and unbinding of the Ena molecule (τ_{end}, Figure 2.12A) denoted the end of a processive run event. The processive run length τ was calculated by averaging the difference ($\tau_{start} - \tau_{end}$) across all processive run events observed across 56 independent simulation runs, each consisting of a total of 2×10^6 timesteps (equivalent to ~10000 seconds). For the final data in Figure 2.11B, the total number of processive run events used for averaging varied depending on the number of Ena arms and number of filaments in the bundle. Based on the range in our TIRFM data (Figure 2.7E), the number of events were in the range of $\sim 1.6 \times 10^5$ for $(N = 4, n = 4)$ and 6.8×10^5 for $(N = 2, n = 1)$. The least number of events used in obtaining data in Figure 2.11, $\sim 4.6 \times 10^3$, corresponded to $(N = 6, n = 6)$.

Free arm time (τ^{arm}_{free}). During each processive run event in the model, individual Ena arms bind to and unbind from filaments independently, but according to their specific rates. The average time between consecutive binding events of an average arm was calculated and denoted as τ^{arm}_{free}. A free Ena arm is available to recruit G-actin from the solution and transfer it to the barbed end with an effective rate that should be independent of the number of filaments in the bundle. Further, since each arm is identical, the effective rate should also be independent of the identity of the arm. It should be noted that in the model Ena arms do not have an identity associated with them and are only used as proxies to obtain statistics related to occupied versus unoccupied states of the barbed end and the sides of filaments. A

rapid exchange of an Ena arm bound to the barbed end with an arm bound to the side of a filament is possible but not explicitly accounted for in the model. Thus, though the kinetic model does not explicitly consider filament elongation, τ_{free}^{arm} is assumed to be approximately proportional to the elongation rate through this implicit effective rate at the resolution of the model.

2.7.2 Supplementary Tables

$k^t_{on,1}$	$k^t_{on} = k^t_{on,4+} = k^l_{on}$	$k^t_{off,1}$	k^t_{off}	$k^t_{off,4+}$	k^l_{off}
0.007	0.0122	0.1488	0.0049	0.0055	0.0195

Table 2.9: **Final set of rate constants in the kinetic model (s^{-1}).**

Run length ratios	$\tau(1,4)/\tau(1,2)$	$\tau(1,3)/\tau(1,2)$	$\tau(2,4)/\tau(1,4)$	$\tau(2,3)/\tau(1,3)$	$\tau(2,2)/\tau(1,2)$	$\tau(4,4)/\tau(1,4)$	$\tau(4,3)/\tau(1,3)$	$\tau(4,2)/\tau(1,2)$
y_{model}	8.3240	3.3356	1.6951	1.2305	1.0902	2.9064	1.7222	1.2969
y_{TIRFM}	7.5727	4.4074	1.8333	1.6875	1.2489	2.8947	2.1236	2.0825

Table 2.10: **Comparison of processive run length ratios defined in Eqn. 2.1 from the model and from TIRFM data.**

CHAPTER 3

BUNDLING PROTEINS' DYNAMICS AND EFFECTS ON ACTIN BINDING PROTEINS

3.1 Abstract[1]

This chapter includes work from three papers that are a collaboration with Cristian Suarez, John Winkelman, Jenna Christensen, and Katie Homa in the Kovar lab to understand the role that different bundlers play when it comes to regulating other actin binding proteins. One interest in the Kovar lab is how different proteins sort to the correct F-actin network at the correct time in the cell cycle. All F-actin networks contain at least one crosslinking protein that can link two actin filaments together. These bundling proteins have different kinetics and facilitate different architectures of F-actin. Since bundling proteins can bind along the side of actin filaments and play an important role for a network's architecture, we hypothesized that they would be good candidates for upstream regulators of other actin binding proteins in each network. Furthermore, these bundling proteins can compete or co-operate with each other as well as other actin binding proteins to contribute to the network's architecture.

In the first paper, in collaboration with Cristian Suarez, we were interested in how long, straight filaments of the filopodia can emerge from the dense, branched lamellipodia. We hypothesized that the bundling protein fascin found in filopodia could inhibit Arp2/3 complex branching. In a collaboration with Jon Winkelman, we were interested in studying the competition between fascin and α-actinin that we found is intrinsically determined due to the size of the two bundling proteins. Cristian Suarez and I performed electron microscopy to visualize at a higher resolution the transition state between fascin and α-actinin domains. For the third paper, in collaboration with Jenna Christensen and Katie Homa, we were interested in the mechanism of how *S. Pombe* tropomyosin can facilitate α-actinin to form more

stable bundles. I performed TIRFM with sparsely labeled α-actinin to measure its dynamics on F-actin in the presence or absence of tropomyosin. Cristian Suarez analyzed this TIRF data to calculate the spot density of α-actinin.

Overall these three works contribute to understanding the role that actin binding proteins, and more specifically bundling proteins, can affect the sorting of actin binding proteins to different F-actin networks, potentially driving the distinct properties of each network. I have presented below the data from the collaborations that I had a role collecting and analyzing and focus on the aspects that are relevant to my contribution.

3.2 Introduction

Many bundling proteins bind cooperatively to sides of filaments, meaning that once one bundling protein binds, another of the same protein is more likely to bind in the next available binding site than random chance [183]. This positive feedback mechanism facilitates bundle formation as many bundlers can bind along the length of the two filaments. Additionally, the cooperativity allows continuous domains of the bundlers to form. We were interested in how different bundling proteins sort to different networks and can affect other actin binding protein sorting. We looked at how fascin affects Arp2/3 complex branching, fascin and α-actinin competition creates separate domains, and tropomyosin's impact on α-actinin binding.

Bundling proteins have a large effect on the different architectures of F-actin networks. Depending on their dynamics and size they can dictate the orientation and spacing of fila-

1. Citations for chapter: [1] Cristian Suarez, Jonathan D. Winkelman, Alyssa J. Harker, Patrick M. McCall, Alisha N. Morganthaler, Margaret L. Gardel, David R. Kovar. Reconsitution of lamellipodia to filopodia transition using pure protein. *In preparation.* [2] Jonathan D. Winkelman, Cristian Suarez, Glen M. Hocky, Alyssa J. Harker, Alisha N. Morganthaler, Jenna R. Christensen, Gregory A. Voth, James R. Bartles, and David R. Kovar. Fascin- and α-Actinin-Bundled Networks Contain Intrinsic Structural Features that Drive Protein Sorting. *Current Biology*, 2620:2697-2706, October 2016. [3] Jenna R. Christensen, Kaitlin E. Homa, Alisha N. Morganthaler, Rachel M. Brown, Cristian Suarez, Alyssa J. Harker, Meghan E. O'Connell, and David R. Kovar. Cooperation between Tropomyosin and α-actinin inhibits fimbrin association with actin filament networks in fission yeast. *In preparation for eLife.*

ments in an actin network as well as the stability of the bundles themselves. For example, filopodia and lamellipodia are spatially similar but have very distinct filament orientations [13]. Lamellipodia filaments are branched by Arp2/3 complex and kept short by capping protein. Fimbrin localizes to the lamellipodia and crosslinks these filaments into a dense meshwork. In contrast, filopodia contain long, straight F-actin bundled primarily by fascin [177]. One open question is how Arp2/3 complex is inhibited from nucleating branched filaments on the F-actin within filopodia. The importance of each bundling protein for initiating and maintaining the network to which it localizes remains unclear.

Another difference in network architecture is in stress fibers compared to filopodia. Filaments are narrowly spaced within filopodia [103], while stress fibers have wider spacing due to the main bundling proteins fascin and α-actinin, respectively. Fascin is a small globular bundling protein compared to the extended homodimer α-actinin. We were interested if the intrinsic properties of the bundling proteins themselves could lead to different sorting between bundling proteins and therefore could lead to different architectures within cells.

Recently we found that two *S. Pombe* bundling proteins, fimbrin and α-actinin, can compete only in the presence of an additional side binding protein, tropomyosin. Tropomyosin is a coiled-coil protein that binds along the sides of F-actin and is known to stabilize F-actin as well as affect other actin binding protein binding [127]. The competition between fimbrin and α-actinin in *S. Pombe* is interesting since fission yeast α-actinin is an especially poor bundling protein. Additionally in cells, we see that tropomyosin and alpha-actinin localize to the cytokinetic ring where fimbrin mainly localizes to endocytic actin patches. That tropomyosin can bolster α-actinin's bundling properties and competition against fimbrin could be important for the different network architectures and how different actin binding proteins are sorted.

3.3 Results

3.3.1 Fascin reduces Arp2/3 complex branch density

Long, straight filaments are found in filopodia which emerge from a dense, branched F-actin network called the lamellipodium. Within the lamelliapodium, actin branches are nucleated by Arp2/3 complex and are kept short by capping protein. We were interested in what factors control the sorting between these two networks that are spatially close together but architecturally distinct. To test our hypothesis that fascin plays a role in reducing Arp2/3 complex branching, we used two-color TIRFM to visualize Arp2/3 branches in the presence and absence of red-labeled fascin (Figure 3.1A-B). We then measured branch density in the presence and absence of fascin and normalized it to control branch density in the absence of fascin and for the number of filaments in a bundle (Figure 3.1D). In order to account for small branches that would be nucleated on the sides of fascin-bundled mother filaments and then quickly incorporated into the bundle, we photobleached the actin. This way we could visualize all new growth of actin filaments (Figure 3.1C). We observe a 2-fold decrease in branch density in the presence of fascin. Therefore, fascin could contribute to the lack of Arp2/3 complex-mediated branch formation on F-actin within filopodia, but it cannot completely block branching alone so other factors must be contributing.

3.3.2 Fascin and α-actinin sort to distinct domains

Fascin and α-actinin have very different structures (Figure 3.2A) and bind to actin using different domains. Fascin is a small globular protein containing four β-trefoil domains. In contrast, α-actinin forms a long homodimer using two to four spectrin repeats, depending on the homolog, and binds to actin using CH domains. We originally observed fascin and α-actinin sorting to distinct domains within actin bundles using *in vitro* TIRFM; however, we were interested in seeing the transition state between the two bundling domains at a higher

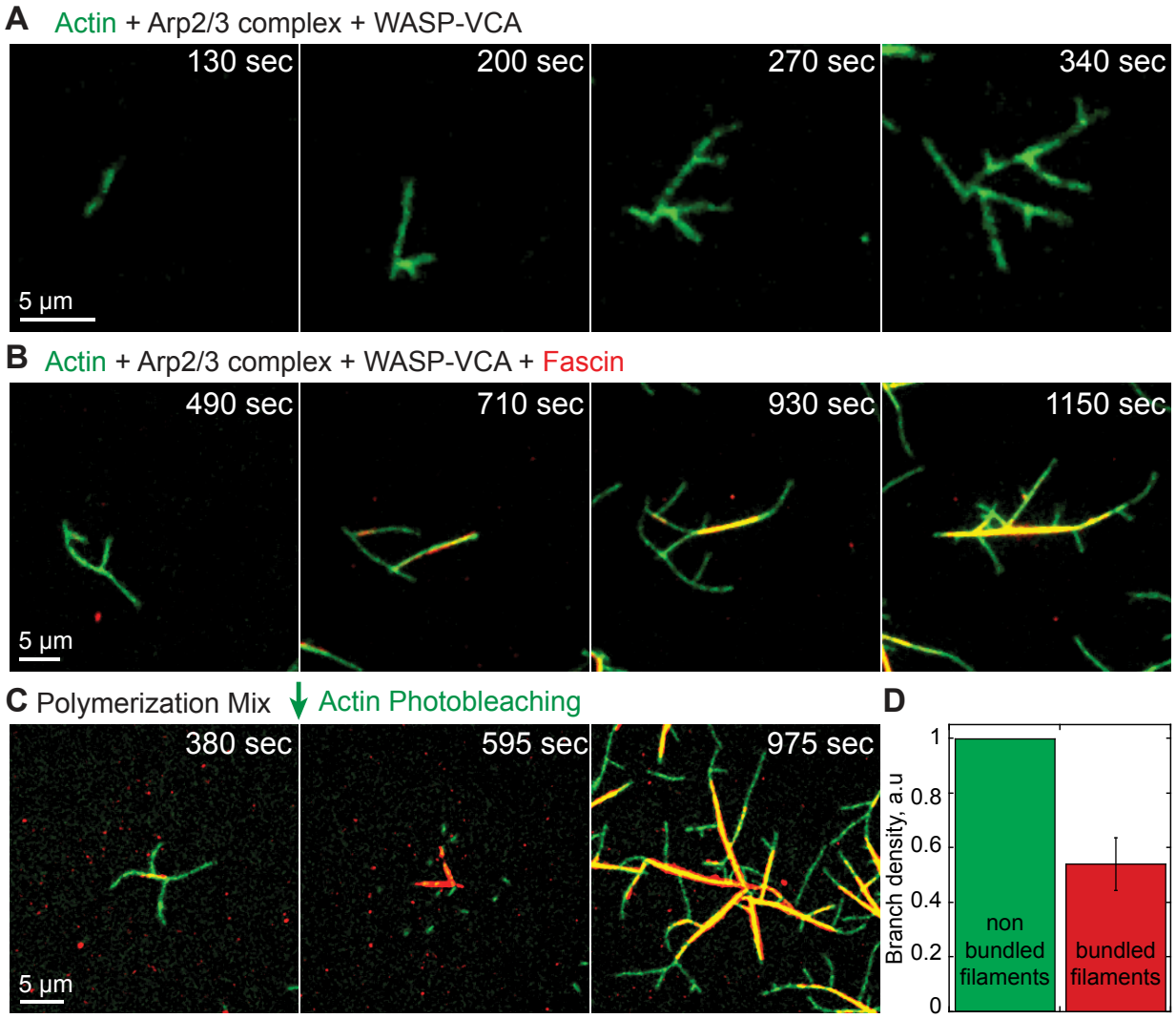

Figure 3.1: **Fascin reduces Arp2/3 complex-mediated branch density** (A-B) Arp2/3 complex-mediated actin polymerization visualized with 1.5 μM Mg-ATP-actin (15% Oregon green labeled) polymerized in the presence of 93 nM Arp2/3 complex, 300 nM WASP-VCA as a NPF, and with or without 500 nM TRM-labeled fascin. Arp2/3 complex-mediated actin branches in absence (A) or presence (B) of fascin. Scale bar 5 μm. (C) 1.5 μM Mg-ATP-actin (15% Oregon green labeled) polymerized in the presence of 50 nM Arp2/3 complex, 100 nM WASP-VCA as a NPF, and 500 nM TRM-labeled fascin. To visualize all barbed ends actin fluorescence was photobleached at t = 380 sec. Scale bar 5 μm. (D) Branch density from single actin filaments and bundled filaments. Error bar, SEM. n = 3. **Figure modified from Suarez et al. in preparation.**

resolution. Therefore, we performed negative-stain electron microscopy (EM) to visualize preformed actin filaments mixed with either fascin or α-actinin alone or both bundling proteins (Figure 3.2B). With fascin alone we see narrow spaced filaments with an interfilament distance of ~8 nm (Figure 3.2D) and a transverse repeat of ~35 nm, which corresponds with one turn of F-actin. α-actinin bundles alone have wider spaced filaments (~32 nm) with a similar transverse repeat of ~35 nm (Figure 3.2C-D). As expected, when both bundlers are mixed together each domain has the characteristics of the respective bundler. The fascin domain is narrow (8 nm) and the α-actinin domain is widely spaced (32 nm) (Figure 3.2C-D). We also observe a transition area (142 $\pm$ 53 nm) between the two domains where the filaments become more widely spaced as you transition from a fascin domain to an α-actinin domain (Figure 3.2B).

3.3.3 Tropomyosin enhances α-actinin dynamics

We recently observed that *S. Pombe* tropomyosin, Cdc8, allows α-actinin, Ain1, to form more stable bundles. Fimbrin, Fim1, can outcompete either tropomyosin and α-actinin to bind to F-actin [31]. However, we discovered that together, α-actinin and tropomyosin are able to overcome fimbrin. To understand the underlying mechanisms of how this cooperation occurs we studied the single molecule dynamics of α-actinin in the presence and absence of tropomyosin using *in vitro* TIRFM. We measured the number of times 0.5% TMR-labeled α-actinin bound F-actin per amount of filament in the presence of polymerizing 1.5 μM Mg-ATP-actin (10% Alexa 488-labeled) and with and without 1 μM unlabeled tropomyosin (Figure 3.3A-B). We found that α-actinin is more dynamic in the presence of tropomyosin. There are 2.3-fold more binding events on F-actin when tropomyosin is also bound (Figure 3.3C). Therefore, tropomyosin enhances α-actinin's association with F-actin and subsequently improves α-actinin's bundling properties.

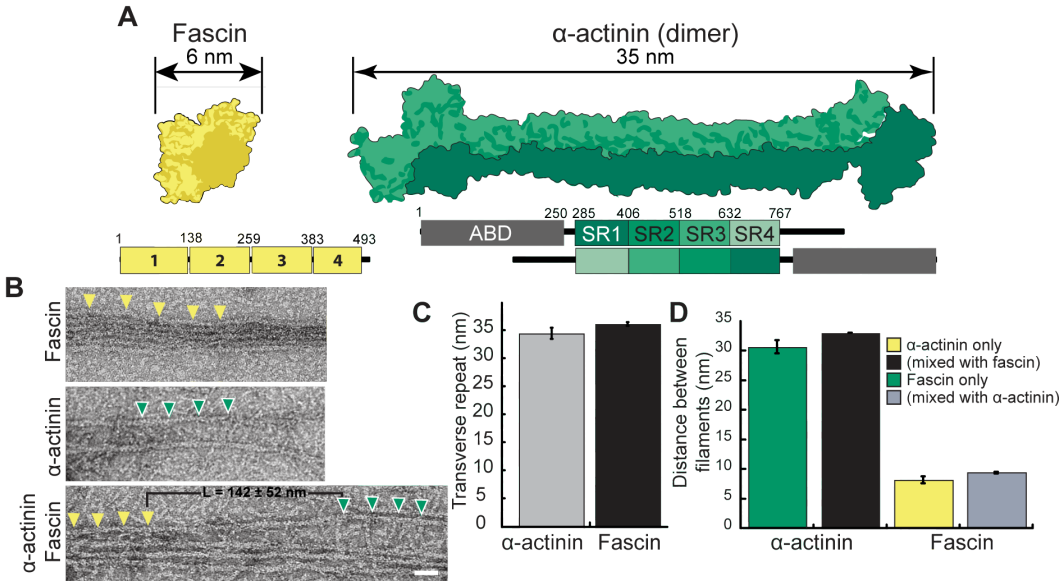

Figure 3.2: **Fascin and α-actinin sort to different domains with different interfilament spacing.** (A) Structural fold (top) and domain organizations (bottom) showing the four β-trefoil domains of fascin (PDB 3P53; [76]) (left) and an α-actinin dimer (PDB 1SJJ; [99]) (right). ABD, Actin-binding domain; SR, spectrin repeat. (B-D) Electron microscopy (EM) of F-actin bundles negatively stained with uranyl acetate, which were formed from 1.5 μM actin. (B) Micrographs of bundles with 1 μM fascin (top), 800 nM α-actinin (middle) or both (1 μM α-actinin and 0.25 μM fascin (bottom). Yellow and green arrowheads indicate fascin and α-actinin molecules, respectively. L is length of transition zone. Scale bar = 30 nm. (C) Distance of transverse repeat in fascin and α-actinin bundles. Error bars indicate SEM; $n \geq 10$ bundles. (D) Distance between filaments in a fascin and α-actinin bundles. Error bars indicate SEM; $n \geq 8$ bundles. **EM in collaboration with Cristian Suarez. Figure modified from [183]**.

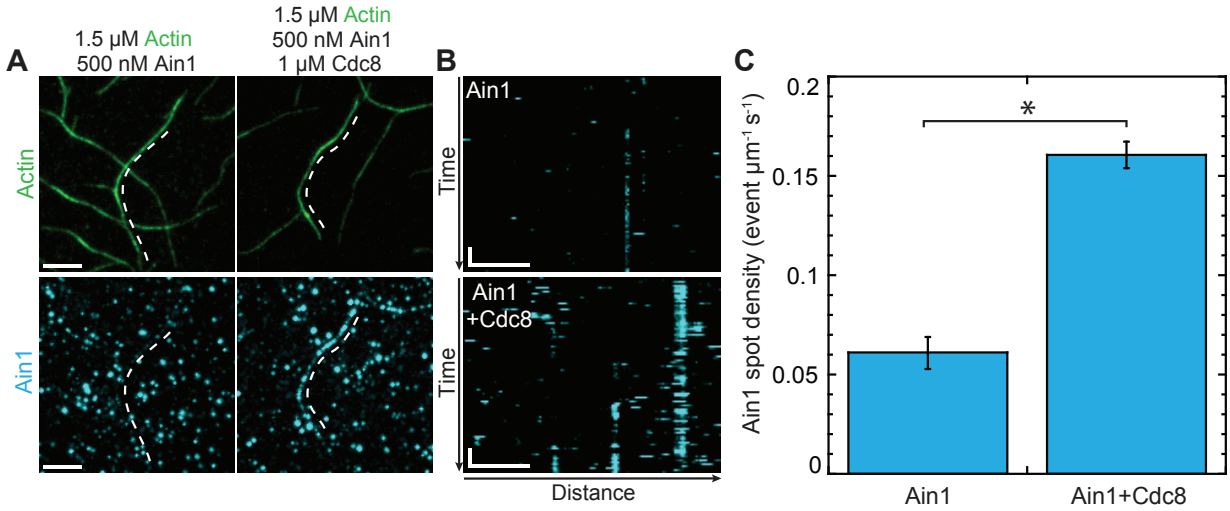

Figure 3.3: **Tropomyosin increases α-actinin dynamics.** TIRFM visualization of 1.5 μM Mg-ATP-actin (10% Alexa 488-actin) with 500 nM 0.5% TMR labeled α-actinin (Ain1), and 1 μM unlabeled tropomyosin (Cdc8). (A) Timelapse micrographs of actin or sparsely labeled α-actinin max projected over 100 frames. Dotted line denotes bundle in both channels. Scale bar, 5 μm. (B) Kymographs of actin bundle length (scale bar, 5 μm) over time (time bar, 10 s) showing α-actinin spot density from E. (C) Quantification of α-actinin spot density in the presence and absence of tropomyosin. Error bars, SEM. n = 2. P value (* = 0.026). **Analysis in collaboration with Cristian Suarez. Figure modified from Christensen et al. in preparation.**

3.4 Materials and Methods

3.4.1 Visualizing Arp2/3 complex branching in TIRFM

TIRFM images were collected at 5 s intervals with a cellTIRF 4Line system (Olympus, Center Valley, PA) fitted to an Olympus IX-71 microscope with through-the-objective TIRF illumination and an iXon EMCCD camera (Andor Technology, Belfast, UK). Mg-ATP-actin (15% Oregon Green-labeled) was mixed with polymerization TIRF buffer [10 mM imidazole (pH 7.0), 50 mM KCl, 1 mM $MgCl_2$, 1 mM EGTA, 50 mM DTT, 0.2 mM ATP, 50 μM $CaCl_2$, 15 mM glucose, 20 μg/mL catalase, 100 μg/mL glucose oxidase, and 0.5% (400 centipoise) methylcellulose] to induce F-actin assembly and Arp2/3 complex and NPF WASP-VCA with or without TMR-labeled (red) fascin was added. This mixture was transferred to a flow cell for imaging at room temperature. For two color TIRFM, we cyclically imaged labeled actin (1 frame, 488 nm excitation for 50ms) and TMR-fascin (1 frame, 561 nm excitation for 50ms). The 488 nm laser at high capacity was used to photobleach actin.

3.4.2 Measuring Arp2/3 complex branch density

First, to calculate the number of filaments in the bundle the fluorescence intensity of actin was recorded for known single filaments 8 frames (40 s) after photobleaching. This was used to calculate the number of filaments in a bundle at this time point by dividing the actin fluorescence by the single filament fluorescence value and was recorded with its corresponding fascin fluorescence value in the 561 channel. The mean gray values for the 561 channel were plotted and a linear equation was fit to calculate the number of filaments in a bundle later in the movie using the TMR-fascin fluorescence. Branch density was calculated from number of observed branches, mean gray value, and length of bundles using TMR-fascin ~5 minutes after photobleaching. The number of branches formed were counted from the end of photobleaching onwards and this number was divided by the total length of the bundle

for branch density. Branches formed before bundling were not counted. The mean gray value was used to calculate the number of filaments in the bundle and this value was used to normalize the branch density to number of filaments.

3.4.3 Visualizing F-actin bundles with negative-stain electron microscopy

Actin (1.5 μM) was polymerized with either 250–500 nM α-actinin, 1–2 μM fascin, or both bundling proteins for 30 min. This solution was then applied to formvar- and carbon-coated 400 mesh copper grids for 1 min, washed, and negatively stained with 1% (w/v) uranyl acetate for 1 min, blotted, and dried. Visualization of the bundles using transmission electron microscopy was performed on an FEI Tecnai G2 Spirit microscope at 120 kV. Images were captured on a Gatan 2k $\times$ 2k CCD camera. Bundle parameters were measured using ImageJ.

3.4.4 Measuring α-actinin Dynamics in TIRFM

TIRFM images were collected with a cellTIRF 4Line system (Olympus, Center Valley, PA) fitted to an Olympus IX-71 microscope with through-the-objective TIRF illumination and an iXon EMCCD camera (Andor Technology, Belfast, UK). 1.5 μM Mg-ATP-actin (10% Alexa 488 labeled) was mixed with polymerization TIRF buffer [10 mM imidazole (pH 7.0), 50 mM KCl, 1 mM $MgCl_2$, 1 mM EGTA, 50 mM DTT, 0.2 mM ATP, 50 μM $CaCl_2$, 15 mM glucose, 20 μg/mL catalase, 100 μg/mL glucose oxidase, and 0.5% (400 centipoise) methylcellulose] to induce F-actin assembly, 0.5 μM 0.5% TMR labeled α-actinin, and 1 μM unlabeled tropomyosin. This mixture was transferred to a flow cell for imaging at room temperature. Once the actin had polymerized and formed bundles we imaged once in the 488 channel to visualize the labeled actin (1 frame, 488 nm excitation for 50ms) and then continuously imaged in the 561 channel to visualize the sparsely labeled α-actinin (100 frames, 561 nm excitation for 50 ms, ~110 ms interval). To measure α-actinin spot density,

we constructed kymographs of bundles for each experiment using ImageJ. α-actinin spots were detected in the kymograph as spots at least 4 pixels wide with fluorescence more than 1.25-fold above background fluorescence. We normalized the spot density to the length of actin filaments present in the bundle by measuring each bundle's length, then multiplying the value by the actin fluorescence ratio between the bundle and single filaments. α-actinin spot density was determined following the formula:

$$\rho = \frac{(n/(L \times r))}{t}$$

Where n is the number of α-actinin spots detected, L the length of the bundle in μm, r the actin fluorescence ratio, and t the time of measurement in seconds.

CHAPTER 4

PATHOGENIC BACTERIA CAN AFFECT THE ENDOGENOUS ACTIN CYTOSKELETON

4.1 Abstract[1]

Vibrio cholera has multiple ways to interfere with a host cell's actin cytoskeletal system. I collaborated on two projects to better understand the different pathways that gram-negative *Vibrio* bacteria can commandeer the actin cytoskeleton. The actin cytoskeleton is an ideal target for pathogenic bacteria for diverse reasons and pathogens target the actin cytoskeleton using different methods. The actin cytoskeleton can be used to prevent or induce the pathogen's phagocytosis as well as facilitate their movement into, around, and out of host cells [100].

The first collaboration with Tom Burke in the Kovar lab focused on the mechanism of actin nucleators, VopL and VopF. These *Vibrio* nucleators assemble actin into unproductive filament within host cells. There were controversial mechanisms proposed for how these proteins were able to nucleate actin filaments and we presented a solution to this controversy, showing that in the presence of physiological conditions that VopL and VopF nucleate and bind to the pointed ends of F-actin. In the second collaboration with the Kudryashov lab at The Ohio State University, I used single-molecule TIRFM to visualize the effect of ACD toxin-formed actin oligomers on Ena/VASP. The Kudryashov lab had previously found that these toxic oligomers affect formin elongation [68], and in this study we expanded to other endogenous actin assembly factors.

Overall these two works contribute to understanding mechanisms for how pathogenic bacteria can interfere with a host's actin cytoskeleton. Understanding how *Vibrio* bacteria can hijack the endogenous actin system allows us to better fight the disease-causing bacteria. I have presented below the data from the collaborations that I had a role collecting and

analyzing and focus on the aspects of the studies that are relevant to my contribution.

4.2 Introduction

Bacterial toxins can effectively compromise a host cell's functions with relatively few molecules, even leading to cell death. These toxins can target signaling cascades (ex. cGMP, adenylate cyclase) or inhibit other enzymes important for cellular processes such as protein synthesis [69]. As the actin cytoskeleton is important for many cellular processes, it is commonly targeted by bacterial toxins. The actin crosslinking domain (ACD) toxins of *Vibrio* species and related bacterial genera are delivered to host cells by type 1 (MARTX toxin) [153] or type VI (VgrG1 toxin) secretion systems [137]. ACD catalyzes formation of actin oligomers through covalent crosslinking of Lys50 in subdomain 2 of an actin monomer with Glu270 in subdomain 3 of another actin monomer by an amide bond [88, 90]. This results in an oligomer that is not suitable for further actin polymerization because the two monomers are oriented similar to actin subunits along the short pitch of an actin filament, except that subdomain 2 has a major twist, disrupting the normal interface for further monomer binding [88].

Surprisingly, though there is a high concentration of actin, only a few ACD molecules are secreted into the host cell. Using *in vitro* determined rates of ACD activity, it would take more than 6 months to covalently crosslink half of all the cytoplasmic actin with a single ACD molecule. This is beyond the timescale for *in vivo* measurements of monolayer disruption [90, 68]. In a previous collaboration with the Kudryashov lab, we found that ACD is effective not by sequestering monomers as previously thought but by using actin

1. Citations for chapter: [1] Thomas A. Burke, Alyssa J. Harker, Roberto Dominguez, and David R. Kovar. The bacterial virulence factors VopL and VopF nucleate actin from the pointed end. *The Journal of Cell Biology*, March 2017. [2] Elena Kudryashova, David B. Heisler, Blake Williams, Alyssa J. Harker, Kyle Shafer, Margot E. Quinlan, David R. Kovar, Dimitrios Vavylonis, and Dmitri S. Kudryashov. Actin Cross-Linking Toxin Is a Universal Inhibitor of Tandem-Organized and Oliogmeric G-Actin Binding Proteins. *Current biology*, 2810:1536-1547.e9, May 2018.

oligomers to target formins [68]. We found that ACD formed toxic actin oligomers that blocked formin-mediated actin polymerization and nucleation. However, the mechanism of how these ACD-formed oligomers block formin activity remains unclear.

Another way that bacteria target the actin cytoskeleton is through type III secretion factors VopF (*Vibrio cholerae*) or VopL (*Vibrio parahaemolyticus*) (VopL/F) [169, 100]. VopL/F contain three tandem WASP homology 2 (WH2) motifs followed by a VopL/F C-terminal Domain (VCD) that facilitates dimerization (Figure 4.2A). This places VopL/F into the class of WH2 nucleators such as cordon-bleu and Spire [138]. The WH2 domain is able to bind to actin monomers in the target-binding cleft between actin subdomains 1 and 3 to facilitate actin filament nucleation [114]. The mechanisms of the WH2 nucleators are not as well studied as other nucleators, Arp2/3 complex and formins.

VopL/F have a 32% sequence identity and 72% sequence similarity and contain the same domain organization, though two competing mechanistic models have been previously proposed. Two groups proposed that VopL nucleates actin filaments from the pointed end and then remains associated with the new filament for only a short time [114, 188] while a third group proposed that VopF binds to the barbed end of growing F-actin and can also sever filaments [126]. In support for the pointed end nucleation model, the crystal structure of VopL in complex with actin was solved and showed that the VCD dimer binds to three actin monomers in an arrangement that is similar to F-actin and allows each actin subunit to bind to a WH2 motif [189]. We set out to clear up this controversy by using single-molecule TIRFM to visualize VopL/F binding to filaments [22].

4.3 Results

4.3.1 Ena/VASP is inhibited by actin crosslinking toxins

Our previous study showed that formin mediated elongation of F-actin is blocked by ACD oligomers in a concentration dependent manner [68]. We measured the IC_{50} of ACD oligomer inhibition of mDia1 to be 1.2 ± 0.6 nM. To further understand the mechanism of how these ACD oligomers affect actin assembly factors we measured their effect on Ena/VASP. We used two-color single-molecule TIRFM to directly visualize the assembly of 1.5 μM Mg-ATP-actin monomers (15% Oregon green-labeled) with 15 pM fluorescently labeled SNAP(549)-EnaΔL (referred to as Ena), 3 μM Chickadee (fly profilin), and an increasing concentration of ACD oligomers (Figure 4.1A-C). We measured the activity of Ena on barbed ends of actin filaments and recorded the barbed end elongation rate while Ena was bound. We found that Ena is affected by the ACD oligomers and will cap filaments, blocking growth (Figure 4.1. We calculated the percentage of capped filaments over a range of ACD oligomers and found that with increasing ACD oligomers, Ena behaved more often as a capping protein than a elongation factor. We also observed that the run length of Ena was much longer when growth of the filament was stopped than while the filament was elongating. This suggests that the oligomers affect Ena's mechanism in a way to reduce the chance of its dissociation from the barbed end.

4.3.2 VopL and VopF assemble endogenous actin

To investigate the molecular mechanism of VopL/F actin nucleation we wanted to directly visualize labeled VopL/F using single-molecule TIRFM. We assembled 1.5 μM Mg-ATP-actin (15% Oregon green-labeled) in the presence of 0.2 nM 549-SNAP-VopL/F to measure the elongation rate of actin filaments and the lifetime of VopL/F bound (Figure 4.2E-F). We observed that in the presence of growing filaments, VopL/F nucleates actin polymerization

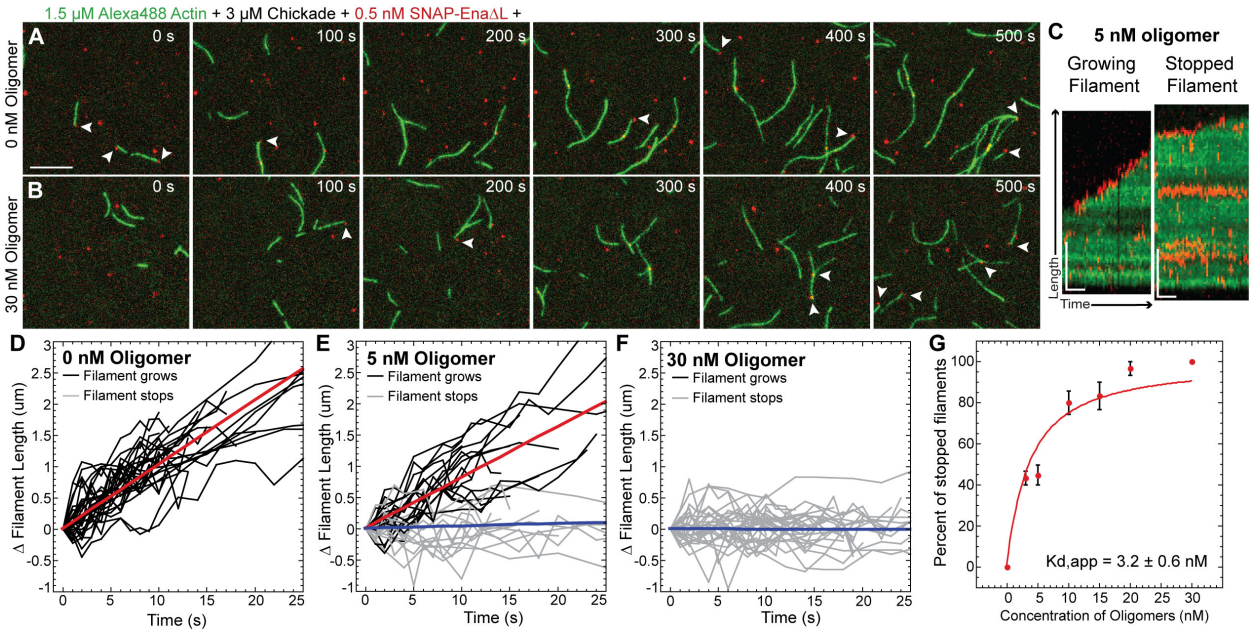

Figure 4.1: **Actin oligomers stop Ena-mediated processive filament elongation.** Two color TIRFM timelapse of 1.5 μM Alexa-488 actin (green) and 0.5 nM SNAP-EnaΔL (red) in the presence of 3 μM Chickadee (fly profilin) and (A) no actin oligomers or (B) 30 nM actin oligomers. Arrows indicate Ena bound barbed ends. Scale bar, 10 μm. Kymographs of a (C) growing Ena bound filament (left) and a stopped Ena bound filament (right). Scale bar, 4 μm and 10 s. Filament elongation traces of Ena bound filaments with (D) 0 nM Oligomers, (E) 5 nM Oligomers, and (F) 30 nM Oligomers. Red fit lines show average growth rates of Ena bound growing filaments and blue fit lines show average growth rates of Ena bound stopped filaments. (G) Kd,app determined by TIRFM by percent of stopped Ena bound filaments over a range of actin oligomers. **Figure modified from [89]**.

and binds to one end of actin filament as the filament continues to elongate. Barbed end associating proteins are known to typically affect the elongation rate of F-actin while they are bound (i.e. formins [84]). Therefore, we measured the elongation rate of VopL/F bound filaments (~13.0 sub/s) and found no difference in elongation rate compared to control filaments (Figure 4.2B-C). We measured the residence time of VopL and VopF to understand its dynamics on ends of filaments. Kaplan-Meier plots were used to calculate the average lifetime of bound VopL/F after nucleating the actin filament. However, since there is dead time required to flow in the reaction (~20 s) and for the time required for nascent filaments to grow long enough to be seen due to the resolution of the microscope (~0.5 μm), we calculated two different residence times. The first residence time (τ_{Obs}) is from the observed timepoint where an actin filament and VopL/F protein are first visualized with TIRFM until the VopL/F protein dissociates from the filament. The second residence time (τ_{Calc}) takes into account how long before the filament is able to be visualized due to the flow delay and resolution of TIRFM. Overall we observe that both VopL and VopF bind to the end of filaments for a similar amount of time using either the observed residence time (VopL_{Obs} τ = 35 s, VopF_{Obs} τ = 27 s) or the calculated residence time ($\text{VopL}_{\text{Calc}}$ τ = 104 s, $\text{VopF}_{\text{Calc}}$ τ = 110 s).

By creating kymographs of the filaments over time we see that VopL/F binds to the pointed, slow-growing end. Another way to identify the pointed end in TIRFM is by using the fluorescence intensity along a filament. Due to photobleaching, the pointed end, which has been assembled for a longer amount of time, is dimmer than the newly assembled actin at the barbed end (Figure 4.2F). We see using linescans that VopL/F associates with this dimmer, pointed end (Figure 4.2H-I). In contrast, formin mDia2, a known barbed end-binding protein, binds to the brighter barbed end (Figure 4.2J). Therefore, VopL/F nucleates filaments and then binds to the dimmer, pointed end of F-actin for ~110 s before dissociating from the filament.

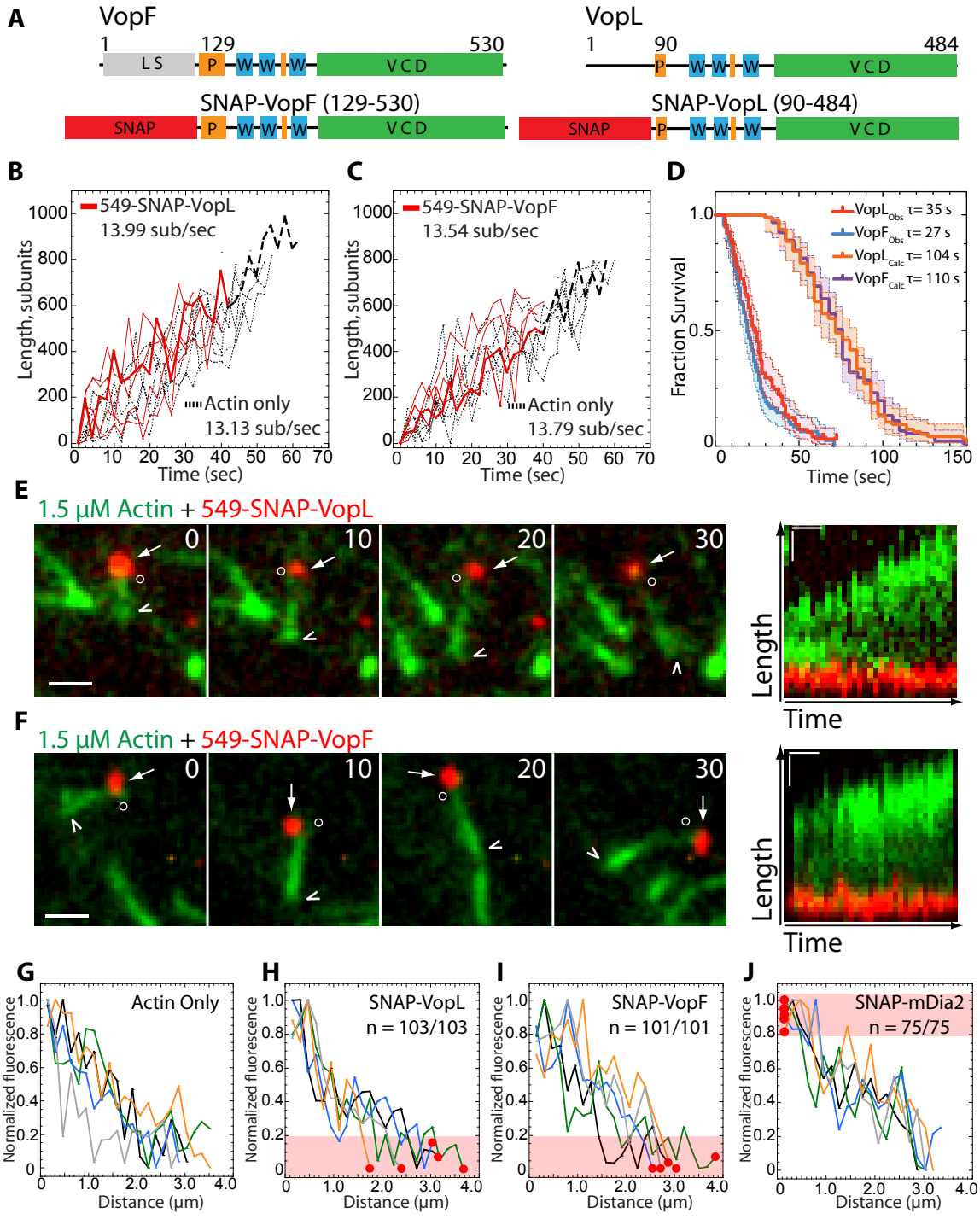

Figure 4.2: **VopL/F nucleate and then remain briefly associated with the pointed end of an actin filament.** (A) Top, domain organization of VopL/F. Orange, proline-rich region (P); blue, WH2 domain (W); green, VCD dimerization domain. Bottom, VopL/F constructs used in this study with SNAP tag (red) for labeling.

Figure 4.2: (continued) (B–J) Slow acquisition (every 2 s, B–D) and rapid acquisition (every second, E–J) two-color TIRFM of the assembly of 1.5 μM Mg-ATP-actin (15% Oregon green actin) with 0.2 nM 549(red)-SNAP-VopL/F. (B and C) Length of individual control (dashed black), 549-SNAP-VopL–associated (B, solid red), or 549-SNAP-VopF-associated (C, solid red) filaments over time ($n \geq 20$). (D) Kaplan–Meier curves representing the mean residence time of 549-SNAP-VopL/F on actin filaments observed (VopL_{Obs}, VopF_{Obs}) or assumed to have been associated because of nucleation ($\text{VopL}_{\text{Calc}}$, $\text{VopF}_{\text{Calc}}$). Error bars indicate 95% CI; $n \geq 90$ events. (E and F, left) Merged timelapse micrographs (in seconds) of individual filaments. White arrowheads and open circles indicate bright and dim filament ends. White arrows indicate 549-SNAP-VopL/F. Scale Bars, 2 μm. (E and F, right) Merged kymographs of filament length (y axis; bar, 1 μm) over time (x axis; bar, 10 s) of the corresponding filaments. (G–J) Linescans of the normalized fluorescence intensity of individual actin filaments measured from their bright to dim (bleached) ends. Red dots indicate position of 549-SNAP-VopL/F or 549-SNAP-mDia2 on the filament traces, and shaded red regions indicate where 100% of VopL/F or mDia2 are bound to the filaments (n $\geq$ 75). **TIRFM, elongation rate, and linescan analysis completed by Tom Burke. Figure modified from [22].**

4.4 Materials and Methods

4.4.1 ACD oligomer and Ena TIRFM

TIRFM images were collected at 1 s intervals with a cellTIRF 4Line system (Olympus, Center Valley, PA) fitted to an Olympus IX-71 microscope with through-the-objective TIRF illumination and an iXon EMCCD camera (Andor Technology, Belfast, UK). Mg-ATP-actin (15% Alexa 488 labeled) was mixed with polymerization TIRF buffer [10 mM imidazole (pH 7.0), 50 mM KCl, 1 mM $MgCl_2$, 1 mM EGTA, 50 mM DTT, 0.2 mM ATP, 50 μM $CaCl_2$, 15 mM glucose, 20 μg/mL catalase, 100 μg/mL glucose oxidase, and 0.5% (400 centipoise) methylcellulose] to induce F-actin assembly and 0.5 nM SNAP(549)-EnaΔL, 3 μM chickadee, and the noted concentration of ACD oligomers. This mixture was transferred to a flow cell for imaging at room temperature. For two color TIRFM, we cyclically imaged labeled actin (1 frame, 488 nm excitation for 50ms) and SNAP(549)-EnaΔL (1 frame, 561 nm excitation for 50ms) [182].

4.4.2 Analysis of Ena/VASP elongation

Barbed end elongation rates were calculated by measuring filament lengths over time with ImageJ software. Measurements of ten filaments with at least 6 length measurements at different time points from three different movies for each condidtion were made. Multiple filament lengths were plotted over time and the distribution was fit with a linear equation using KaleidaGraph 4.5 (Synergy Software, Reading, PA). Filaments were counted as stopped if they had an elongation rate less than 5 sub/s and growing if the elongation rate was greater than 15 sub/s. The apparent Kd was calculated using the following quadratic equation,

$$f(x) = \frac{(x + m1 + 1) - \sqrt{(x + m1 + 1)^2 - 4 * x * 1)}}{2}$$

where m1 was set equal to 1, as the data was normalized from 0 to 1 [131].

4.4.3 Analysis of VopL/F lifetime

Residence times for 549-SNAP-VopL/F on nucleated actin filaments in spontaneous TIRFM assays were determined through back-calculation by measuring the length of actin filaments immediately before the 549-SNAP-VopL/F dissociated and converting that length into total actin subunits (1 μm = 375 subunits). The subunit length was divided by the mean elongation rate of the filaments. Barbed-end elongation rates were calculated by measuring filament lengths over time with ImageJ. Residence times for single 549-SNAP-VopL/F dimers were determined by fitting a Kaplan-Meier [80] survival curve with a single exponential equation, $f(x) = x_0 * exp^{(-x/\tau)}$ to calculate the average lifetime. Kaplan-Meier survival curves were used to account for processive runs that started before imaging began or ended after imaging terminated. Log rank statistical significance tests were done using Prism 7 (GraphPad Software, San Diego, CA). We reported two average lifetimes, one from observed time bound (τ_{Obs}) and other that is calculated accounting for the dead time required to flow

the reaction into the chamber (∼20 s) and for the filaments to reach an observable length (∼0.5 μm) (τ_{Calc}).

CHAPTER 5

CONCLUSIONS AND FUTURE DIRECTIONS

5.1 Ena/VASP's processive mechanism

Initially Ena/VASP was thought to be processive only when clustered together, which was observed *in vitro* with Ena/VASP clustered onto polystyrene beads [18]. With the advancement of imaging technology, further observations of single molecules of Ena/VASP showed short processive runs in solution [61]. Furthermore, previous work in the Kovar lab discovered that Ena/VASP is more processive on trailing barbed ends of fascin bundles [182]. We wanted to further understand this enhanced processivity as well as Ena/VASP's underlying molecular mechanism. Our hypothesis for the enhanced processivity is that the tetrameric Ena/VASP could use its arms that were not actively adding monomer to the barbed end to bind to the sides of surrounding filaments when bound to the barbed end. This would result in the observed longer run lengths on trailing barbed ends.

With the goal of further elucidating Ena/VASP's processive molecular mechanism, we have found that Ena is more processive specifically on trailing barbed ends of fascin bundles. We saw no enhanced processivity on fimbrin or α-actinin bundles, yet we did see enhancement with two homologs of fascin. We also discovered that the number of Ena's arms and the number of filaments within a fascin bundle are both positively correlated with enhanced processivity on trailing barbed ends. This "avidity" effect supports our hypothesis about Ena/VASP's enhanced processivity. Furthermore, we tested two other Ena/VASP homologs, human VASP and *C. elegans* UNC-34, and saw the same trend with increasing processivity with increasing fascin bundle size. We tested the effect of our oligomerization mutants, $\text{Ena}_{\text{Dimer}}$ and $\text{Ena}_{\text{Trimer}}$, and saw that cells transfected with the mutants produced significantly less filopodia than wildtype $\text{Ena}_{\text{Tetramer}}$. This result suggests that the oligomerization of Ena/VASP into tetramers is important for its function within filopodia

initiation and maintenance.

Ena/VASP's molecular mechanism still contains some gaps in understanding. One interesting question revolves around the role that each Ena/VASP arm plays during filament elongation. These arms could all be equal players in adding monomer as well as binding sides of filaments or certain arms could be designated for each activity (Figure 5.1). This designation need not be by chemical modification, though that is possible in cells. Rather, it could be a random distribution of arms that initially bind either monomer or the sides of filaments, and once these arms are designated by initial binding they do not switch during that processive run. Another possibility is that the arms all fulfill each role, but they do it within the same rotation. For example, an arm could bind a monomer and this begins the process of first adding the monomer to the barbed end, then binding the elongating filament sides, then searching space for either nearby filament sides or if none are available, another actin monomer to start the process over again. Furthermore, if this is the standard process of the arms, how often interruptions to the rotation occur would be important to elucidate. This would lead to understanding the efficiency of Ena/VASP-mediated elongation.

Another open question is whether Ena/VASP follows along the actin's helical pitch as it elongates. Formin has been shown to rotate as it processively elongates [107]. Since both proteins processively track the barbed end, it is unclear whether rotation along the actin helix is necessary. The structural differences between formin and Ena/VASP (FH2 ring vs. four floppy arms) suggest that it would be harder for Ena/VASP to coordinate following the actin helical pitch. Additionally, since Ena/VASP is thought to cluster in cells and elongate bundled actin filaments it would not leave room for rotation of either the Ena/VASP or the actin filaments. If Ena/VASP did not need to rotate to elongate F-actin it could be one way that Ena/VASP and formin differentiate between activities in cells. However, if rotation is necessary for Ena/VASP's processive elongation it would open up many new questions on its mechanism as well as its function in cells.

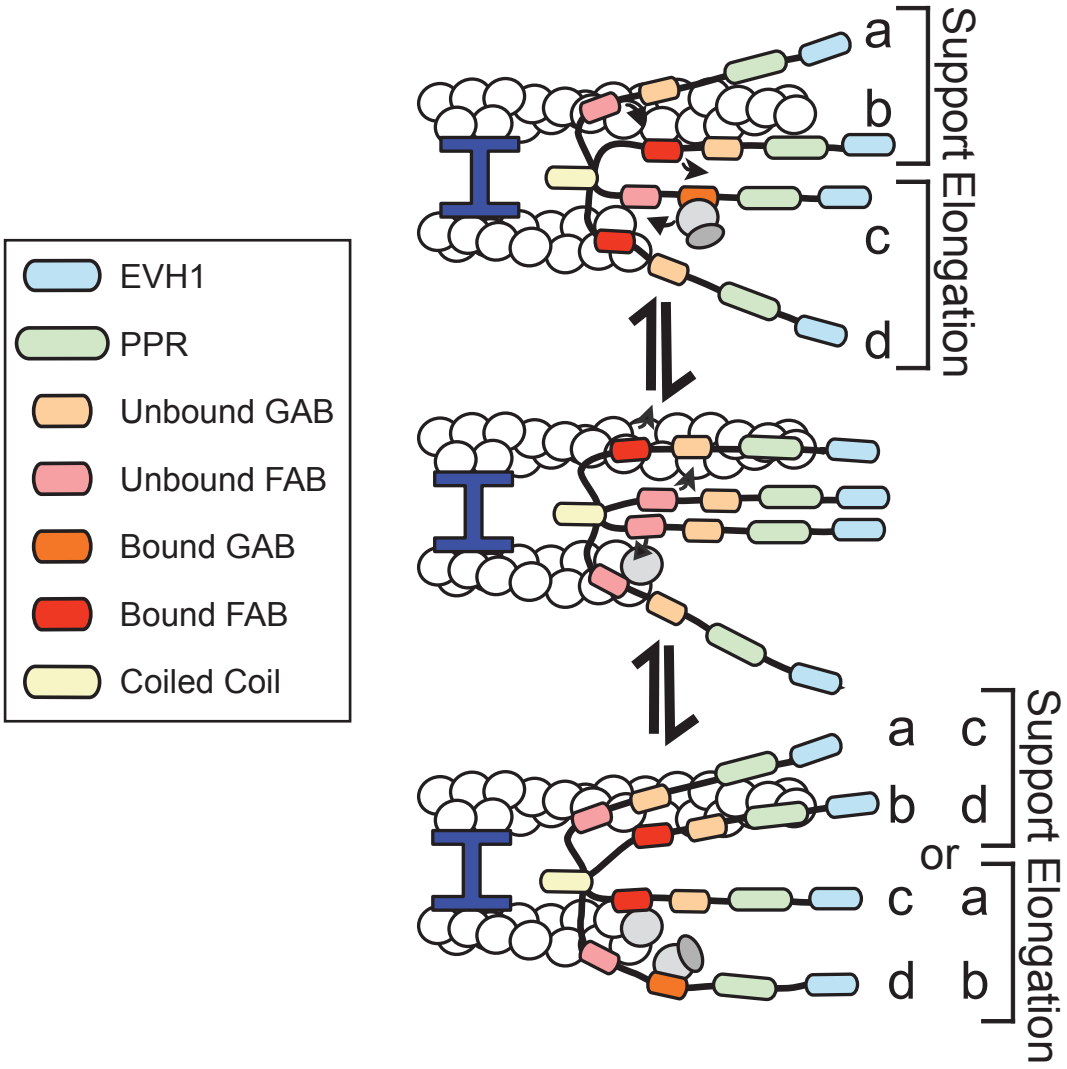

Figure 5.1: **Switching arms in Ena/VASP's molecular mechanism.** Cartoon model showing Ena/VASP adding new actin monomers on the trailing barbed end. The cartoon shows additional arms are able to bind to the trailing or leading actin filament with the dark red FAB domains. The dark orange shows when the monomer is bound to the GAB domain. Light colored domains are unbound GAB/FAB domains. Numbered arms show possibility of all arms being equal elongation contributors or two arms being dedicated for elongation and two arms dedicated for binding surrounding filaments.

Recent studies of Ena/VASP have opened new questions about Ena/VASP tetramerization. Brühmann et al. showed elongation and processivity are different for chimeric VASP oligomerization mutants on single filaments [21]. Here, we showed that processivity is positively correlated with both the number of Ena arms and number of filaments in a fascin bundle. We further tested the Ena oligomerization mutants' ability to form filopodia in *Drosophila* culture cells and found that they had reduced ability compared to a wildtype tetramer. These results suggest that a tetramer is better at both elongation of F-actin and staying associated with the barbed end compared to dimer and trimers. Additionally, *in vivo* we see that a tetramer is more efficient at forming filopodia. Evolutionarily, having tetrameric ENa/VASP could have given cells an advantage over cells having Ena/VASP with lesser oligomerization states.

Furthermore, Brühmann et al. showed that higher oliogmers were better than tetramers for VASP-mediated elongation and barbed end processivity on single filaments. However, Ena/VASP does not form a higher oligomer, which suggests there could be a reason that evolution halted at a tetramer. One simple argument is that producing a functional molecule from six versus four monomers puts more strain on the cell for protein production. However, with our kinetic model we also measured a proxy for Ena/VASP-mediated elongation, τ_{free}^{arm}, or the time that an arm is free to bind actin monomers from solution. This measurement showed decreasing returns with higher oligomers of Ena/VASP on bundled filaments. Therefore, this could add an additional explanation for why higher oligomers of Ena/VASP did not evolve. We hypothesize that an Ena/VASP tetramer lies at an ideal spot that allows for efficient elongation and processivity on F-actin, but does not require more protein production to form active molecules that do not give cells an advantage, at least within the bundled filopodia.

5.2 Ena/VASP's role in filopodia formation

Following the convergent elongation model of filopodia initiation [168], barbed ends at the leading edge must be protected from capping protein so that these filaments can continue to elongate. Ena/VASP has been shown to compete with capping proteins for barbed ends [2, 7, 182], and having longer processive runs should also lead to better competition against capping protein during filopodia initiation. Thus these protected filaments can then continue to grow faster through Ena/VASP-mediated elongation. Once the filaments are bundled by fascin, Ena/VASP would "target" shorter filaments within the filopodial bundle because of its enhanced processivity on trailing barbed ends. This would protect shorter filaments in the bundle for a longer time against capping protein as well as increase their length faster through Ena/VASP-mediated elongation. Therefore, in a mature filopodia, the filaments would all be the same length and Ena/VASP would be localized to the tip.

Beyond Ena/VASP's role in protecting trailing filaments, Ena/VASP can also be clustered in the tip complex to continue to elongate filaments. Many open questions remain about how this process works in cells, and clarifying what roles Ena/VASP plays within the process and what roles are its main function is needed. Within different cell types and even within different types of filopodia within a cell this mechanism can vary. Formin likely also plays a role within convergent elongation in most cell types, so understanding how formin and Ena/VASP cooperate within this process and their concurrent regulation opens up interesting questions. These two different types of processive polymerases are mechanistically interesting to compare and contrast to understand how different proteins maintain actin filament contact as well as how they are regulated within the cell. Understanding their individual functions as well as how they work together will give a clearer picture of what is happening at filopodia and the leading edge of the cell. Ena/VASP is also known to localize to other locations within cells such as sites of stress fiber repair and focal adhesions, but is not found to be required in these processes. It could be playing a different role at these locations since fascin bundles

are not prevalent. In summary, bundling proteins could regulate actin binding proteins throughout the cell so that they preform their proper function within each actin network to which they localize.

Though Ena/VASP has been shown to compete with capping protein, the mechanism for competition is not known. Ena/VASP is thought to occlude the barbed end by sterically blocking capping protein from binding to the barbed end. Similarly, previous genetic and biochemical work suggested that formins and capping protein were entirely antagonistic [87]. However, recent studies using single-molecule TIRFM have shown that a "decision complex" of both capping protein and formin can be found at the barbed end. Two different formins, mDia1 and FMNL2, can form a decision complex with capping protein and it binds for a set amount of time before one protein gains sole control [14, 155]. These studies open up the possibility that Ena/VASP can also share the barbed end with capping protein in another sort of decision complex. Since Ena/VASP and formin are both involved in filopodia formation and capping protein competition it would be important to understand how the formin/capping protein decision complex responds to Ena/VASP. It is possible that Ena/VASP could help formin gain control, or even become a part of the decision complex at the barbed end. Following up these different interactions between the various barbed end binding proteins will be necessary for fully understanding processes happening at the leading edge as well as filopodia formation.

Another notable aspect of Ena/VASP's activity is its ability to use both profilin-actin and free actin monomers to facilitate F-actin elongation. It is known that Ena/VASP GAB domains bind more strongly to profilin-actin than free actin monomers [29], yet this could be a way to regulate the activity of formin-mediated filopodia formation versus Ena/VASP. Recently, it was shown that profilin is antagonistic to Arp2/3 complex as Arp2/3 complex is more efficient using free actin monomers over profilin-actin [167, 146]. Since formins are more efficient at facilitating actin elongation with profilin-actin compared to Ena/VASP, perhaps

its when profilin-actin is low that both Arp2/3 complex and Ena/VASP activity is preferred in the cell over formin activity. Yet, since Ena/VASP is still able to use profilin-actin more efficiently than free actin monomers, it could also cooperate with formins using profilin-actin. It would be interesting to measure the efficiency of profilin-actin versus free actin use by Ena/VASP and formins that are thought to bind and work together at the leading edge. In this case both proteins could use profilin-actin, but depending on the differences in affinity and efficiency of adding profilin-actin to F-actin between the two proteins, formins could predominantly use profilin-actin where Ena/VASP would be subjugated to using free-actin monomer. Adding in different profilin isoforms could expand further the complex balance of how the elongating and nucleating proteins utilize profilin-actin. Ena/VASP and formin can both differentially use different profilin isoforms [61, 112, 157], so understanding their perferred source of actin monomer and how this source is distributed between Ena/VASP, formin, and Arp2/3 will further our understanding of actin polymerization at the leading edge.

5.3 Regulation with actin filament bundling proteins

One major discovery in my work has been that different actin bundling proteins can regulate the binding of actin elongation factors at the barbed end of the actin filament. We found the Ena/VASP has enhanced processivity on trailing barbed ends of multiple homologs of fascin bundles, but not fimbrin or α-actinin bundles. Though we do not yet know the mechanism behind this regulation, it suggests that all bundled networks are not created equally and this is due to a property of the bundle itself. Further support for bundling proteins regulating other actin binding proteins is that we have shown bundling proteins intrinsically sort into domains, separating by their intrinsic spacing. [183]. In this case, fimbrin and fascin sort to their narrowly-spaced bundle regions while α-actinin sorts to its own wider spaced bundled regions. In both of these situations we see differentiation of protein activity,

either Ena processivity or bundler localization, due to an intrinsic property of a bundling protein. Though this differentiation is most likely not due to the same intrinsic property of the bundler since we see different sized bundlers failing to enhance Ena's processivity, these results do contribute to the possibility that bundling proteins can regulate a wide range of different actin binding proteins and their dynamics within different actin networks.

The mechanism of how fascin contributes to Ena's enhanced processivity on trailing barbed ends is still unknown. In our study we were able to test if fascin facilitates a specific spacing or polarity of filaments that allows Ena to bind longer. We found that having fascin-like spacing or polarity was not sufficient to enhance Ena's processivity. Direct binding of fascin does not seem likely since Ena needs to track the barbed end of the growing trailing filament and Ena's enhanced processivity is consistent with increasing fascin concentration. Additionally, there are no known Ena binding domains within fascin. Another possibility is that fascin is holding a filament in a certain twist or reducing the filament's natural range of helical twist. An actin filament has a measured twist, but EM studies have shown that actin filaments actually fall within a range of degrees of twist. Fascin could reduce or shift the range of degrees that the actin can explore. One study did find that fascin has a slight rotation of the filament, but this rotation was only a single degree, which is not thought to be a large enough scale to affect actin binding proteins [32]. A final possibility is that fascin bundles closer to the growing end of the trailing barbed end which holds the trailing barbed end closer to the side of the leading filament, allowing Ena to use the leading filament sides as additional binding sites. If fimbrin and α-actinin allow for more flexibility of the trailing barbed end away from the leading filament, this could explain why only fascin is able to enhance Ena's processivity. Using higher resolution microscopy such as atomic force microscopy (AFM) could measure how rapidly the growing trailing barbed end is bundled with different bundling proteins. Since we measured that Ena has a longer lifetime only on the sides of fascin bundles, our hypothesis is differences in binding to the side of F-actin is

the root of Ena's enhanced processivity on trailing barbed ends. This could be tested by making mutations within the FAB domain to reduce side binding and measuring any changes to Ena's processivity. Testing these different possibilities for how fascin is able to regulate Ena will give deeper understanding into Ena's molecular mechanism and also give insight into Ena's role in filopodia, as fascin is the predominant bundling protein in filopodia.

Though we have found that bundling proteins can regulate a wide variety of actin binding proteins, we have also shown that other side binding proteins can in return affect the dynamics of bundling proteins. This suggests that though bundling proteins could regulate the sorting and activity of many actin binding proteins to form different actin networks, there are still upstream actin binding proteins that could regulate the bundling proteins as well. One example that we found is that tropomyosin helps *S. Pombe* α-actinin form more stable bundles. Using single-molecule TIRFM we saw that tropomyosin increases α-actinin's dynamics on actin bundles. However, we also previously found that fimbrin can outcompete tropomyosin as it bundles F-actin [31]. We also recently found that fimbrin can compete off α-actinin. However, both tropomyosin and α-actinin can compete against fimbrin. This is a complex regulation network where tropomyosin can help one bundling protein, while being removed by another. Interestingly both α-actinin and fimbrin use the same CH domain to bind to actin and bind actin in the same region. The molecular and structural mechanism of how tropomyosin binding to F-actin can assist one bundling protein and be removed by another is still an open question.

Our studies of different bundling proteins have shown that they can regulate different protein's localization and activity. It is important to understand how the bundling proteins are able to regulate different actin binding proteins, perhaps without any direct interaction. One possibility is that long range effects of the bundling could cause changes in other actin binding proteins. One recent study has proposed that different bundling proteins can have long range effects of the actin filament [173]. Also understanding how different actin bundling

proteins are regulated by typical signaling molecules as well as other actin binding proteins will be important for understanding how different actin networks are built at certain times and locations within the cell. Targeting bundling proteins for further investigation of their effects on different actin network formation is ideal since bundling proteins can bind along the sides of actin filaments, which increases the number of binding sites and can dramatically impact an actin network's architecture.

5.4 Actin bundling proteins and their effect on convergent elongation

Interestingly, we have found that the same bundling protein that allows for longer processive runs of Ena is also the main bundling protein in the actin network that is formed of long, straight parallel bundles, filopodia. Fascin is important for filopodia formation, but may play a role beyond just forming F-actin bundles that can create force to extend the cell membrane [177, 26]. Fascin bundles within the nascent filopodia could regulate Ena/VASP to allow for increased processivity on trailing barbed ends within the bundle. This increased processivity would allow for better inhibition of capping protein and longer filaments, allowing the trailing barbed ends to catch up to the leading barbed ends.

Moreover, another protein we've found to be regulated by fascin bundling is Arp2/3 complex, which is another player within filopodia formation via the convergent elongation model. The convergent elongation model proposes that actin filaments found in filopodia are initially nucleated by Arp2/3 complex. However, within a filopodium itself there is no branching of actin filaments, which raises the question of how Arp2/3 complex is inhibited along the filopodial filaments. We found that fascin bundles facilitate a decrease in Arp2/3 complex-mediated branching. Although fascin does not completely inhibit branching, it does significantly reduce Arp2/3 complex-mediated branching 2-fold. This suggests that fascin could play a role in inhibiting Arp2/3 complex, but it is not sufficient on its own

to completely stop branching. Therefore, another factor must be in play to stop Arp2/3 complex from forming branches off the sides of filopodia filaments.

Ena/VASP was shown to have anti-branching properties in early studies [10, 129, 147, 163]. However, recent studies have found that VASP can bind to the NPF WAVE complex and enhance Arp2/3 complex-mediated actin assembly [28, 66]. Though these results seem contradictory, both of these activities could be taking place depending on the localization of Ena/VASP to the leading edge with WAVE complex, or within filopodia bundles. Further investigation is needed to understand how Ena/VASP is functioning at the leading edge and within filopodia, especially related to its relationship to Arp2/3 complex and its NPFs.

5.5 Pathogenic bacteria target the host actin cytoskeleton

Actin is a good target for pathogenic bacteria as the actin cytoskeleton plays many vital roles within cells. ACD toxin-mediated actin oligomers can regulate endogenous actin assembly proteins, such as Ena/VASP and Arp2/3 complex. The oligomers bind to these proteins' actin binding domains but cannot be formed into F-actin. In the presence of the oligomers, actin elongating proteins such as formin and Ena/VASP turn into capping proteins. This can be explained by either the actin binding domains having a higher affinity for the oligomers compared to G-actin or, if the affinity is equalivalent, that the addition of free actin monomer to F-actin is the main pathway for release of actin monomers from the elongation factor's actin binding domains. Since the oligomers cannot be added to a filament in this situation, they remain bound to the actin binding domains. However, when observing Ena in the presence of ACD actin oligomers it appeared that Ena binds much longer to filaments when actin assembly is stopped in the presence of actin oligomers than during normal elongation. How the oligomer can maintain the association of Ena with the barbed end is not clear. Understanding how the oligomer is binding to Ena/VASP and affecting its assembly properties would give, not only insight into the ACD toxin's mechanism, but also

the mechanism of Ena/VASP. Interestingly, VopL/F which are *Vibrio* nucleating proteins also fall victim to ACD oligomers. The ratio of VopL/F compared to all the endogenous actin assembly proteins could be small enough that the side effect of blocking VopL/F is not detrimental, yet understanding how these two processes work in tandem within cells will be important for a complete picture of *Vibrio* bacteria's pathogenic mechanism.

In our study of VopL/F we found that the concentration of profilin, and such the free monomer available for nucleation, affects VopL/F's binding localization along the filament [22]. With saturating profilin we still see a majority of VopL/F nucleating from the pointed end, but do see some (<15%) molecules binding to the barbed end as well. Additionally, when no actin monomers are present VopL/F can bind to the barbed end of pre-assembled filaments for 25-30 s, which is much shorter than they stay bound to the pointed end during nucleation, 110 s. This switching of activity in the presence or absence of free actin monomer suggests that VopL/F can bind to actin monomers, profilin-actin, and F-actin. To fully understand how these molecules choose these different binding partners we must carefully measure the affinity. The TIRFM experiments suggest that VopL/F bind the strongest to actin monomers, followed by profilin-actin, and finally F-actin. VopL/F has been suggested to be structurally similar to Ena/VASP proteins and this switching of activity suggests that VopL/F's WH2 domains could act as a GAB or FAB domain. Comparing the structure and binding of Ena/VASP's GAB and FAB domain with VopL/F's WH2 domains could give an overall categorization of how WH2-like domains bind to actin differently when in different forms (i.e. G-actin, profilin-actin, F-actin).

5.6 Concluding Remarks

We have further elucidated the molecular mechanism of Ena/VASP on single and bundled filaments and found that Ena/VASP has enhanced processivity specifically on trailing barbed ends of fascin bundles. This shows a novel mechanism for regulation of actin assembly

proteins mediated by actin bundling proteins. We have also seen that fascin bundling can reduce Arp2/3 complex-mediated branching. Both of these processes are regulated by fascin and may be important for filopodia formation via the convergent elongation model. Further observations that two different bundling proteins, α-actinin and fascin, sort to different domains due to an intrinsic spacing property adds to the importance of actin bundling proteins for regulating actin binding proteins in general. In addition, these actin bundling proteins can be regulated by other proteins as well, such as we have found with tropomyosin increasing *S. Pombe* α-actinin's dynamics. Overall actin binding proteins are ideal targets for pathogenic bacteria and we have found actin assembly proteins such as Ena/VASP are targeted by ACD toxin-mediated actin oligomers. Studying the actin binding proteins of the pathogenic bacteria, such as VopL/F, can give us not only insight into their disease causing mechanisms, but also how they are related to a host cell's actin binding proteins. Here, I've shown that understanding how different actin binding proteins regulate other proteins' activities and affect their molecular mechanisms is a complicated goal, yet in the past years and from work shown here great strides have been made to understand down to a molecular level how these hundreds of proteins function to form the diverse actin networks that are necessary for vital cellular processes.

References

[1] S. M. Ahern-Djamali, C. Bachmann, P. Hua, S. K. Reddy, A. S. Kastenmeier, U. Walter, and F. M. Hoffmann. Identification of profilin and src homology 3 domains as binding partners for Drosophila enabled. *Proceedings of the National Academy of Sciences of the United States of America*, 96(9):4977–4982, April 1999.

[2] Derek A. Applewhite, Melanie Barzik, Shin-Ichiro Kojima, Tatyana M. Svitkina, Frank B. Gertler, and Gary G. Borisy. Ena/VASP proteins have an anti-capping independent function in filopodia formation. *Molecular Biology of the Cell*, 18(7):2579–2591, July 2007.

[3] Christiane Bachmann, Lieselore Fischer, Ulrich Walter, and Matthias Reinhard. The EVH2 Domain of the Vasodilator-stimulated Phosphoprotein Mediates Tetramerization, F-actin Binding, and Actin Bundle Formation. *Journal of Biological Chemistry*, 274(33):23549–23557, August 1999.

[4] Linda J. Ball, Jarchau Thomas, Oschkinat Hartmut, and Walter Ulrich. EVH1 domains: structure, function and interactions. *FEBS Letters*, 513(1):45–52, December 2001.

[5] Linda J. Ball, Ronald Kühne, Berit Hoffmann, Angelika Häfner, Peter Schmieder, Rudolf Volkmer-Engert, Martin Hof, Martin Wahl, Jens Schneider-Mergener, Ulrich Walter, Hartmut Oschkinat, and Thomas Jarchau. Dual epitope recognition by the VASP EVH1 domain modulates polyproline ligand specificity and binding affinity. *The EMBO Journal*, 19(18):4903–4914, September 2000.

[6] Francesca Bartolini, James B. Moseley, Jan Schmoranzer, Lynne Cassimeris, Bruce L. Goode, and Gregg G. Gundersen. The formin mDia2 stabilizes microtubules independently of its actin nucleation activity. *The Journal of Cell Biology*, 181(3):523–536, May 2008.

[7] Melanie Barzik, Tatyana I. Kotova, Henry N. Higgs, Larnele Hazelwood, Dorit Hanein, Frank B. Gertler, and Dorothy A. Schafer. Ena/VASP proteins enhance actin polymerization in the presence of barbed end capping proteins. *The Journal of Biological Chemistry*, 280(31):28653–28662, August 2005.

[8] Melanie Barzik, Leslie M. McClain, Stephanie L. Gupton, and Frank B. Gertler. Ena/VASP regulates mDia2-initiated filopodial length, dynamics, and function. *Molecular Biology of the Cell*, 25(17):2604–2619, September 2014.

[9] James E. Bear and Frank B. Gertler. Ena/VASP: towards resolving a pointed controversy at the barbed end. *Journal of Cell Science*, 122(12):1947–1953, June 2009.

[10] James E. Bear, Tatyana M. Svitkina, Matthias Krause, Dorothy A. Schafer, Joseph J. Loureiro, Geraldine A. Strasser, Ivan V. Maly, Oleg Y. Chaga, John A. Cooper, Gary G. Borisy, and Frank B. Gertler. Antagonism between Ena/VASP proteins and actin filament capping regulates fibroblast motility. *Cell*, 109(4):509–521, May 2002.

[11] Peter M. Benz, Constanze Blume, Stefanie Seifert, Sabine Wilhelm, Jens Waschke, Kai Schuh, Frank Gertler, Thomas Münzel, and Thomas Renné. Differential VASP phosphorylation controls remodeling of the actin cytoskeleton. *J Cell Sci*, 122(21):3954–3965, November 2009.

[12] Colleen G. Bilancia, Jonathan D. Winkelman, Denis Tsygankov, Stephanie H. Nowotarski, Jennifer A. Sees, Kate Comber, Iwan Evans, Vinal Lakhani, Will Wood, Timothy C. Elston, David R. Kovar, and Mark Peifer. Enabled Negatively Regulates Diaphanous-Driven Actin Dynamics In Vitro and In Vivo. *Developmental Cell*, 28(4):394–408, February 2014.

[13] Laurent Blanchoin, Rajaa Boujemaa-Paterski, Cécile Sykes, and Julie Plastino. Actin Dynamics, Architecture, and Mechanics in Cell Motility. *Physiological Reviews*, 94(1):235–263, January 2014.

[14] Jeffrey P. Bombardier, Julian A. Eskin, Richa Jaiswal, Ivan R. Corrêa, Ming-Qun Xu, Bruce L. Goode, and Jeff Gelles. Single-molecule visualization of a formin-capping protein 'decision complex' at the actin filament barbed end. *Nature Communications*, 6:8707, 2015.

[15] Thomas Bornschlögl. How filopodia pull: What we know about the mechanics and dynamics of filopodia. *Cytoskeleton*, 70(10):590–603, October 2013.

[16] Dennis Breitsprecher and Bruce L. Goode. Formins at a glance. *J Cell Sci*, 126(1):1–7, January 2013.

[17] Dennis Breitsprecher, Richa Jaiswal, Jeffrey P. Bombardier, Christopher J. Gould, Jeff Gelles, and Bruce L. Goode. Rocket launcher mechanism of collaborative actin assembly defined by single-molecule imaging. *Science (New York, N.Y.)*, 336(6085):1164–1168, June 2012.

[18] Dennis Breitsprecher, Antje K. Kiesewetter, Joern Linkner, Claus Urbanke, Guenter P. Resch, J. Victor Small, and Jan Faix. Clustering of VASP actively drives processive, WH2 domain-mediated actin filament elongation. *The EMBO Journal*, 27(22):2943–2954, November 2008.

[19] Dennis Breitsprecher, Antje K. Kiesewetter, Joern Linkner, Marlene Vinzenz, Theresia E. B. Stradal, John Victor Small, Ute Curth, Richard B. Dickinson, and Jan Faix. Molecular mechanism of Ena/VASP-mediated actin-filament elongation. *The EMBO Journal*, 30(3):456–467, February 2011.

[20] N. P. Brindle, M. R. Holt, J. E. Davies, C. J. Price, and D. R. Critchley. The focal-adhesion vasodilator-stimulated phosphoprotein (VASP) binds to the proline-rich domain in vinculin. *The Biochemical Journal*, 318 (Pt 3):753–757, September 1996.

[21] Stefan Brühmann, Dmitry S. Ushakov, Moritz Winterhoff, Richard B. Dickinson, Ute Curth, and Jan Faix. Distinct VASP tetramers synergize in the processive elongation of

individual actin filaments from clustered arrays. *Proceedings of the National Academy of Sciences*, 114(29):E5815–E5824, July 2017.

[22] Thomas A. Burke, Alyssa J. Harker, Roberto Dominguez, and David R. Kovar. The bacterial virulence factors VopL and VopF nucleate actin from the pointed end. *The Journal of Cell Biology*, March 2017.

[23] Keith Burridge and Christophe Guilluy. Focal adhesions, stress fibers and mechanical tension. *Experimental Cell Research*, 343(1):14–20, April 2016.

[24] E. Butt, K. Abel, M. Krieger, D. Palm, V. Hoppe, J. Hoppe, and U. Walter. cAMP- and cGMP-dependent protein kinase phosphorylation sites of the focal adhesion vasodilator-stimulated phosphoprotein (VASP) in vitro and in intact human platelets. *The Journal of Biological Chemistry*, 269(20):14509–14517, May 1994.

[25] Kenneth G. Campellone and Matthew D. Welch. A Nucleator Arms Race: Cellular Control of Actin Assembly. *Nature reviews. Molecular cell biology*, 11(4):237–251, April 2010.

[26] Kelly Cant, Brenda A. Knowles, Mark S. Mooseker, and Lynn Cooley. Drosophila singed, a fascin homolog, is required for actin bundle formation during oogenesis and bristle extension. *The Journal of Cell Biology*, 125(2):369–380, April 1994.

[27] M. F. Carlier and D. Pantaloni. Direct evidence for ADP-Pi-F-actin as the major intermediate in ATP-actin polymerization. Rate of dissociation of Pi from actin filaments. *Biochemistry*, 25(24):7789–7792, December 1986.

[28] Xing Judy Chen, Anna Julia Squarr, Raiko Stephan, Baoyu Chen, Theresa E. Higgins, David J. Barry, Morag C. Martin, Michael K. Rosen, Sven Bogdan, and Michael Way. Ena/VASP proteins cooperate with the WAVE complex to regulate the actin cytoskeleton. *Developmental Cell*, 30(5):569–584, September 2014.

[29] David Chereau and Roberto Dominguez. Understanding the role of the G-actin-binding domain of Ena/VASP in actin assembly. *Journal of Structural Biology*, 155(2):195–201, August 2006.

[30] Ekta Seth Chhabra and Henry N. Higgs. INF2 Is a WASP Homology 2 Motif-containing Formin That Severs Actin Filaments and Accelerates Both Polymerization and Depolymerization. *Journal of Biological Chemistry*, 281(36):26754–26767, September 2006.

[31] Jenna R. Christensen, Glen M. Hocky, Kaitlin E. Homa, Alisha N. Morganthaler, Sarah E. Hitchcock-DeGregori, Gregory A. Voth, and David R. Kovar. Competition between Tropomyosin, Fimbrin, and ADF/Cofilin drives their sorting to distinct actin filament networks. *eLife*, 6, 2017.

[32] Mireille M. A. E. Claessens, Mark Bathe, Erwin Frey, and Andreas R. Bausch. Actin-binding proteins sensitively mediate F-actin bundle stiffness. *Nature Materials*, 5(9):748–753, September 2006.

[33] J. A. Cooper, E. L. Buhle, S. B. Walker, T. Y. Tsong, and T. D. Pollard. Kinetic evidence for a monomer activation step in actin polymerization. *Biochemistry*, 22(9):2193–2202, April 1983.

[34] Naomi Courtemanche, Ja Yil Lee, Thomas D. Pollard, and Eric C. Greene. Tension modulates actin filament polymerization mediated by formin and profilin. *Proceedings of the National Academy of Sciences of the United States of America*, 110(24):9752–9757, June 2013.

[35] Naomi Courtemanche and Thomas D. Pollard. Interaction of Profilin with the Barbed End of Actin Filaments. *Biochemistry*, 52(37):6456–6466, September 2013.

[36] Joshua D. Currie and Stephen L. Rogers. Using the Drosophila melanogaster D17-c3 cell culture system to study cell motility. *Nature Protocols*, 6(10):1632–1641, September 2011.

[37] Pascale Daou, Salma Hasan, Dennis Breitsprecher, Emilie Baudelet, Luc Camoin, Stéphane Audebert, Bruce L. Goode, and Ali Badache. Essential and nonredundant roles for Diaphanous formins in cortical microtubule capture and directed cell migration. *Molecular Biology of the Cell*, 25(5):658–668, March 2014.

[38] E. M. De La Cruz and T. D. Pollard. Nucleotide-free actin: stabilization by sucrose and nucleotide binding kinetics. *Biochemistry*, 34(16):5452–5461, April 1995.

[39] Roberto Dominguez. Actin filament nucleation and elongation factors – structure–function relationships. *Critical Reviews in Biochemistry and Molecular Biology*, 44(6):351–366, October 2009.

[40] Roberto Dominguez and Kenneth C. Holmes. Actin Structure and Function. *Annual review of biophysics*, 40:169–186, June 2011.

[41] Julian von der Ecken, Mirco Müller, William Lehman, Dietmar J. Manstein, Pawel A. Penczek, and Stefan Raunser. Structure of the F-actin–tropomyosin complex. *Nature*, 519(7541):114–117, March 2015.

[42] Marc Edwards, Adam Zwolak, Dorothy A. Schafer, David Sept, Roberto Dominguez, and John A. Cooper. Capping protein regulators fine-tune actin assembly dynamics. *Nature Reviews. Molecular Cell Biology*, 15(10):677–689, October 2014.

[43] Robert A. Edwards and Joseph Bryan. Fascins, a family of actin bundling proteins. *Cell Motility and the Cytoskeleton*, 32(1):1–9, January 1995.

[44] J. Faix, D. Breitsprecher, T. E.B Stradal, and K. Rottner. Filopodia: Complex models for simple rods. *The International Journal of Biochemistry & Cell Biology*, 41(8-9):1656–1664, 2009.

[45] Jan Faix and Klemens Rottner. The making of filopodia. *Current Opinion in Cell Biology*, 18(1):18–25, February 2006.

[46] Alexander A. Fedorov, Elena Fedorov, Frank Gertler, and Steven C. Almo. Structure of EVH1, a novel proline-rich ligand-binding module involved in cytoskeletal dynamics and neural function. *Nature Structural & Molecular Biology*, 6(7):661–665, July 1999.

[47] François Ferron, Grzegorz Rebowski, Sung Haeng Lee, and Roberto Dominguez. Structural basis for the recruitment of profilin-actin complexes during filament elongation by Ena/VASP. *The EMBO journal*, 26(21):4597–4606, October 2007.

[48] Kenneth N. Fish. Total Internal Reflection Fluorescence (TIRF) Microscopy. *Current protocols in cytometry / editorial board, J. Paul Robinson, managing editor ... [et al.]*, 0 12:Unit12.18, October 2009.

[49] Tinya Fleming, Shih-Chieh Chien, Pamela J. Vanderzalm, Megan Dell, Megan K. Gavin, Wayne C. Forrester, and Gian Garriga. The role of C. elegans Ena/VASP homolog UNC-34 in neuronal polarity and motility. *Developmental Biology*, 344(1):94–106, August 2010.

[50] C. Frieden. Polymerization of actin: mechanism of the Mg2+-induced process at pH 8 and 20 degrees C. *Proceedings of the National Academy of Sciences of the United States of America*, 80(21):6513–6517, November 1983.

[51] F. B. Gertler, J. S. Doctor, and F. M. Hoffmann. Genetic suppression of mutations in the Drosophila abl proto-oncogene homolog. *Science*, 248(4957):857–860, May 1990.

[52] Frank B Gertler, Kirsten Niebuhr, Matthias Reinhard, Jürgen Wehland, and Philippe Soriano. Mena, a Relative of VASP and Drosophila Enabled, Is Implicated in the Control of Microfilament Dynamics. *Cell*, 87(2):227–239, October 1996.

[53] Bruce L. Goode and Michael J. Eck. Mechanism and Function of Formins in the Control of Actin Assembly. *Annual Review of Biochemistry*, 76(1):593–627, 2007.

[54] Christopher J. Gould, Sankar Maiti, Alphée Michelot, Brian R. Graziano, Laurent Blanchoin, and Bruce L. Goode. The formin DAD domain plays dual roles in autoinhibition and actin nucleation. *Current biology: CB*, 21(5):384–390, March 2011.

[55] Stephanie L. Gupton and Frank B. Gertler. Filopodia: the fingers that do the walking. *Science's STKE: signal transduction knowledge environment*, 2007(400):re5, August 2007.

[56] Pinar S. Gurel, Mu A, Bingqian Guo, Rui Shu, Dale F. Mierke, and Henry N. Higgs. Assembly and turnover of short actin filaments by the formin INF2 and profilin. *The Journal of Biological Chemistry*, 290(37):22494–22506, September 2015.

[57] Sarah Güthe, Larisa Kapinos, Andreas Möglich, Sebastian Meier, Stephan Grzesiek, and Thomas Kiefhaber. Very Fast Folding and Association of a Trimerization Domain from Bacteriophage T4 Fibritin. *Journal of Molecular Biology*, 337(4):905–915, April 2004.

[58] M. Halbrügge and U. Walter. Analysis, purification and properties of a 50,000-dalton membrane-associated phosphoprotein from human platelets. *Journal of Chromatography*, 521(2):335–343, November 1990.

[59] Cheri M. Hampton, Dianne W. Taylor, and Kenneth A. Taylor. Novel structures for α-actinin: F-actin interactions and their implications for actin-membrane attachment and tension sensing in the cytoskeleton. *Journal of molecular biology*, 368(1):92–104, April 2007.

[60] Dorit Hanein, Niels Volkmann, Sharon Goldsmith, Anne-Marie Michon, William Lehman, Roger Craig, David DeRosier, Steve Almo, and Paul Matsudaira. An atomic model of fimbrin binding to F-actin and its implications for filament crosslinking and regulation. *Nature Structural & Molecular Biology*, 5(9):787–792, September 1998.

[61] Scott D. Hansen and R. Dyche Mullins. VASP is a processive actin polymerase that requires monomeric actin for barbed end association. *The Journal of Cell Biology*, 191(3):571–584, November 2010.

[62] Jean Hanson and J. Lowy. The structure of F-actin and of actin filaments isolated from muscle. *Journal of Molecular Biology*, 6(1):46–IN5, January 1963.

[63] Birgit Harbeck, Stefan Hüttelmaier, Kathrin Schlüter, Brigitte M. Jockusch, and Susanne Illenberger. Phosphorylation of the Vasodilator-stimulated Phosphoprotein Regulates Its Interaction with Actin. *Journal of Biological Chemistry*, 275(40):30817–30825, October 2000.

[64] P. B. Harbury, T. Zhang, P. S. Kim, and T. Alber. A switch between two-, three-, and four-stranded coiled coils in GCN4 leucine zipper mutants. *Science*, 262(5138):1401–1407, November 1993.

[65] M. Amanda Hartman and James A. Spudich. The myosin superfamily at a glance. *J Cell Sci*, 125(7):1627–1632, April 2012.

[66] Svitlana Havrylenko, Philippe Noguera, Majdouline Abou-Ghali, John Manzi, Fahima Faqir, Audrey Lamora, Christophe Guérin, Laurent Blanchoin, and Julie Plastino. WAVE binds Ena/VASP for enhanced Arp2/3 complex–based actin assembly. *Molecular Biology of the Cell*, 26(1):55–65, January 2015.

[67] Ernest G. Heimsath and Henry N. Higgs. The C Terminus of Formin FMNL3 Accelerates Actin Polymerization and Contains a WH2 Domain-like Sequence That Binds Both Monomers and Filament Barbed Ends. *The Journal of Biological Chemistry*, 287(5):3087–3098, January 2012.

[68] D. B. Heisler, E. Kudryashova, D. O. Grinevich, C. Suarez, J. D. Winkelman, K. G. Birukov, S. R. Kotha, N. L. Parinandi, D. Vavylonis, D. R. Kovar, and D. S. Kudryashov. ACD toxin-produced actin oligomers poison formin-controlled actin polymerization. *Science*, 349(6247):535–539, July 2015.

[69] James S. Henkel, Michael R. Baldwin, and Joseph T. Barbieri. Toxins from bacteria. *EXS*, 100:1–29, 2010.

[70] Jessica L. Henty-Ridilla, Aneliya Rankova, Julian A. Eskin, Katelyn Kenny, and Bruce L. Goode. Accelerated actin filament polymerization from microtubule plus ends. *Science*, 352(6288):1004–1009, May 2016.

[71] Chiharu Higashida, Tai Kiuchi, Yushi Akiba, Hiroaki Mizuno, Masahiro Maruoka, Shuh Narumiya, Kensaku Mizuno, and Naoki Watanabe. F- and G-actin homeostasis regulates mechanosensitive actin nucleation by formins. *Nature Cell Biology*, 15(4):395–405, April 2013.

[72] Henry N. Higgs. Formin proteins: a domain-based approach. *Trends in Biochemical Sciences*, 30(6):342–353, June 2005.

[73] Catarina C F Homem and Mark Peifer. Exploring the roles of diaphanous and enabled activity in shaping the balance between filopodia and lamellipodia. *Molecular Biology of the Cell*, 20(24):5138–5155, December 2009.

[74] Alan K. Howe, Brian P. Hogan, and R. L. Juliano. Regulation of Vasodilator-stimulated Phosphoprotein Phosphorylation and Interaction with Abl by Protein Kinase A and Cell Adhesion. *Journal of Biological Chemistry*, 277(41):38121–38126, October 2002.

[75] H. E. Huxley. Electron Microscope Studies on the Structure of Natural and Synthetic Protein Filaments from Striated Muscle. *Journal of Molecular Biology*, 7:281–308, September 1963.

[76] Silvia Jansen, Agnieszka Collins, Changsong Yang, Grzegorz Rebowski, Tatyana Svitkina, and Roberto Dominguez. Mechanism of Actin Filament Bundling by Fascin. *Journal of Biological Chemistry*, 286(34):30087–30096, August 2011.

[77] P. Jenö, T. Mini, S. Moes, E. Hintermann, and M. Horst. Internal sequences from proteins digested in polyacrylamide gels. *Analytical Biochemistry*, 224(1):75–82, January 1995.

[78] Antoine Jégou, Marie-France Carlier, and Guillaume Romet-Lemonne. Formin mDia1 senses and generates mechanical forces on actin filaments. *Nature Communications*, 4:1883, 2013.

[79] Fan Kang, Roney O. Laine, Michael R. Bubb, Frederick S. Southwick, and Daniel L. Purich. Profilin Interacts with the Gly-Pro-Pro-Pro-Pro-Pro Sequences of Vasodilator-Stimulated Phosphoprotein (VASP): Implications for Actin-Based Listeria Motility. *Biochemistry*, 36(27):8384–8392, July 1997.

[80] E. L. Kaplan and Paul Meier. Nonparametric Estimation from Incomplete Observations. *Journal of the American Statistical Association*, 53(282):457–481, 1958.

[81] Michael G Klein, Wuxian Shi, Udupi Ramagopal, Yiider Tseng, Denis Wirtz, David R Kovar, Christopher J Staiger, and Steven C Almo. Structure of the Actin Crosslinking Core of Fimbrin. *Structure*, 12(6):999–1013, June 2004.

[82] Andreas Klostermann, Beat Lutz, Frank Gertler, and Christian Behl. The Orthologous Human and Murine Semaphorin 6a-1 Proteins (SEMA6a-1/Sema6a-1) Bind to the Enabled/Vasodilator-stimulated Phosphoprotein-like Protein (EVL) via a Novel Carboxyl-terminal Zyxin-like Domain. *Journal of Biological Chemistry*, 275(50):39647–39653, December 2000.

[83] E. D. Korn, M. F. Carlier, and D. Pantaloni. Actin polymerization and ATP hydrolysis. *Science (New York, N.Y.)*, 238(4827):638–644, October 1987.

[84] David R Kovar. Molecular details of formin-mediated actin assembly. *Current Opinion in Cell Biology*, 18(1):11–17, February 2006.

[85] David R. Kovar, Elizabeth S. Harris, Rachel Mahaffy, Henry N. Higgs, and Thomas D. Pollard. Control of the Assembly of ATP- and ADP-Actin by Formins and Profilin. *Cell*, 124(2):423–435, January 2006.

[86] David R. Kovar and Thomas D. Pollard. Insertional assembly of actin filament barbed ends in association with formins produces piconewton forces. *Proceedings of the National Academy of Sciences of the United States of America*, 101(41):14725–14730, October 2004.

[87] David R. Kovar, Jian-Qiu Wu, and Thomas D. Pollard. Profilin-mediated Competition between Capping Protein and Formin Cdc12p during Cytokinesis in Fission Yeast. *Molecular Biology of the Cell*, 16(5):2313–2324, May 2005.

[88] Dmitri S. Kudryashov, Zeynep A. Oztug Durer, A. Jimmy Ytterberg, Michael R. Sawaya, Inna Pashkov, Katerina Prochazkova, Todd O. Yeates, Rachel R. Ogorzalek Loo, Joseph A. Loo, Karla J. Fullner Satchell, and Emil Reisler. Connecting actin monomers by iso-peptide bond is a toxicity mechanism of the Vibrio cholerae MARTX toxin. *Proceedings of the National Academy of Sciences*, 105(47):18537–18542, November 2008.

[89] Elena Kudryashova, David B. Heisler, Blake Williams, Alyssa J. Harker, Kyle Shafer, Margot E. Quinlan, David R. Kovar, Dimitrios Vavylonis, and Dmitri S. Kudryashov. Actin Cross-Linking Toxin Is a Universal Inhibitor of Tandem-Organized and Oligomeric G-Actin Binding Proteins. *Current biology*, 28(10):1536–1547.e9, May 2018.

[90] Elena Kudryashova, Caitlin Kalda, and Dmitri S. Kudryashov. Glutamyl phosphate is an activated intermediate in actin crosslinking by actin crosslinking domain (ACD) toxin. *PloS One*, 7(9):e45721, 2012.

[91] Jeffrey R. Kuhn and Thomas D. Pollard. Real-time measurements of actin filament polymerization by total internal reflection fluorescence microscopy. *Biophysical Journal*, 88(2):1387–1402, February 2005.

[92] Karin Kuhnel, Thomas Jarchau, Eva Wolf, Ilme Schlichting, Ulrich Walter, Alfred Wittinghofer, and Sergei V. Strelkov. The VASP tetramerization domain is a right-handed coiled coil based on a 15-residue repeat. *Proceedings of the National Academy of Sciences of the United States of America*, 101(49):17027–17032, December 2004.

[93] Adam V. Kwiatkowski, Frank B. Gertler, and Joseph J. Loureiro. Function and regulation of Ena/VASP proteins. *Trends in Cell Biology*, 13(7):386–392, July 2003.

[94] Sonja Kühn, Constanze Erdmann, Frieda Kage, Jennifer Block, Lisa Schwenkmezger, Anika Steffen, Klemens Rottner, and Matthias Geyer. The structure of FMNL2-Cdc42 yields insights into the mechanism of lamellipodia and filopodia formation. *Nature Communications*, 6:7088, 2015.

[95] Anja Lambrechts, Adam V. Kwiatkowski, Lorene M. Lanier, James E. Bear, Joel Vandekerckhove, Christophe Ampe, and Frank B. Gertler. cAMP-dependent Protein Kinase Phosphorylation of EVL, a Mena/VASP Relative, Regulates Its Interaction with Actin and SH3 Domains. *Journal of Biological Chemistry*, 275(46):36143–36151, November 2000.

[96] Lorene M Lanier, Monte A Gates, Walter Witke, A. Sheila Menzies, Ann M Wehman, Jeffrey D Macklis, David Kwiatkowski, Philippe Soriano, and Frank B Gertler. Mena Is Required for Neurulation and Commissure Formation. *Neuron*, 22(2):313–325, February 1999.

[97] Lorene M Lanier and Frank B Gertler. From Abl to actin: Abl tyrosine kinase and associated proteins in growth cone motility. *Current Opinion in Neurobiology*, 10(1):80–87, February 2000.

[98] Yujie Li, Jenna R. Christensen, Kaitlin E. Homa, Glen M. Hocky, Alice Fok, Jennifer A. Sees, Gregory A. Voth, and David R. Kovar. The F-actin bundler α-actinin Ain1 is tailored for ring assembly and constriction during cytokinesis in fission yeast. *Molecular Biology of the Cell*, 27(11):1821–1833, June 2016.

[99] Jun Liu, Dianne W. Taylor, and Kenneth A. Taylor. A 3-D reconstruction of smooth muscle alpha-actinin by CryoEm reveals two different conformations at the actin-binding region. *Journal of Molecular Biology*, 338(1):115–125, April 2004.

[100] Amy D. B. Liverman, Hui-Chun Cheng, Jennifer E. Trosky, Daisy W. Leung, Melanie L. Yarbrough, Dara L. Burdette, Michael K. Rosen, and Kim Orth. Arp2/3-independent assembly of actin by Vibrio type III effector VopL. *Proceedings of the National Academy of Sciences*, 104(43):17117–17122, October 2007.

[101] Joseph J. Loureiro, Douglas A. Rubinson, James E. Bear, Gretchen A. Baltus, Adam V. Kwiatkowski, and Frank B. Gertler. Critical roles of phosphorylation and actin binding motifs, but not the central proline-rich region, for Ena/vasodilator-stimulated phosphoprotein (VASP) function during cell migration. *Molecular Biology of the Cell*, 13(7):2533–2546, July 2002.

[102] Sankar Maiti, Alphee Michelot, Christopher Gould, Laurent Blanchoin, Olga Sokolova, and Bruce L. Goode. Structure and activity of full-length formin mDia1. *Cytoskeleton (Hoboken, N.J.)*, 69(6):393–405, June 2012.

[103] Pieta K. Mattila and Pekka Lappalainen. Filopodia: molecular architecture and cellular functions. *Nature Reviews Molecular Cell Biology*, 9(6):446–454, June 2008.

[104] Erik Meijering, Oleh Dzyubachyk, and Ihor Smal. Chapter nine - Methods for Cell and Particle Tracking. In P. Michael conn, editor, *Methods in Enzymology*, volume 504 of *Imaging and Spectroscopic Analysis of Living Cells*, pages 183–200. Academic Press, January 2012.

[105] Harry Mellor. The role of formins in filopodia formation. *Biochimica et Biophysica Acta (BBA) - Molecular Cell Research*, 1803(2):191–200, February 2010.

[106] Mithilesh Mishra, Junqi Huang, and Mohan K. Balasubramanian. The yeast actin cytoskeleton. *FEMS microbiology reviews*, 38(2):213–227, March 2014.

[107] Hiroaki Mizuno, Chiharu Higashida, Yunfeng Yuan, Toshimasa Ishizaki, Shuh Narumiya, and Naoki Watanabe. Rotational movement of the formin mDia1 along the double helical strand of an actin filament. *Science (New York, N.Y.)*, 331(6013):80–83, January 2011.

[108] Stephen C. Mockrin and Edward D. Korn. Acanthamoeba profilin interacts with G-actin to increase the rate of exchange of actin-bound adenosine 5'-triphosphate. *Biochemistry*, 19(23):5359–5362, November 1980.

[109] Pierre Montaville, Antoine Jégou, Julien Pernier, Christel Compper, Bérengère Guichard, Binyam Mogessie, Melina Schuh, Guillaume Romet-Lemonne, and Marie-France Carlier. Spire and Formin 2 synergize and antagonize in regulating actin assembly in meiosis by a ping-pong mechanism. *PLoS biology*, 12(2):e1001795, February 2014.

[110] Pierre Montaville, Sonja Kühn, Christel Compper, and Marie-France Carlier. Role of the C-terminal Extension of Formin 2 in Its Activation by Spire Protein and Processive Assembly of Actin Filaments. *The Journal of Biological Chemistry*, 291(7):3302–3318, February 2016.

[111] James B. Moseley and Bruce L. Goode. Differential Activities and Regulation of Saccharomyces cerevisiae Formin Proteins Bni1 and Bnr1 by Bud6. *Journal of Biological Chemistry*, 280(30):28023–28033, July 2005.

[112] Ghassan Mouneimne, Scott D. Hansen, Laura M. Selfors, Lara Petrak, Michele M. Hickey, Lisa L. Gallegos, Kaylene J. Simpson, James Lim, Frank B. Gertler, John H. Hartwig, R. Dyche Mullins, and Joan S. Brugge. Differential remodeling of actin cytoskeleton architecture by profilin isoforms leads to distinct effects on cell migration and invasion. *Cancer Cell*, 22(5):615–630, November 2012.

[113] Anita C.H. Murphy and Paul W. Young. The actinin family of actin cross-linking proteins – a genetic perspective. *Cell & Bioscience*, 5, August 2015.

[114] Suk Namgoong, Malgorzata Boczkowska, Michael J. Glista, Jonathan D. Winkelman, Grzegorz Rebowski, David R. Kovar, and Roberto Dominguez. Mechanism of actin filament nucleation by *Vibrio* VopL and implications for tandem W domain nucleation. *Nature Structural & Molecular Biology*, 18(9):1060–1067, September 2011.

[115] P. Naumanen, P. Lappalainen, and P. Hotulainen. Mechanisms of actin stress fibre assembly. *Journal of Microscopy*, 231(3):446–454, September 2008.

[116] Erin M. Neidt, Colleen T. Skau, and David R. Kovar. The cytokinesis formins from the nematode worm and fission yeast differentially mediate actin filament assembly. *The Journal of Biological Chemistry*, 283(35):23872–23883, August 2008.

[117] Kirsten Niebuhr, Frank Ebel, Ronald Frank, Matthias Reinhard, Eugen Domann, Uwe D. Carl, Ulrich Walter, Frank B. Gertler, Jürgen Wehland, and Trinad Chakraborty. A novel proline-rich motif present in ActA of Listeria monocytogenes and cytoskeletal proteins is the ligand for the EVH1 domain, a protein module present in the Ena/VASP family. *The EMBO Journal*, 16(17):5433–5444, September 1997.

[118] Stephanie H. Nowotarski, Natalie McKeon, Rachel J. Moser, and Mark Peifer. The actin regulators Enabled and Diaphanous direct distinct protrusive behaviors in different tissues during Drosophila development. *Molecular Biology of the Cell*, 25(20):3147–3165, October 2014.

[119] Kyoko Okada, Francesca Bartolini, Alexandra M. Deaconescu, James B. Moseley, Zvonimir Dogic, Nikolaus Grigorieff, Gregg G. Gundersen, and Bruce L. Goode. Adenomatous polyposis coli protein nucleates actin assembly and synergizes with the formin mDia1. *The Journal of Cell Biology*, 189(7):1087–1096, June 2010.

[120] Takanori Otomo, Diana R. Tomchick, Chinatsu Otomo, Sanjay C. Panchal, Mischa Machius, and Michael K. Rosen. Structural basis of actin filament nucleation and processive capping by a formin homology 2 domain. *Nature*, 433(7025):488–494, February 2005.

[121] Katerina Papanikolopoulou, Vincent Forge, Pierrette Goeltz, and Anna Mitraki. Formation of Highly Stable Chimeric Trimers by Fusion of an Adenovirus Fiber Shaft Fragment with the Foldon Domain of Bacteriophage T4 Fibritin. *Journal of Biological Chemistry*, 279(10):8991–8998, March 2004.

[122] Lejla Pasic, Tatyana Kotova, and Dorothy A. Schafer. Ena/VASP proteins capture actin filament barbed ends. *The Journal of Biological Chemistry*, 283(15):9814–9819, April 2008.

[123] Aditya Paul and Thomas Pollard. The Role of the FH1 Domain and Profilin in Formin-Mediated Actin-Filament Elongation and Nucleation. *Current biology : CB*, 18(1):9–19, January 2008.

[124] Aditya S. Paul and Thomas D. Pollard. Review of the mechanism of processive actin filament elongation by formins. *Cell motility and the cytoskeleton*, 66(8):606–617, August 2009.

[125] Markos Pechlivanis, Annette Samol, and Eugen Kerkhoff. Identification of a Short Spir Interaction Sequence at the C-terminal End of Formin Subgroup Proteins. *Journal of Biological Chemistry*, 284(37):25324–25333, September 2009.

[126] Julien Pernier, Jozsef Orban, Balendu Sankara Avvaru, Antoine Jégou, Guillaume Romet-Lemonne, Bérengère Guichard, and Marie-France Carlier. Dimeric WH2 domains in *Vibrio* VopF promote actin filament barbed-end uncapping and assisted elongation. *Nature Structural & Molecular Biology*, 20(9):1069–1076, September 2013.

[127] S. V. Perry. Vertebrate tropomyosin: distribution, properties and function. *Journal of Muscle Research and Cell Motility*, 22(1):5–49, 2001.

[128] J. Petersen, O. Nielsen, R. Egel, and I. M. Hagan. FH3, a domain found in formins, targets the fission yeast formin Fus1 to the projection tip during conjugation. *The Journal of cell biology*, 141(5):1217–1228, June 1998.

[129] Julie Plastino, Stéphane Olivier, and Cécile Sykes. Actin Filaments Align into Hollow Comets for Rapid VASP-Mediated Propulsion. *Current Biology*, 14(19):1766–1771, October 2004.

[130] Thomas D. Pollard. Rate constants for the reactions of ATP- and ADP-actin with the ends of actin filaments. *The Journal of Cell Biology*, 103(6):2747–2754, December 1986.

[131] Thomas D. Pollard. A Guide to Simple and Informative Binding Assays. *Molecular Biology of the Cell*, 21(23):4061–4067, December 2010.

[132] Thomas D. Pollard. Actin and Actin-Binding Proteins. *Cold Spring Harbor Perspectives in Biology*, 8(8), August 2016.

[133] Thomas D. Pollard and Gary G. Borisy. Cellular motility driven by assembly and disassembly of actin filaments. *Cell*, 112(4):453–465, February 2003.

[134] Thomas D. Pollard and John A. Cooper. Actin, a central player in cell shape and movement. *Science (New York, N.Y.)*, 326(5957):1208–1212, November 2009.

[135] K. E. Prehoda, D. J. Lee, and W. A. Lim. Structure of the enabled/VASP homology 1 domain-peptide complex: a key component in the spatial control of actin assembly. *Cell*, 97(4):471–480, May 1999.

[136] Martin Pring, Marie Evangelista, Charles Boone, Changsong Yang, and Sally H. Zigmond. Mechanism of Formin-Induced Nucleation of Actin Filaments. *Biochemistry*, 42(2):486–496, 2002.

[137] Stefan Pukatzki, Amy T. Ma, Andrew T. Revel, Derek Sturtevant, and John J. Mekalanos. Type VI secretion system translocates a phage tail spike-like protein into target cells where it cross-links actin. *Proceedings of the National Academy of Sciences*, 104(39):15508–15513, September 2007.

[138] Britta Qualmann and Michael M. Kessels. New players in actin polymerization – WH2-domain-containing actin nucleators. *Trends in Cell Biology*, 19(6):276–285, June 2009.

[139] Margot E. Quinlan, John E. Heuser, Eugen Kerkhoff, and R. Dyche Mullins. *Drosophila* Spire is an actin nucleation factor. *Nature*, 433(7024):382–388, January 2005.

[140] Nagendran Ramalingam, Hongxia Zhao, Dennis Breitsprecher, Pekka Lappalainen, Jan Faix, and Michael Schleicher. Phospholipids regulate localization and activity of mDia1 formin. *European Journal of Cell Biology*, 89(10):723–732, October 2010.

[141] M Reinhard, M Halbrugge, U Scheer, C Wiegand, B M Jockusch, and U Walter. The 46/50 kDa phosphoprotein VASP purified from human platelets is a novel protein associated with actin filaments and focal contacts. *The EMBO Journal*, 11(6):2063–2070, June 1992.

[142] M. Reinhard, T. Jarchau, and U. Walter. Actin-based motility: stop and go with Ena/VASP proteins. *Trends in Biochemical Sciences*, 26(4):243–249, April 2001.

[143] Daisy N. Riquelme, Aaron S. Meyer, Melanie Barzik, Amy Keating, and Frank B. Gertler. Selectivity in subunit composition of Ena/VASP tetramers. *Bioscience Reports*, 35(5), 2015.

[144] Stéphane Romero, Christophe Le Clainche, Dominique Didry, Coumaran Egile, Dominique Pantaloni, and Marie-France Carlier. Formin is a processive motor that requires profilin to accelerate actin assembly and associated ATP hydrolysis. *Cell*, 119(3):419–429, October 2004.

[145] Elizabeth A. Roth-Johnson, Christina L. Vizcarra, Justin S. Bois, and Margot E. Quinlan. Interaction between microtubules and the Drosophila formin Cappuccino and its effect on actin assembly. *The Journal of Biological Chemistry*, 289(7):4395–4404, February 2014.

[146] Jeremy D. Rotty, Congying Wu, Elizabeth M. Haynes, Cristian Suarez, Jonathan D. Winkelman, Heath E. Johnson, Jason M. Haugh, David R. Kovar, and James E. Bear. Profilin-1 serves as a gatekeeper for actin assembly by Arp2/3-dependent and –independent pathways. *Developmental cell*, 32(1):54–67, January 2015.

[147] Stanislav Samarin, Stéphane Romero, Christine Kocks, Dominique Didry, Dominique Pantaloni, and Marie-France Carlier. How VASP enhances actin-based motility. *The Journal of Cell Biology*, 163(1):131–142, October 2003.

[148] Antje Schirenbeck, Rajesh Arasada, Till Bretschneider, Theresia E. B. Stradal, Michael Schleicher, and Jan Faix. The bundling activity of vasodilator-stimulated phosphoprotein is required for filopodium formation. *Proceedings of the National Academy of Sciences*, 103(20):7694–7699, May 2006.

[149] Caroline A Schneider, Wayne S Rasband, and Kevin W Eliceiri. NIH Image to ImageJ: 25 years of image analysis. *Nature Methods*, 9:671, June 2012.

[150] Bonnie J. Scott, Erin M. Neidt, and David R. Kovar. The functionally distinct fission yeast formins have specific actin-assembly properties. *Molecular Biology of the Cell*, 22(20):3826–3839, October 2011.

[151] Arnau Sebé-Pedrós, Pawel Burkhardt, Núria Sánchez-Pons, Stephen R. Fairclough, B. Franz Lang, Nicole King, and Iñaki Ruiz-Trillo. Insights into the Origin of Metazoan Filopodia and Microvilli. *Molecular Biology and Evolution*, 30(9):2013–2023, September 2013.

[152] D. Sept and J. A. McCammon. Thermodynamics and kinetics of actin filament nucleation. *Biophysical Journal*, 81(2):667–674, August 2001.

[153] Kerri-Lynn Sheahan, Christina L. Cordero, and Karla J. Fullner Satchell. Identification of a domain within the multifunctional Vibrio cholerae RTX toxin that covalently crosslinks actin. *Proceedings of the National Academy of Sciences*, 101(26):9798–9803, June 2004.

[154] Mark Sheffield, Timothy Loveless, Jeff Hardin, and Jonathan Pettitt. C. elegans Enabled exhibits novel interactions with N-WASP, Abl, and cell-cell junctions. *Current biology: CB*, 17(20):1791–1796, October 2007.

[155] Shashank Shekhar, Mikael Kerleau, Sonja Kühn, Julien Pernier, Guillaume Romet-Lemonne, Antoine Jégou, and Marie-France Carlier. Formin and capping protein together embrace the actin filament in a ménage à trois. *Nature Communications*, 6:8730, 2015.

[156] Tom Shemesh, Takanori Otomo, Michael K. Rosen, Alexander D. Bershadsky, and Michael M. Kozlov. A novel mechanism of actin filament processive capping by formin. *The Journal of Cell Biology*, 170(6):889–893, September 2005.

[157] William T. Silkworth, Kristina L. Kunes, Grace C. Nickel, Martin L. Phillips, Margot E. Quinlan, Christina L. Vizcarra, and Laurent Blanchoin. The neuron-specific formin Delphilin nucleates nonmuscle actin but does not enhance elongation. *Molecular Biology of the Cell*, 29(5):610–621, December 2017.

[158] Orit Siton-Mendelson and Anne Bernheim-Groswasser. Functional Actin Networks under Construction: The Cooperative Action of Actin Nucleation and Elongation Factors. *Trends in Biochemical Sciences*, 42(6):414–430, June 2017.

[159] B. Sjöblom, A. Salmazo, and K. Djinović-Carugo. Alpha-actinin structure and regulation. *Cellular and molecular life sciences: CMLS*, 65(17):2688–2701, September 2008.

[160] Colleen T. Skau, David S. Courson, Andrew J. Bestul, Jonathan D. Winkelman, Ronald S. Rock, Vladimir Sirotkin, and David R. Kovar. Actin Filament Bundling by Fimbrin Is Important for Endocytosis, Cytokinesis, and Polarization in Fission Yeast. *Journal of Biological Chemistry*, 286(30):26964–26977, July 2011.

[161] Colleen T. Skau and David R. Kovar. Fimbrin and tropomyosin competition regulates endocytosis and cytokinesis kinetics in fission yeast. *Current biology: CB*, 20(16):1415–1422, August 2010.

[162] Colleen T. Skau and Clare M. Waterman. Specification of Architecture and Function of Actin Structures by Actin Nucleation Factors. *Annual Review of Biophysics*, 44(1):285–310, 2015.

[163] Justin Skoble, Victoria Auerbuch, Erin D. Goley, Matthew D. Welch, and Daniel A. Portnoy. Pivotal role of VASP in Arp2/3 complex–mediated actin nucleation, actin branch-formation, and Listeria monocytogenes motility. *J Cell Biol*, 155(1):89–100, October 2001.

[164] J. Victor Small, Theresia Stradal, Emmanuel Vignal, and Klemens Rottner. The lamellipodium: where motility begins. *Trends in Cell Biology*, 12(3):112–120, March 2002.

[165] Duncan Sousa, Anthony Cammarato, Ken Jang, Philip Graceffa, Larry S. Tobacman, Xiaochuan (Edward) Li, and William Lehman. Electron Microscopy and Persistence Length Analysis of Semi-Rigid Smooth Muscle Tropomyosin Strands. *Biophysical Journal*, 99(3):862–868, August 2010.

[166] J. A. Spudich and S. Watt. The regulation of rabbit skeletal muscle contraction. I. Biochemical studies of the interaction of the tropomyosin-troponin complex with actin and the proteolytic fragments of myosin. *The Journal of Biological Chemistry*, 246(15):4866–4871, August 1971.

[167] Cristian Suarez, Robert T. Carroll, Thomas A. Burke, Jenna R. Christensen, Andrew J. Bestul, Jennifer A. Sees, Michael L. James, Vladimir Sirotkin, and David R.

Kovar. Profilin Regulates F-Actin Network Homeostasis by Favoring Formin over Arp2/3 Complex. *Developmental Cell*, 32(1):43–53, January 2015.

[168] Tatyana M. Svitkina, Elena A. Bulanova, Oleg Y. Chaga, Danijela M. Vignjevic, Shin-ichiro Kojima, Jury M. Vasiliev, and Gary G. Borisy. Mechanism of filopodia initiation by reorganization of a dendritic network. *The Journal of Cell Biology*, 160(3):409–421, February 2003.

[169] Vincent C. Tam, Davide Serruto, Michelle Dziejman, William Brieher, and John J. Mekalanos. A Type III Secretion System in Vibrio cholerae Translocates a Formin/Spire Hybrid-like Actin Nucleator to Promote Intestinal Colonization. *Cell Host & Microbe*, 1(2):95–107, April 2007.

[170] J. Tang, D. W. Taylor, and K. A. Taylor. The three-dimensional structure of alpha-actinin obtained by cryoelectron microscopy suggests a model for Ca(2+)-dependent actin binding. *Journal of Molecular Biology*, 310(4):845–858, July 2001.

[171] S. Tojkander, G. Gateva, and P. Lappalainen. Actin stress fibers - assembly, dynamics and biological roles. *Journal of Cell Science*, 125(8):1855–1864, April 2012.

[172] Denis Tsygankov, Colleen G. Bilancia, Eric A. Vitriol, Klaus M. Hahn, Mark Peifer, and Timothy C. Elston. CellGeo: A computational platform for the analysis of shape changes in cells with complex geometries. *J Cell Biol*, 204(3):443–460, February 2014.

[173] Katalin Türmer, József Orbán, Pál Gróf, and Miklós Nyitrai. FASCIN and alpha-actinin can regulate the conformation of actin filaments. *Biochimica Et Biophysica Acta*, 1850(9):1855–1861, September 2015.

[174] Andreas Untergasser, Ioana Cutcutache, Triinu Koressaar, Jian Ye, Brant C. Faircloth, Maido Remm, and Steven G. Rozen. Primer3—new capabilities and interfaces. *Nucleic Acids Research*, 40(15):e115, August 2012.

[175] Peter A. C. van Gisbergen, Ming Li, Shu-Zon Wu, and Magdalena Bezanilla. Class II formin targeting to the cell cortex by binding PI(3,5)P(2) is essential for polarized growth. *The Journal of Cell Biology*, 198(2):235–250, July 2012.

[176] Dimitrios Vavylonis, David R. Kovar, Ben O'Shaughnessy, and Thomas D. Pollard. Model of Formin-Associated Actin Filament Elongation. *Molecular cell*, 21(4):455–466, February 2006.

[177] Danijela Vignjevic, Shin-ichiro Kojima, Yvonne Aratyn, Oana Danciu, Tatyana Svitkina, and Gary G. Borisy. Role of fascin in filopodial protrusion. *J Cell Biol*, 174(6):863–875, September 2006.

[178] Danijela Vignjevic, Defne Yarar, Matthew D. Welch, John Peloquin, Tatyana Svitkina, and Gary G. Borisy. Formation of filopodia-like bundles in vitro from a dendritic network. *The Journal of Cell Biology*, 160(6):951–962, March 2003.

[179] Valda K. Vinson, Enrique M. De La Cruz, Henry N. Higgs, and Thomas D. Pollard. Interactions of Acanthamoeba Profilin with Actin and Nucleotides Bound to Actin. *Biochemistry*, 37(31):10871–10880, August 1998.

[180] Christina L. Vizcarra, Batbileg Bor, and Margot E. Quinlan. The role of formin tails in actin nucleation, processive elongation, and filament bundling. *The Journal of Biological Chemistry*, 289(44):30602–30613, October 2014.

[181] Christina L. Vizcarra, Barry Kreutz, Avital A. Rodal, Angela V. Toms, Jun Lu, Wei Zheng, Margot E. Quinlan, and Michael J. Eck. Structure and function of the interacting domains of Spire and Fmn-family formins. *Proceedings of the National Academy of Sciences*, 108(29):11884–11889, July 2011.

[182] Jonathan D. Winkelman, Colleen G. Bilancia, Mark Peifer, and David R. Kovar. Ena/VASP Enabled is a highly processive actin polymerase tailored to self-assemble parallel-bundled F-actin networks with Fascin. *Proceedings of the National Academy of Sciences*, 111(11):4121–4126, March 2014.

[183] Jonathan D. Winkelman, Cristian Suarez, Glen M. Hocky, Alyssa J. Harker, Alisha N. Morganthaler, Jenna R. Christensen, Gregory A. Voth, James R. Bartles, and David R. Kovar. Fascin- and α-Actinin-Bundled Networks Contain Intrinsic Structural Features that Drive Protein Sorting. *Current Biology*, 26(20):2697–2706, October 2016.

[184] R. P. Woychik, R. L. Maas, R. Zeller, T. F. Vogt, and P. Leder. 'Formins': proteins deduced from the alternative transcripts of the limb deformity gene. *Nature*, 346(6287):850–853, August 1990.

[185] Yoshihiko Yamakita, Shoichiro Ono, Fumio Matsumura, and Shigeko Yamashiro. Phosphorylation of Human Fascin Inhibits Its Actin Binding and Bundling Activities. *Journal of Biological Chemistry*, 271(21):12632–12638, May 1996.

[186] Changsong Yang and Tatyana Svitkina. Filopodia initiation: focus on the Arp2/3 complex and formins. *Cell Adhesion & Migration*, 5(5):402–408, October 2011.

[187] Shengyu Yang, Fang-Ke Huang, Jianyun Huang, Shuai Chen, Jean Jakoncic, Alejandra Leo-Macias, Ruben Diaz-Avalos, Lin Chen, J. Jillian Zhang, and Xin-Yun Huang. Molecular mechanism of fascin function in filopodial formation. *The Journal of Biological Chemistry*, 288(1):274–284, January 2013.

[188] Bingke Yu, Hui-Chun Cheng, Chad A. Brautigam, Diana R. Tomchick, and Michael K. Rosen. Mechanism of actin filament nucleation by the bacterial effector VopL. *Nature Structural & Molecular Biology*, 18(9):1068–1074, September 2011.

[189] Jacob A. Zahm, Shae B. Padrick, Zhucheng Chen, Chi W. Pak, Ali A. Yunus, Lisa Henry, Diana R. Tomchick, Zhe Chen, and Michael K. Rosen. The Bacterial Effector VopL Organizes Actin into Filament-like Structures. *Cell*, 155(2):423–434, October 2013.

[190] Sally H Zigmond. Formin-induced nucleation of actin filaments. *Current Opinion in Cell Biology*, 16(1):99–105, February 2004.

[191] Dennis Zimmermann, Kaitlin E. Homa, Glen M. Hocky, Luther W. Pollard, Enrique M. De La Cruz, Gregory A. Voth, Kathleen M. Trybus, and David R. Kovar. Mechanoregulated inhibition of formin facilitates contractile actomyosin ring assembly. *Nature Communications*, 8(1):703, September 2017.

[192] Dennis Zimmermann, Alisha N. Morganthaler, David R. Kovar, and Cristian Suarez. In Vitro Biochemical Characterization of Cytokinesis Actin-Binding Proteins. In *Yeast Cytokinesis*, Methods in Molecular Biology, pages 151–179. Humana Press, New York, NY, 2016.